Intrinsic Constraints on Cross-modal Plasticity

By

Charlene Ellsworth

B.S. Biology and Mathematics
Tufts University, 1997

Submitted to the Department of Brain and Cognitive Sciences in
Partial Fulfillment of the Requirements for the Degree of

Doctor of Philosophy
at the
Massachusetts Institute of Technology

September 2004

Signature of Author .....
Department of Brain and Cognitive Sciences
August 2, 2004

Certified by .....
Mriganka Sur
Sherman Fairchild Professor of Neuroscience
Head, Department of Brain and Cognitive Sciences
Thesis Supervisor

Accepted by .....
Earl K. Miller
Picower Professor of Neuroscience
Chair, Department of Brain and Cognitive Sciences Graduate Committee

Intrinsic Constraints on Cross-modal Plasticity

by

Charlene Ellsworth

Submitted to the Department of Brain and Cognitive Sciences in
Partial Fulfillment of the Requirements for the Degree of
Doctor of Philosophy

Abstract

Over the last two decades numerous examples have demonstrated the remarkable plasticity of the developing brain. This plasticity occurs from the level of a single synapse to the repatterning of sensory input. One paradigm that demonstrates this plasticity is the re-routing of sensory input to inappropriate targets. This cross-modal plasticity in an animal model is reminiscent of similar rearrangements in deaf and blind human patients. In these animal models, visual input is induced to innervate the auditory or somatosensory thalamus, MGN and VB respectively, as a result of deafferentation of these nuclei. Such experiments have demonstrated that structures are influenced by their input, and therefore sensory input is able to use alternative pathways for function. This thesis examines the extent to which cues intrinsic to the target provide information to these novel retino-MGN projections. It will consider two examples in which the target structure imposes order onto the incoming sensory input; via intra-nuclei patterning and via a behaviorally relevant efferent pathway. We demonstrate that retinal axons use an ephrin gradient present in the MGN to acquire orderly connections, akin to retinal patterning in visual targets. Using fear conditioning, we show that learning of a visual cue changes when visual input is routed through the auditory pathway. To better understand the intrinsic cues present in a target, we identify a set of genes differentially expressed in the LGN and MGN, which includes a list of transcription factors and putative downstream targets. Furthermore, we demonstrate that deafferentation of the MGN does not influence these sensory-specific molecular profiles but does create a permissive environment which induces innervation by local axons.

Thesis Supervisor: Mriganka Sur
Title: Sherman Fairchild Professor of Neuroscience

Acknowledgments

First and foremost, I would like to thank my advisor Dr. Mriganka Sur for his support, insight, and continued patience. This work has been brought to you as a result of his encouragement and high expectations. He attracted to the laboratory a group of exceptional scientists and terrific people which I was honored to be among. And as chair of the department, he built a community that has been a true source of motivation and support.

I thank also my committee members Dr. Susumu Tonegawa, Dr. Carlos Lois, and Dr. M. Christian Brown. Dr. Tonegawa and his laboratory provided much needed technical assistance and knowledge throughout the past four years. His enthusiasm for science has been truly motivating. Dr. Brown was my source of information on all things auditory. Through his courses and our conversations, I gained a better appreciation of this exciting field. I extend a special thank you to Dr. Lois for his advice, both scientific and personal, and for his continued interest in my research.

Perhaps most importantly, I thank the Sur Lab. They have been an instrumental source of knowledge and support during my graduate career. I especially thank Al Lyckman who taught me most everything I know. He helped me to become a better scientist and a better writer. My collaboration with Jessica Newton was the most productive, efficient, and enjoyable experiences that I have been a part of, and I am grateful for that opportunity. Additional thanks go to Cathy Leamey and Ania Majewska, for being scientific and

personal role models, and more importantly for always being up for a drink at the Muddy. The lab would not have been nearly as organized or fun without Christine Waite and Casey Johnson, so perhaps they deserve the most thanks. And of course, thank you to all the grad students in the Sur Lab, most especially Serkan Oray and Brandon Farley. I grew as a scientist in their company and I thank them for the many random scientific musings, their open ears, and their constant support.

I thank the Department of Brain and Cognitive Sciences at MIT and all of the students, staff, and faculty that have contributed to my graduate school career. A special thank you to Denise Heintze and Carla Ashton-Cohen for keeping all of us graduate students healthy, happy, and productive. I would also like to acknowledge the many people in the department who have provided scientific advice and equipment through the years, including but not limited to the members of the Lois, Tonegawa, and Nedivi Lab. Also to BioMicroCenter, Gabriel, Cam, Sam, and Sonal who worked very hard to help me along during the last weeks of my thesis. Of course, I am indebted to my fellow graduate students. The four years would not have been possible without Jodi, Amy, Brandon, and Nathan who helped me keep all things in perspective and sane during the bad days and were always willing to celebrate the good ones. Most especially, I acknowledge my qualifying exam study partners: Nathan Wilson, Amy Pooler, Corey Harwell, Marnie Phillips, and Wei Allen Lee for sharing in my most productive study hours ever.

Finally, I extend my most sincere thank yous to my friends and family, who have been with me through these grueling years. Thank you to the Catholic Community at MIT, to

Phil and Carolyn who were my family here in Cambridge, and to Rachel, Nora, and Jeanne who supported me through the ups and downs of graduate school and beyond. This research would not have been possible without Mom, Dad, Lisa, Renee, Tara, Paul, Paul, Emily, Morgan, and Grandma. It is only because of their continued love and happy thoughts and prayers that this research, in fact my life thus far, has been possible.

All things are possible to him who believes. *Mark 9:23*

Collaborations

The behavioral experiments were done in close collaboration with Jessica Reeves-Newton, with the help of Tsuyoshi Miyakawa. The ephrin experiments were done with Alvin Lyckman. Ephrin/Eph probes were obtained from Drs. David Feldheim and John Flanagan. Retinal Eph receptor staining in Figure 2-3 was graciously provided by David Feldheim. Affymetrix microarray processing was performed by Manlin Lo at the MIT BioMicro Center. Data Analysis was performed with the help of Sanchita Bhattacharya. Promoter analysis of genes identified in chapter three was done in collaboration with Dr. Gabriel Kreiman. In situ hybridizations were performed with the help of Ning Dong Kang, Monique Brouillette, Sam Horng, and Sonal Jhaveri.

Table of Contents

Chapter 1 : Introduction

Several examples over the last two decades have demonstrated the remarkable plasticity of the brain. One example has been a growing interest in the ability to use regions of the brain previously assigned to other tasks. For example, there is evidence that congenitally blind or deaf patients can use regions of the brain previously assigned to their unused sense to enhance function of remaining senses. An animal model for this cross-modal plasticity has been as promising. In multiple examples, visual input has been rerouted to either the auditory or somatosensory pathways following deafferentation of their target structures. Visual input can use this denervated pathway to transmit visual information. Neurons in the auditory and somatosensory cortex become responsive to visual input. Furthermore, visual information is organized in a manner consistent with the visual pathway. This organization suggests that the auditory pathways can function to process visual information. Further research has demonstrated that this novel route is behaviorally functional. Together, this demonstrates the remarkable plasticity of the brain and alters the notion of a *sensory-specific* pathway.

However remarkable this plasticity, there has been little research asking how sensory information is constrained by the innate properties of the pathway it innervates. In order to appreciate the feasibility of such cross modal plasticity for functional recovery, it is equally important to understand how sensory input is influenced by the target structure. In this thesis, we examine how molecular cues innate to a target influence the processing of sensory input.

The second chapter of this thesis will discuss the role of the ephrins in shaping visual information that is routed through the auditory pathway. In normal development, retinotopic organization is dependent on graded ephrin expression in the LGN and SC, with complementary retinal Eph expression. We ask whether a similar graded expression in the MGN shapes aberrant retinal projections to the MGN. The third chapter will examine how fear conditioning to a visual cue compares when it is routed through the auditory instead of the visual thalamus. Normal animals will learn to associate an auditory cue more rapidly than a visual cue when paired with a noxious stimulus. This difference may be mediated by direct connections between the auditory thalamus and the lateral amygdala. We ask whether visual input, when routed through the auditory thalamus, acquires this rapid fear association. The fourth chapter begins to identify the array of molecular cues that differentiate the LGN and MGN. More specifically, we use cDNA microarray analysis to ask what genes are differentially expressed in the two nuclei. In the fifth chapter, we induce cross modal rewiring and ask how the genetic profile of these two nuclei differs in response to this perturbation.

Chapter 2: Ephrin –A2 and –A5 shape retino-MGN projections in rewired mice

Introduction

Under certain experimental conditions, inputs of one modality can be induced to innervate thalamic nuclei of a different modality. Comparisons of projections in normal targets with those in novel targets should provide insight as to how afferent and target derived factors influence the development of modality-specific patterns. The lateral geniculate nucleus (LGN, including its dorsal and ventral divisions, LGd and LGv respectively) is the primary thalamic recipient of visual fibers from retinal ganglion cell axons, while the medial geniculate nucleus (MGN) is the principal target of auditory fibers from the inferior colliculus. Surgical deafferentation of the MGN in neonatal animals induces axons of retinal ganglion cells to innervate this nucleus [1-3]. Similarly, deafferentation of the ventrobasal nucleus (VB), which normally receives somatosensory input, also induces aberrant visual innervation. Retino-MGN and retino-VB projections have features that are characteristic of retino-LGN projections, such as retinotopy and local eye-specific segregation [4-6]. Auditory cortex that develops with visual input also has a retinotopic map of visual space, as well as orientation selective cells and an orientation map [7,8].

In the visual system, retinotopic ordering of inputs to visual targets depends on ephrin-Eph interactions. Rodent retinal ganglion cells show a graded pattern of expression for the EphA5 receptor [9], while the LGd and superior colliculus express a gradient of the

ligands ephrin-A2 and -A5. Repulsive interactions mediated by the EphA5 receptor on retinal ganglion cell axons in the presence these dual ephrin-A gradients are essential to the development of retinotopic maps in both visual targets [9-16]. Several members of the ephrin family are differentially expressed in the developing thalamus [1,9,17]. We previously reported an ephrin A gradient in the MGN that is similar in orientation and expression level to that in the LGd [1]. Here we asked whether ephrin-A gradients regulate the patterning of a surgically induced retino-MGN projection, analogous to their function in normal visual targets.

In rodents, ipsilateral axons arise from cells in the ventrotemporal retina, a region with high EphA5 receptor expression. These axons may be especially sensitive to the parallel ephrin gradients in the LGN and MGN, targeting cells with low ephrin expression in both nuclei (Fig. 2-1A). If the ephrin gradient directly contributes to retino-MGN organization, we would expect ipsilateral patterning in the MGN to be different in wild-type and ephrin knockout mice (Fig. 2-1B). Furthermore, we would expect that any differences we see between the mice should be similar in the MGN and LGN. We show here that *ipsilateral* retino-MGN projections preferentially target areas of the MGN that show low ephrin expression in normal mice, while in ephrin-knock out mice they are more extensive and have greater topographic spread than in wild-type mice. The changes in the patterning for the retino-MGN projections are comparable to those for the retino-LGN projection. Despite changes in patterning, eye-specific segregation is maintained in the knockout mice in the LGN, and rewired MGN. These data suggest that guidance interactions mediated by relatively few receptor-ligand systems have important consequences for

afferent patterning in multiple thalamic nuclei, including normal and novel targets of retinal axons.

Methods

Animals. Surgeries were performed on wild-type 129/SvEv mice (Taconic, Germantown, NY) and on ephrin-A2/A5 double knockout mice that were bred and maintained in our in-house colony (Division of Comparative Medicine, MIT). The ephrin-A2/A5 double knockout mouse (Feldheim et al., 2000) was generated by crossing a homozygous ephrin-A2 knockout in a pure 129/SvEv background with a homozygous ephrin-A5 knockout in a mixed Swiss-Webster/C57BL/6 background [16]. Live animal procedures were approved by the Committee on Animal Care at MIT and conformed to National Institutes of Health guidelines.

Rewiring Surgery. 129/SvEv and ephrin-A2/A5 knockout mice were anesthetized one day after birth by deep hypothermia. Using high temperature microcautery, we lesioned the left superior colliculus and the left inferior colliculus, and severed the left brachium of the inferior colliculus using an 18-gauge needle. These combined procedures effectively deafferent the left MGN, by removing ipsilateral inputs that arise in the inferior colliculus and ascend through the brachium of the inferior *colliculus, as well as* contralateral inputs that cross the midline at the level of the superior colliculus [1,5]. Pups were revived under a heat lamp and were reared to adulthood.

Ephrin-A and EphA expression. Expression patterns of ephrin-A proteins and EphA receptor tyrosine kinases were obtained by staining with alkaline phosphatase

(AP)-coupled affinity probes [9]. For ephrin-A staining of the MGN, we used 100μm vibrotome sections from P0 mouse brains, unperfused and fixed for 20 minutes in paraformaldehyde. For Eph-A staining of the retina, we used 20μm whole mount cryostat sections, fixed with paraformaldehyde for 15 seconds. Sections were incubated with ephrinA5-coupled AP or EphA3-coupled AP in HBAH buffer (Hanks Balanced Salt Solution, BSA (0.5 mg/mL), 0.1% (w/v) NaN_3, 20 mM HEPES, pH 7.0) for 90 minutes. Endogenous phosphatase activity was quenched by incubating the sections overnight at 65 °C. Alkaline phosphatase activity was detected using NBT (Nitro blue tetrazolium, chloride) and BCIP (5-bromo-4-choro-3indolyl-phosphate-p-toluidine salt). Probe intensity in the MGN and retina was quantified on grayscale images using Scion Image software. For the MGN, a line was drawn along the descending ephrin gradient from the ventral and lateral corner (in coronal section) or anterior and lateral corner (in horizontal section). For the retina, a line was drawn along the retinal ganglion cell layer from nasal to temporal retina. Luminance values were measured, inverted, and scaled from 0 (light; low probe intensity) to 1 (dark; high probe intensity).

Retrograde labeling of ipsilateral retinal axons. With a picospritzer, we made five injections of Alexafluor-488 conjugated CTB into the superficial layers of the left superior colliculus of a P0 mouse. A single injection delivered approximately 1uL of CTB. Pups were sacrificed 24 hours after injections. Whole heads were removed, frozen in isopentane, and sectioned at 20μm on a cryostat. Images of the ipsilateral retina were taken with a Zeiss fluorescent microscope. Pixel intensity values were calculated as described above without inversion.

Fluorescent tracing. Adult mice (> 6 weeks) were anesthetized using Avertin (320mg/kg). We injected a saturating volume (2uL) of 1% cholera toxin B-subunit conjugated to either Alexafluor - 488 or –596 (CTB; Molecular Probes, Eugene, OR) into the left and right eyes, respectively. Thus, in the left, rewired, hemisphere, ipsilateral eye projections were labeled green while contralateral eye projections were labeled red. Mice were euthanized 2-3 days after injection using sodium pentobarbital (50mg/kg), and perfused sequentially with phosphate buffered saline and 4% paraformaldehyde. Brains were removed from the skull, equilibrated in 30% sucrose, and sectioned frozen in the coronal or horizontal plane at 50um. Sections were imaged by confocal microscopy. The LGN and MGN were identified on representative sections using Alexa-640/660 Nissl stain (Molecular Probes, Eugene, OR).

Identification of retinal label in standard sections. To compare the extent and location of retinal label in matched locations within the MGN of wild-type and ephrin knockout mice, the LGd was used as a positional reference to define the anterior, posterior, dorsal and ventral borders of the MGN. In the coronal plane, retinal projections to the MGN were consistently observed in six serial 50um sections (labeled "C1" - "C6", as indicated on the horizontal schematic of Fig. 2-2C). Section C1, the most anterior section, was defined as the third section rostral to the posterior boundary of the LGd (approximately located at –2.8 bregma). This section and the next (section C2) were used for measuring the amount and extent of retinal label in "anterior" MGN sections. Sections C5 and C6 were used for measuring label in "posterior" MGN sections.

In the horizontal plane, rewired projections were consistently observed in at least eight sections (labeled "H1"-"H8"). The lateral posterior nucleus (LP) lies dorsal to the LGd and MGN, and also receives enhanced retinal projections after rewiring. We ensured that projections into the LP were not included in the calculations by conservatively including only 6 serial sections in our data analysis. Section H1 was defined as the most ventral section containing LGd. This section was used for measurements in "ventral" MGN sections. We designated the most dorsal section H6; this section was used for measurements in "dorsal" sections.

Retinal labeling in the MGN. Sections were examined by confocal microscopy to produce 8-bit digital images of red and green fluorescence. Images were normalized to contain gray values of 0-255 for each channel. A region of interest (ROI) encompassing all label in the rewired MGN was defined in Adobe Photoshop for each coronal or horizontal section. The LGN, or in more posterior sections the optic tract, was used as the lateral border for the MGN. The ROI never extended past the medial border of the MGN as determined by Nissl staining on representative sections. In order to quantify the degree of retinal innervation from the ipsilateral and contralateral eyes in each ROI, we counted the total number of red and green pixels in each ROI that exceeded a pixel intensity threshold of 200. From these measurements we determined the total number of pixels, and the totals in each channel for each ROI. The percentage of ipsilateral pixels was defined as the number of green pixels in that ROI divided by the total number of rewired pixels in the same ROI.

Location and extent of ipsilateral terminations. For analyzing the location and extent of ipsilateral projections in the LGd and MGN, we analyzed data from five serial coronal sections each from the LGd and the rewired MGN. The most anterior LGd section used in this analysis was the fifth section caudal to the anterior end of LGd (section "C0" in Fig. 2-2C). In some cases, we used the control hemisphere of rewired mice for LGd data. Rewired MGN data included coronal sections C1-C5 as defined above. In NIH ImageJ, a line 45° from horizontal was drawn on each image from the most ventral to the most dorsal retinal projection in the LGd or MGN (see Fig. 2-6). The smallest region encompassing all green pixels (ipsilateral) was outlined by hand. The centroid position of this region was calculated using NIH ImageJ and projected normally onto the 45-degree line. Relative centroid position was defined as the distance of the centroid from the ventral-most retinal projection, divided by total line length. To measure the spread of ipsilateral label, the most ventral and dorsal ipsilateral label was projected normally onto the 45-degree line. The relative extent of ipsilateral label was defined as the distance between these ventral and dorsal points divided by the total line length.

Results

Early in development, retinal fibers traverse the lateral edge of the thalamus via the optic tract en route to the superior colliculus. Subsequently, they branch into the principal visual nucleus of the thalamus, the LGd. In mice, early deafferentation of the MGN causes retinal projections to overshoot the expected medial and posterior boundaries of the LGN and project into this aberrant target [1] (Fig. 2-2). Coronal sections through the posterior thalamus (Fig. 2-2A,B) show retinal projections into the LGd in control, unlesioned mice, and to the LGd and the MGN in rewired mice. Horizontal sections through the thalamus (Fig. 2-2C,D) show retinal projections to the LGd in unlesioned mice, and additionally to the MGN in rewired mice. Here, we sought to understand the patterning of retinal projections in the MGN, and whether ephrin-A proteins contribute to the specification of this patterning.

Ephrin expression in the mouse MGN

The mouse MGN shows graded expression of ephrin-A2 and ephrin-A5 mRNAs and ephrin-A proteins with highest expression at the ventrolateral border of the MGN [1]. We have confirmed this ephrin-A gradient in coronal sections, showing that it decreases towards the dorsal and medial part of the MGN (Fig. 2-3A), and have further characterized it in horizontal sections of the MGN at P0. Alkaline phosphatase staining using an EphA3 affinity probe revealed graded ephrin-A protein expression in horizontal sections. In these sections, the highest ephrin-A expression was seen at the anterolateral border of the MGN. The expression then decreased posteriorly and medially from this

border (Fig. 2-3B). The high lateral ephrin-A expression in the MGN, seen in both coronal and horizontal sections, abuts either the medial edge of the LGd or, in more posterior sections, the posterior LGd and optic tract. The pattern of ephrin expression is similar in the LGd: ephrin-A2 and –A5 mRNA expression is high at the lateral, ventral and anterior edge and decreases towards the medial, dorsal and posterior end [9]. This results in a head-to-tail organization pattern between these two nuclei; low ephrin expression in the LGN abuts high ephrin expression in the MGN. The absence of Eph3-AP staining in the thalamus of ephrin-A2/A5 knockout mice indicates that ephrin-A2 and -A5 account for all the ephrin-A staining in these thalamic nuclei but does not absolutely rule out the presence of other ephrin-A ligands [15].

Retinal origin of ipsilateral axons

In wild-type mice, temporal retinal ganglion cell axons express high levels of receptors for ephrin-A2 and ephrin-A5 (EphA3 in chick:[10]; EphA5 in mice:[9]). Using an ephrin-A5 alkaline phosphatase probe, we confirmed that the pattern of receptor expression is the same in ephrin-A2/A5 knockout mice [15] (Fig. 2-3C,E). We hypothesized that ipsilateral axons, which arise from the temporal retina, would have high levels of receptor expression. To verify this hypothesis, we retrogradely labeled ipsilateral axons from the superior colliculus of wild-type and ephrin-A2/A5 knockout mice (n=2 for each). Unilateral injections of cholera toxin B in the superior colliculus labeled retinal ganglion cells in the ventro-temporal retina of the same side (Fig. 2-3D). Comparisons of the receptor staining to corresponding sections of back-labeled retinal neurons demonstrated that ipsilateral axons arise from regions of the retina with high receptor expression.

Importantly, there was no difference between wild-type and ephrin knockout mice (Fig. 2-3F).

Effects of ephrin expression on patterning eye-specific projections in the rewired MGN

Patterning in the anterior-posterior dimension. Different mean levels of Eph receptor expression in contralateral and ipsilateral retinal ganglion cells indicate that ephrin expression may contribute to eye-specific targeting. For example, ephrin is expressed from a high anterior to low posterior gradient in the MGN (Fig 2-2B). Ipsilateral axons, which show high receptor expression, should avoid areas of the MGN with high ligand expression, namely anterior MGN (Fig.2-4A). We examined eye-specific projections in coronal sections through anterior and posterior MGN (Fig. 2-4). Intraocular injections of Alexafluor 488 (green) and 596 (red) CTB were made, respectively, into the left and right eyes of adult, unilaterally rewired mice. In all cases, ipsilateral projections were labeled with green CTB. In rewired wild-type mice, ipsilateral retinal axons consistently avoided areas of high ephrin expression, namely anterior MGN, and preferentially occupied the posterior region of this nucleus (Fig. 2-4B). We quantified the total number of labeled pixels in the rewired MGN for each section. From this, we calculated the percentage of those pixels that were from the ipsilateral eye (labeled with green CTB). The percentage of rewired axons representing the ipsilateral eye was significantly higher in posterior sections compared to anterior sections (Fig. 2-4C; $p<0.01$, t-test; $n=5$ animals; this and all subsequent comparisons treat each animal as a single datum).

To determine whether this patterning is influenced by ephrin expression, we performed the same analysis on ephrin-A2/A5 knockout mice. We suspected that ipsilateral projections would be specifically enhanced in anterior MGN, where ephrin is highly expressed in the wild type (Fig. 2-4D). Indeed, tracing retinal projections in rewired ephrin-A2/A5 knockout mice revealed ipsilateral patterning that differed from that in the wild type (Fig. 2-4E). In these mice, the percentage of ipsilateral label in anterior MGN significantly increased compared to wild type. A comparison of matched anterior sections demonstrated significantly more ipsilateral projections in ephrin knockout versus wild-type mice (Fig. 2-4C,F; $p<0.05$, t-test; n=5 animals each). Ipsilateral representation in posterior MGN was still higher than in anterior MGN, but this difference was not significant ($p>0.1$, t-test; n=5 animals). There was no significant change in the amount of ipsilateral representation in matched posterior sections of knockout versus wild-type mice ($p>0.45$, t-test; n=5 animals each). There were no apparent changes in the patterning of contralateral projections in the rewired MGN of ephrin-A2/A5 knockout mice.

Patterning in the dorso-ventral dimension. As can be seen in coronal sections, ipsilateral axons not only project more posteriorly within the MGN but also more dorsally and medially than contralateral axons (Fig. 2-4B, see also Fig. 2-2A). This patterning is also consistent with a repulsive role for the ephrin gradient. In both the LGN and the MGN, ephrin is also expressed in a gradient in the dorsoventral dimension, from high ventral to low dorsal (Fig. 2-3A). Using the same reasoning as above, we suspected that ipsilateral axons would preferentially target dorsal MGN (Fig. 2-5A). To confirm this, we performed the same analysis as above on horizontal sections. In wild-type mice,

rewired ipsilateral axons consistently avoided ventral MGN (Fig. 2-5B), preferring the dorsal part of the nucleus. The proportion of ipsilateral label per section was significantly higher in dorsal MGN sections compared to ventral MGN sections (Fig. 2-5C; $p<0.005$, t-test; n=5 animals). In ephrin-A2/A5 knockout mice there was a major increase in the proportion of ipsilateral innervation in ventral MGN (Fig. 2-5D,E). The proportion of ipsilateral label was now much more evenly spread across the nucleus, with no difference between ventral and dorsal sections (Fig. 2-5F; $p>0.2$, t-test; n=5 animals). The most ventral horizontal sections in ephrin knockout mice received significantly greater ipsilateral innervation than matched sections in wild-type mice (Fig. 2-5C,F; $p<0.01$, t-test; n=5 animals each).

Ipsilateral projections in the MGN and LGd of wild-type and ephrin knockout mice

The changes in patterning of ipsilateral projection that we see in the rewired MGN of ephrin knockout mice are reminiscent of the distribution of retinal terminations in normal visual targets, which show similar ephrin expression patterns. For example, in ephrin-A5 knockout mice, temporal axons extend more anteriorly in the LGd [9]. For a more direct comparison, we measured the centroid location of the ipsilateral projection, as well as the spread of ipsilateral label along the axis of ephrin gradient, in both the LGd and MGN of wild-type and ephrin knockout mice (Fig. 2-6). We focused our analysis on coronal sections, as the ipsilateral projection to the LGd is best characterized in this orientation. In wild-type mice, ipsilateral projections target the dorsal and medial edge of the LGd. In ephrin-A2/A5 knockout mice, ipsilateral projections to the LGd spread farther ventrally

and laterally and appeared more widespread compared to the wild-type (Fig. 2-6A). Our metrics demonstrate that in the LGd of ephrin knockout mice, the ipsilateral projection shifted significantly ventrally (Fig. 2-6B; $p<0.01$, t-test; n=5 animals each) and tended to spread further along the dorsoventral dimension (Fig. 2-6C; $p<0.09$, t-test; n=5 animals each) compared to wild type. Such spread is expected in the LGd of knockout mice if high ventrolateral ephrin expression constrains ipsilateral axons in the wild type. We compared this shift in patterning to the position and spread of ipsilateral label along the ephrin gradient axis in the rewired MGN (Fig. 2-6D). Here, the centroid of the ipsilateral label also shifted significantly (Fig. 2-6E; $p<0.05$, t-test; n=5 animals each) and tended to spread further ventrally (Fig. 2-6F; $p<0.07$, t-test; n=5 animals each) in knockout mice compared to wild type. These data, derived from coronal sections, are consistent with the horizontal sections shown in Fig. 2-5. In fact, the shift and spread of the ipsilateral label in ephrin knockout mice appeared to be more pronounced in the rewired MGN compared to the LGd.

Spread of retino-MGN terminations in wild-type and ephrin knockout mice

In a previous study, Lyckman et al.[1] demonstrated that retino-MGN projections are more extensive in ephrin knockout mice compared to wild type, although the relative contributions of ipsilateral and contralateral retinal projections were not evaluated. Here, we also found a roughly 2-fold increase in the total number of labeled pixels in the rewired MGN of ephrin knockout mice compared to wild type (Fig. 2-7, circles; $p<0.05$, t-test; n=10 animals each). This increase was evident despite any obvious differences in cell number or density in the deafferented MGN of these strains. Our results described so

far suggested that ipsilateral projections were specifically increased in ephrin knockout mice. We asked whether an increase in the total number of rewired terminals in the ephrin knockout mice versus the wild type could be accounted for solely by an increase in ipsilateral terminals. We calculated, per mouse, the average number of ipsilateral and contralateral pixels in the rewired MGN of wild-type and ephrin knockout mice. There was a small increase in the number of contralateral projections between ephrin and wild-type mice, although it was not significant ($p>0.35$, t-test; $n=10$ animals each). There was a much greater, roughly 4-fold, increase in the total number of ipsilateral projections in ephrin knockout compared to wild-type mice ($p<0.001$, t-test; $n=10$ animals each). Thus the increase in retinal innervation of the MGN in ephrin knockout mice is due almost entirely to an increase in ipsilateral input.

Inter-ocular segregation in the rewired MGN

In mice, not only are projections from each eye targeted to characteristic eye-specific zones within the LGd, but also ipsilateral and contralateral projections show little to no overlap of termination at the boundaries between these zones. Eye-specific segregation into small focal clusters is observed in the rewired MGN of ferrets, although stereotyped eye-specific zones are not observed [5]. Here, we used dual color (red and green) intraocular injections, as described above, to examine the extent of segregation of retino-MGN projections in wild-type and ephrin-knockout mice. The extent of overlap from the two eyes is indicated by the presence of yellow pixels. Our data indicated that retino-MGN projections were well segregated in wild-type mice: only 0.9% of pixels showed overlap between projections from the two eyes. The degree of eye segregation in rewired

retino-MGN projections was comparable to that of normal retino-LGd projections (Fig. 2-2A,C, 2-4B, 2-5B), where, using our measure, 0.02% of pixels showed inter-ocular overlap. In rewired ephrin-A2/A5 knockout mice, ipsilateral axons projected widely throughout the MGN and were no longer targeted to well-defined zones. However, the changes in ipsilateral targeting did not lead to an increase in the overlap of projections (Fig. 2-4E, 2-5E): 1.3% of pixels showed overlap, a proportion not different from that in rewired wild-type mice ($p>0.1$, t-test; $n=5$ animals each). Similarly, in the LGd of ephrin knock-out mice, 0.1% of pixels showed overlap between the two eyes, which was similar to the proportion in wild type mice ($p>0.05$, t-test; $n=5$ animals each). Thus, consistent with more detailed studies of the LGd (David Feldheim, personal communication), while the targeting of eye-specific projections into zones was significantly influenced by ephrin expression, the segregation of eye-specific terminals was not.

Discussion

We have confirmed that there is a graded pattern of ephrin-A protein expression in the mouse MGN that is similar in orientation and expression levels to that in the LGd. High ephrin-A expression in the MGN occurs at the border of the LGd and optic tract. In the MGN, rewired ipsilateral retinal ganglion cell axons avoid areas of high ephrin expression. Rewired ipsilateral axons develop highly stereotyped patterns of innervation in wild-type mice, preferentially targeting posterior, dorsal and medial MGN. The preferential targeting of ipsilateral axons is significantly altered in location and extent in ephrin-A2/A5 knockout mice suggesting that the ephrin-A gradients are necessary for the establishment of this pattern (Fig. 2-1). This change in targeting also results in an overall increase in ipsilateral representation in the rewired MGN of ephrin knockout mice compared to wild type. We posit that a specific increase in ipsilateral projections may account for the expansion of rewired projections previously reported in ephrin knockout mice. We also report changes in ipsilateral patterning in the LGd of ephrin-A2/A5 knockout mice. Our data suggest that graded topographic labels, such as the ephrins, can serve to shape multiple aspects of afferent patterning, including discrete eye-specific projections, and can do so in both normal and novel targets.

Regulation of patterning by ephrin/Eph interaction

Sensory axons faithfully reach their appropriate subcortical targets; once there they develop modality-specific patterns of innervation. Results from previous rewiring experiments have been used to suggest a role for patterned sensory activity in the fine-

tuning of connections, including retinotopy and eye segregation[4,5]. It has also been suggested that the patterning of rewired projections indicates a role for interactions among developing axons as a key factor in organizing orderly connections[19]. Our data, however, offer an additional hypothesis. Molecular cues common to the visual and auditory pathway are available to shape rewired patterning. While this paper focuses on the auditory thalamus, similar graded ephrin expression is seen in the somatosensory thalamus and cortex. This expression influences the establishment of a somatotopic map in S1[17,20]. Interestingly, visual axons can also be induced to innervate the ventrobasal nucleus, which traditionally receives somatosensory input [19,21] The retinotopic map that develops in the rewired somatosensory thalamus may also be influenced by the ephrin/ Eph interaction.

In addition to offering an explanation for the patterning of aberrant cross-modal projections, our findings demonstrate a direct and simple way by which multimodal maps may be aligned within a target during normal development [9,10]. Sensitivity to a common molecular signaling system would provide a parsimonious mechanism to align multiple input pathways, as occurs in the superior colliculus. Although there is less information on direct ephrin involvement in the auditory pathway, the EphA4 receptor and ephrin-B2 ligand are expressed along the tonotopic axis in the chick auditory brainstem. Ephrin expression in the mouse inner ear [22,23] along with the graded ephrin expression shown here, indicates that the ephrins likely participate in axon guidance in regions of the developing auditory pathway as well. The ephrins are also expressed in multiple sensory

pathways in the developing cortex[24]. Thus, we suspect Eph/ephrin interactions may also serve to align multimodal input in higher cortical areas.

Arealization in the developing thalamus

Deafferentation of the MGN in ephrin-A2/A5 knockout mice leads to increased retinal innervation compared to the same surgery performed on wild-type mice. Here, we demonstrate a specific increase in ipsilateral retino-MGN input in these mice. These findings suggest that the ephrins may contribute to specifying nuclear boundaries in the thalamus. However, retinal axons do not project into the MGN in ephrin knockout mice without surgery [1] demonstrating that the ephrin boundary is not the sole factor in compartmentalization. A similar relationship is seen at the boundary of the superior and inferior colliculus, where ephrin-A5 expression is also high. In wild-type and ephrin-A5 knockout mice, visual axons initially overshoot the posterior border of the SC and project into the inferior colliculus. In ephrin-A5 knockout mice, compared to wildtype, significantly more temporal axons extend into the IC, indicating that high ephrin expression limits this anomalous projection. However, by P14 these projections disappear for both mice, indicating that the auditory brainstem does not support this visual input. This is quite reminiscent of the patterning we see at the LGN/MGN border. Deafferentation of the MGN is apparently necessary to induce visual axon input into this inappropriate target. These findings together support the idea that sensory axons have an *a priori* competitive advantage in their intended target. It is possible that this originates from molecular cues differentially expressed in the thalamus. It is yet unclear why deafferentation permits this anomalous input to exist but insight may come from the vast

literature on deafferentation induced sprouting in the developing and adult brain (eg., Deller and Frotscher, 1997).

The previous discussion assumes that an enhanced ipsilateral retino-MGN projection is due to additional axons overshooting the LGN/MGN boundary in ephrin knockout mice, compared to wild-type. However, it remains possible that this result is instead due to increased arborization of retinal afferents within the MGN. Disruption of ephrin expression within the MGN may permit a *constant* number of rewired retinal axons to innervate areas of the MGN previously avoided, causing an enhancement of retinal termination. This hypothesis is also supported by the spread of ipsilateral termination we see in the LGd of ephrin-A2/A5 knockout mice. If so, this suggests that targets directly influence the degree of afferent arborization, and presynaptic neurons can have a variable, rather than constant, extent of terminal arbors [2].

In the ephrin knockout LGd, expansion of the ipsilateral projection results in a compensatory reduction of the contralateral projection (Fig. 2-6A). One interpretation of this finding is that the topographic spread of the ipsilateral terminal zone, as would be predicted by removing the ephrin gradient, induces a readjustment of the retinotopically matched contralateral input. As a result, the binocular region of the LGd expands, while the monocular region shrinks. Indeed, optical imaging of primary visual cortex in ephrin –A2/A5 knockout mice demonstrates an expansion of binocular cortex and a contraction of monocular cortex. Interestingly, this compensatory rearrangement is not evident in visual projections to the MGN. In the MGN, expansion of the ipsilateral input has no

obvious influence on contralateral representation. It is possible that our measures cannot detect these changes. Alternatively, it is possible that the MGN is not equipped for aligning matched retinotopic input from the ipsilateral and contralateral eye. A final possibility is that the lack of contralateral loss in the MGN may simply result from a more complex competition for space within the deafferented MGN. In the LGN, ipsilateral axons directly compete with contralateral axons for space within the nucleus. In the deafferented MGN, however, these axons are also competing for space with remaining ascending and descending auditory input. While it is likely that some input must shrink as a result of ipsilateral expansion, it is less clear that this will be the contralateral input.

Ephrins and inter-ocular segregation

We find that in ephrin -A2/A5 knockout mice, the ipsilateral retinal zone is displaced and extended in both the rewired MGN and the LGd; however, the terminations remain sharply clustered and show no greater overlap than in wild type mice. Thus, local segregation between terminals from the two eyes is unaffected. These data are consistent with the hypothesis that the formation of eye-specific layers, or zones, and local inter-ocular segregation are dissociable processes. Indeed, two recent studies have argued that the formation of eye-specific zones in the LGd can be dissociated from segregation of retinal axons into local eye-specific clusters [25,26]. It is likely that the former process requires the presence of labeling molecules such as the ephrins, while the segregation of eye-specific terminations may be driven by a separate mechanism, such as synchronous electrical activity in retinal ganglion cells of either eye. Similarly, retinal terminations

from the two eyes in the MGN of rewired ferrets initially overlap extensively, and progressively segregate into small eye-specific clusters[5]. However, they do not form eye-specific layers similar to those in the LGd. It is likely that additional, perhaps molecular, cues are necessary to guide the complex lamination seen in the ferret LGN and that these cues are not present in the MGN. However, the data from this paper indicates that axon guidance cues in general, and the ephrin family of molecules in particular, are integrally involved in the segregation of retinal input into eye-specific regions in central targets.

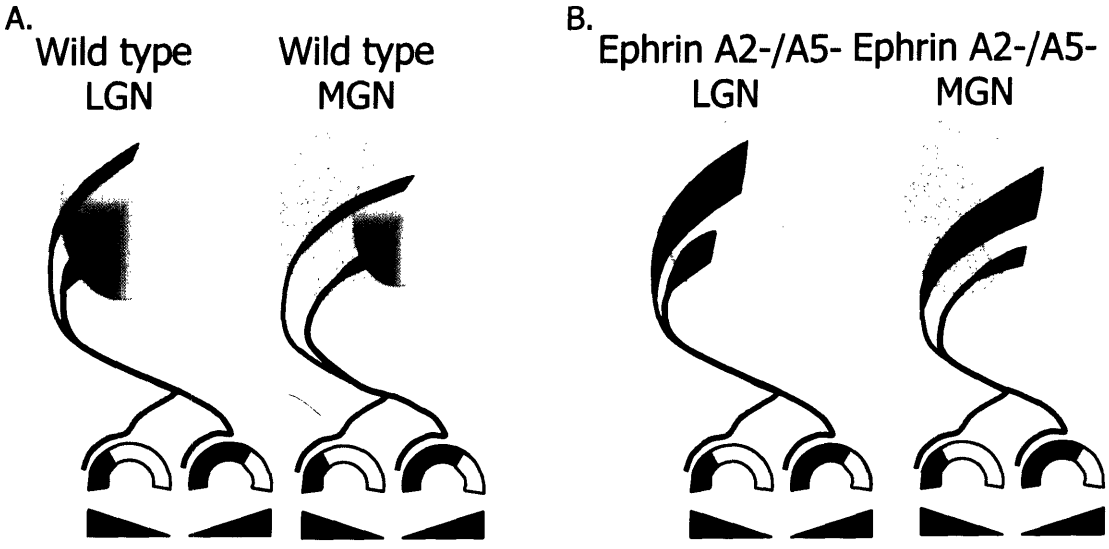

Figure 2-1. Schematic representation of visual projections in wild-type and ephrin knockout mice.

Contralateral projections are labeled in red. Ipsilateral projections are labeled in green. Ephrin expression is represented by the blue gradient, while Eph receptor expression is depicted by the dark blue triangles. *A,* In normal and rewired wild-type mice, ipsilateral axons arise from the temporal retina and express high levels of EphA5 receptor. As a result, these axons target regions of the LGN with low ephrin expression. An identical ephrin gradient is also apparent in the MGN. In rewired wild-type mice, ipsilateral retino-MGN projections target regions of the MGN with low ephrin expression. As a result of these parallel ephrin gradients, eye-specific patterning is the same in the LGN and rewired MGN. *B,* In ephrin knockout mice, ipsilateral axons still show high EphA5 receptor expression but target broader regions of the LGN and MGN. Ipsilateral axons spread ventrally in both the LGN and MGN of ephrin knockout mice.

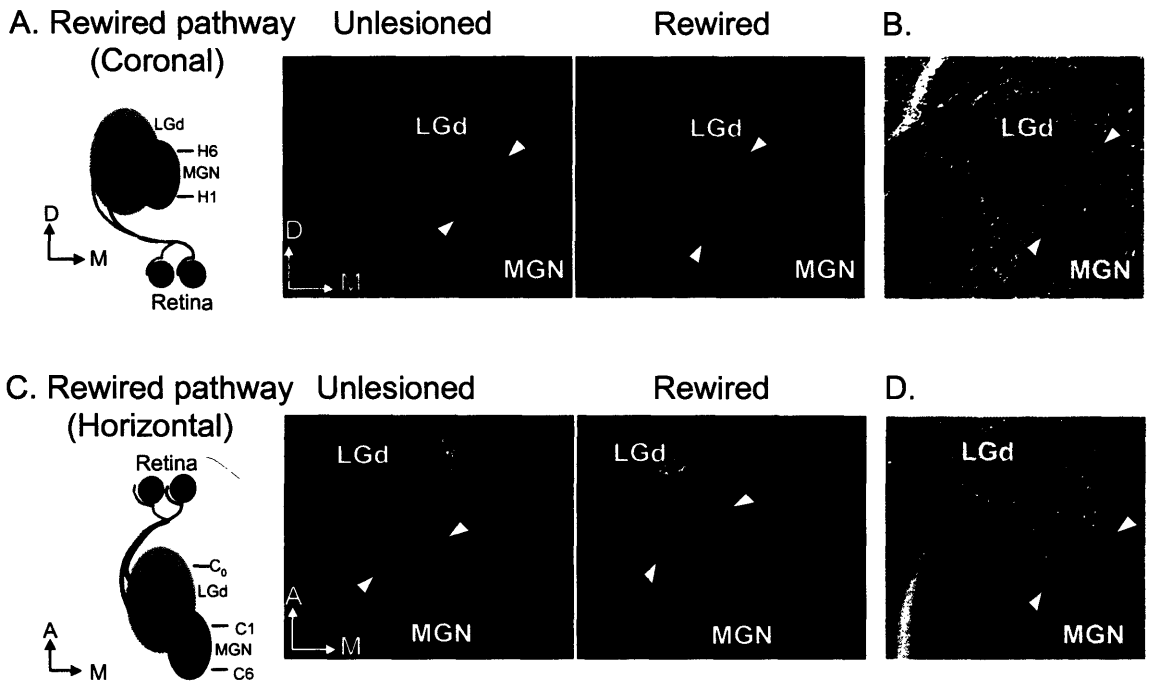

Figure 2-2. Rewired projections in coronal and horizontal sections.

A,C, Schematic representation of rewired visual projections in coronal and horizontal sections. In unlesioned animals, retinal axons innervate the lateral geniculate nucleus (LGN) (orange) while auditory input reaches the medial geniculate nucleus (MGN) (blue) from the inferior colliculus (IC). In 'rewired' animals, SC and IC lesions deafferent the MGN and induce retinal axons to innervate the MGN. A, h1 (most ventral) and h6 (most dorsal) mark the approximate locations used for horizontal sections. C, c1 (most anterior) and c6 (most posterior) mark the approximate locations used for coronal sections. c_0 marks the approximate location of the LGd section show in Fig. 6. A,B, Coronal. In representative coronal sections (section c1) we can view retinal axons overshooting the medial boundary of the LGN and projecting into the MGN. We also see enhanced retinal projections into the lateral posterior nucleus (LP). Retinal axons are labeled with alexafluor conjugated CTB. Contralateral projections are labeled in red. Ipsilateral projections are labeled in green. White arrowheads mark the LGN/MGN boundary. Left panels – unlesioned animals, middle panels- rewired animals. Right panels show matched Alexa 640/660 Nissl-stained sections. 50um sections. C,D. Horizontal. In horizontal sections (section h6), we can view retinal axons overshooting the posterior boundary of the LGN. Details same as for coronal sections. Scale bar: 0.1mm

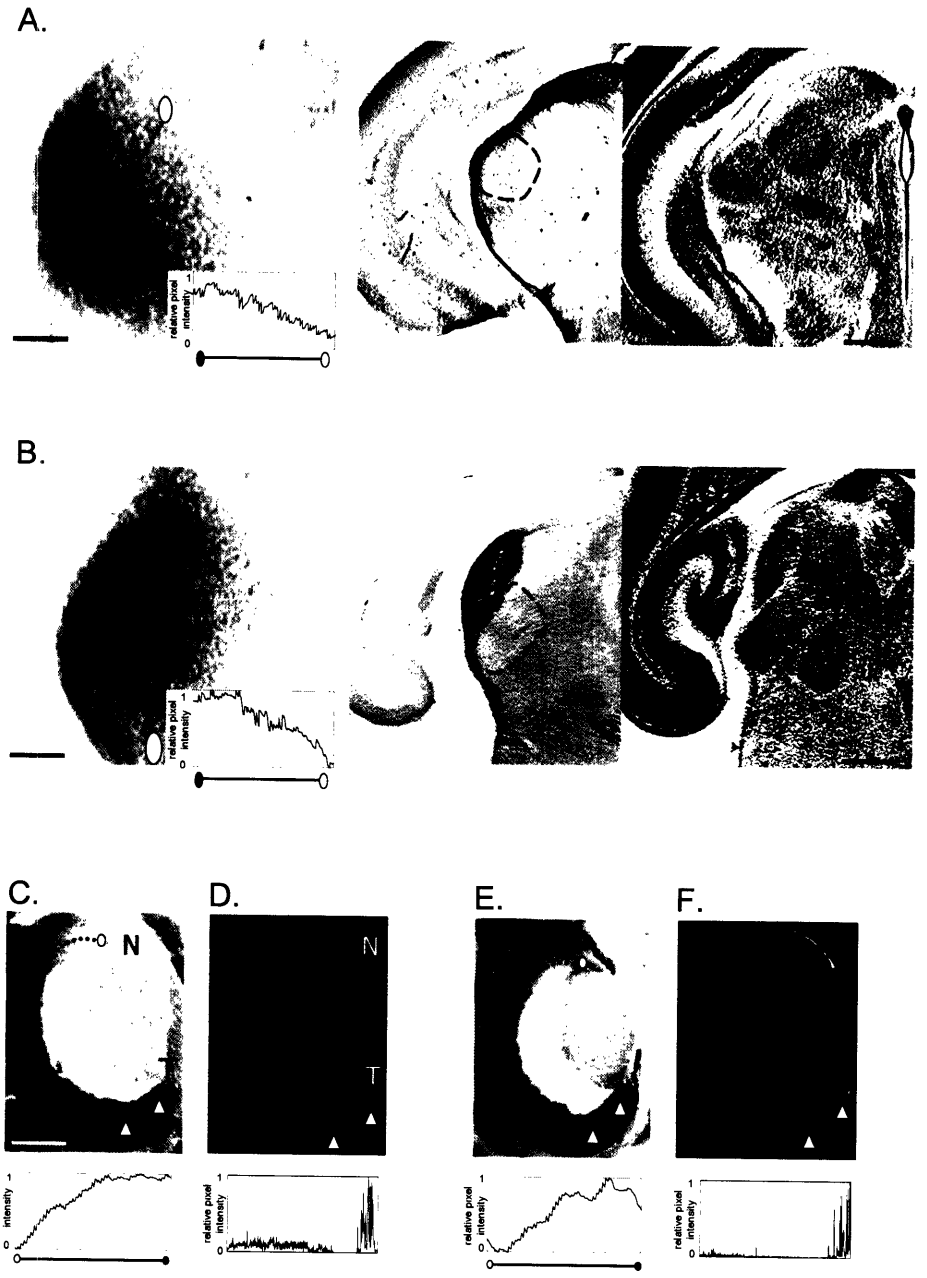

Figure 2-3. Ephrin protein expression in the MGN.

A,B, Left panels - EphA3 alkaline phosphatase probe staining to show ephrin-A ligand expression in a p0 mouse. Inset – pixel intensity profile of EphA3-AP affinity-probe staining through MGN along black line from open to closed oval. Y-axis indicates gray scale pixel values. Right panels – matched p0 sections stained with cresyl violet. Outlines mark the boundaries of the MGN. A. 100 um coronal section. B.100um horizontal section. C. Ephrin-A affinity-probe staining of a horizontal section through wildtype retina. In this view, temporal retina is located in bottom right of the figure (T, temporal; N, nasal). Arrows mark the position of ipsilateral cells labeled in D. Below – pixel intensity profile of Ephrin-AP affinity-probe staining through retinal ganglion cell layer along dotted line from open to closed oval. D. Ipsilaterally projecting retinal ganglion cells, retrogradely labeled with CTB from the superior colliculus. 50*um* section. *Below* – pixel intensity profile of CTB label through retinal ganglion cell layer. *E,F* Same as *C, D* for ephrin-A2/A5 knockout mice.

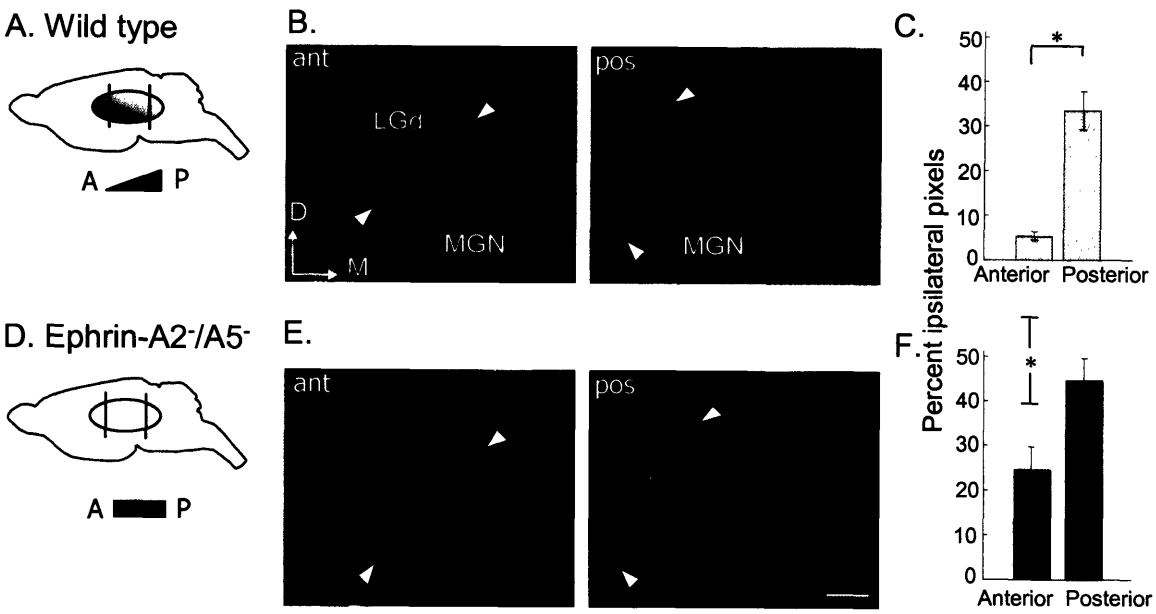

Figure 2-4. Anterior-posterior patterning of ipsilateral projections in rewired MGN of wild-type and ephrin-A2/A5 double knockout mice.

A,D, Schematic sagittal section depicting the anteroposterior ephrin gradient in wildtype (A) and ephrin-A2/A5 double knockout (D) MGN. Below - the corresponding expected distribution of ipsilateral visual projections to the MGN. B,E,50um coronal sections. Contralateral projections are labeled in red. Ipsilateral projections are labeled in green. Left panels – representative anterior sections (c1) Right panels – representative posterior sections (c6). White arrowheads mark the LGN/MGN boundary. *B,* Wild type *E,* Ephrin-A2/A5 double knockout. Scale bar: 0.1mm. *C,F,* Percentage of rewired projections from the ipsilateral eye in anterior and posterior coronal sections, quantified by calculating total number of green pixels versus total labeled pixels in each section using confocal images. Error bars in this and all graphs show standard errors of the mean. *C,* Wild type . *F,* Ephrin-A2/A5 double knockout .

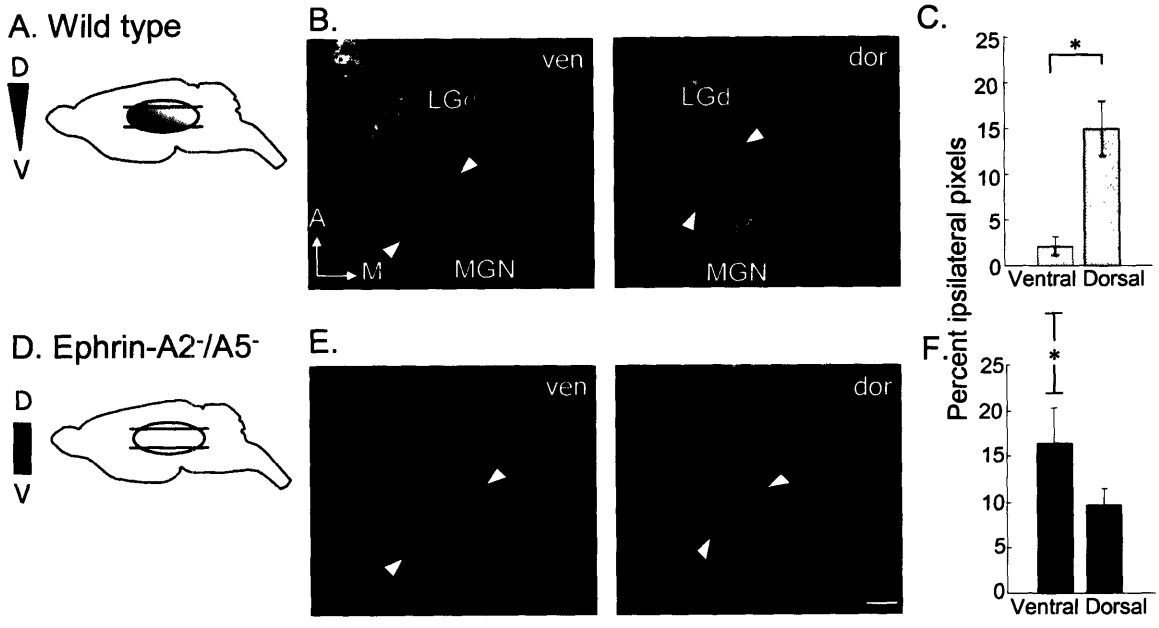

Figure 2-5. Dorsal-ventral patterning of ipsilateral projections in rewired MGN of wild-type and ephrin-A2/A5 double knockout mice.

A,D, Schematic sagittal section depicting the dorsoventral ephrin gradient in wildtype (A) and ephrin-A2/A5 double knockout (D) MGN. Left - the corresponding expected distribution of ipsilateral visual projections to the MGN.,B,E, 50um horizontal sections. Contralateral projections are labeled in red. Ipsilateral projections are labeled in green. Left panels – representative ventral sections (h1). Right panels – representative dorsal sections (h6). White arrowheads mark the LGN/MGN boundary. B, Wild type E, Ephrin-A2/A5 double knockout. Scale bar: 0.1mm. C,F, Percentage of rewired projections from the ipsilateral eye in ventral and dorsal horizontal sections, quantified as in figure 3. B, Wild type . D, Ephrin-A2/A5 double knockout .

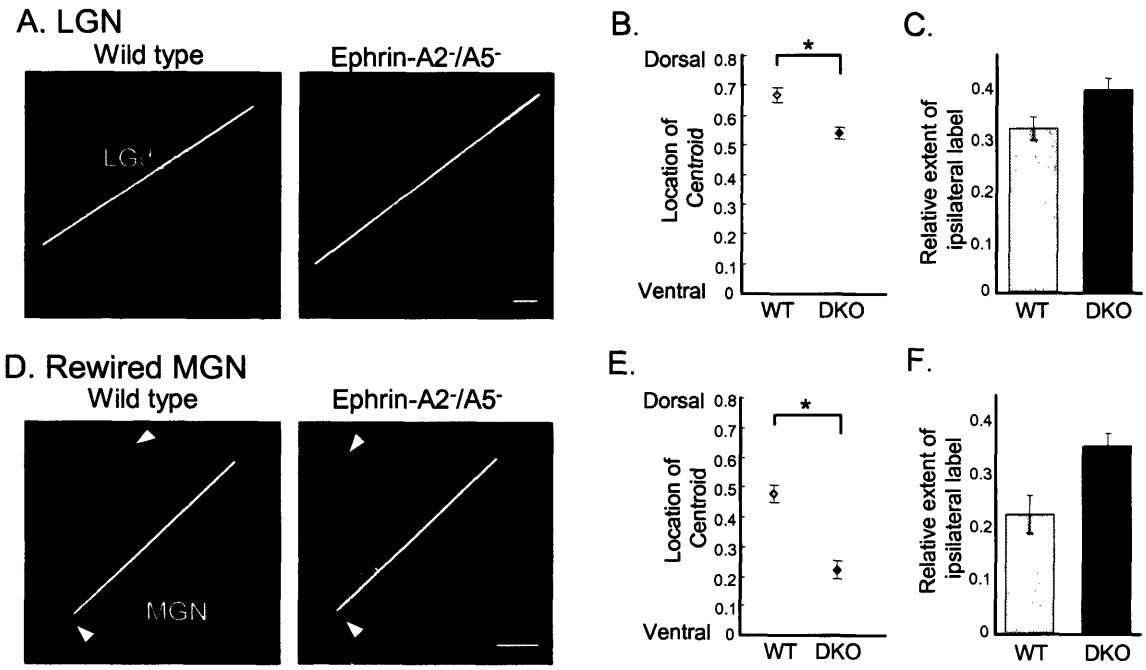

Figure 2-6. Comparison of dorsoventral patterning of ipsilateral projections in the LGd and rewired MGN of wild-type and ephrin-A2/A5 double knockout mice.

A,D, Representative 50um coronal sections in wild-type (left) and ephrin-A2/A5 knockout mice (right). A, LGd (section c_0). D, Rewired MGN (section c5). White line represents the ephrin gradient in wild-type mice, from high ventral to low dorsal. Scale bar: 0.1mm. B,E, Dorsoventral position of ipsilateral centroid in LGd (B) and rewired MGN (E) of wild type (yellow circle) and ephrin-A2/A5 double knockout (blue circle). Y-axis represents the position of the ipsilateral centroid as a fraction of the full length of retinal projection along the ephrin gradient [0 = most ventral projection, 1= most dorsal projection]. C, F, Spread of ipsilateral projection in the LGd and rewired MGN of wild type (yellow) vs. ephrin-A2/A5 double knockout (blue). Y-axis represents the length of ipsilateral representation along the ephrin gradient as a fraction of the full length of retinal projection along the same gradient.

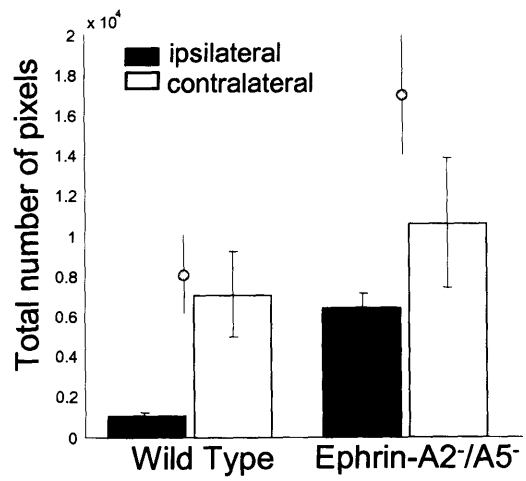

Figure 2-7. Increase in ipsilateral and contralateral pixels in the rewired MGN of wildtype and ephrin-A2/A5 double knockout mice.

Y-axis represents the number of pixels in the rewired MGN per mouse. Bar graph: Wild type (left), Ephrin-A2/A5 knockout (right). White depicts the average number of ipsilateral pixels in the rewired MGN per mouse. Black depicts the average number of contralateral pixels. Closed circles represent the total number of labeled pixels per mouse in the rewired MGN in wild-type and ephrin knockout mice.

Chapter 3: Retino-MGN projections accelerate visually cued fear conditioning

Introduction

In the early 19th century, Muller posited that the qualities of the sensory nerves are specific to the various senses, the nerve of vision being normally as insensible to sound as the nerve of audition is to light. A modern interpretation of this theory is that sensory-specific pathways give identity to a stimulus – such that any activation of that pathway will elicit a sensory-specific perception. It is not clear, however, how the perceptual specificity of a sensory-specific pathway emerges. The literal interpretation of the labeled line theory is not supported by work in rewired ferrets. In these animals, visual cues routed through the auditory pathway are treated as visual and not auditory [27]. By developing under the direction of visual cues, the auditory cortex rearranges its inter- and intra-cortical connections to assume a visual identity. The alternative view, one more in line with Muller's proposal, is that these sensory- specific qualities are inherent in the innate connectivity of the developing organism. Molecular information early on in development may determine how sensory-nuclei connect.

It is not possible to ask a rewired ferret his or her perceptual understanding of a stimulus. Therefore, we can not determine whether visual activation of the auditory cortex is perceived as light or sound. A more robust behavioral paradigm for accessing how an animal is fear conditioning. During fear conditioning, a neutral stimulus is paired with a noxious stimulus, such as a foot-shock. After learning the association, presentation of the

conditioned cue will henceforth elicit a fear response. This response can come in the form of increased heart rate and enhanced acoustic startle, as well as defensive behaviors such as freezing. Fear conditioning is mediated through the amygdala [28]. Research in both humans and rodents has demonstrated the necessity of the amygdala for fear learning, evident from lesion, electrophysiological, and anatomical studies. Discrete lesions of sub-nuclei in the amygdala (see below) result in the impaired acquisition or expression of fear-conditioned response [29]. Cued learning is also marked by the acquisition of a potentiated signal in the amygdala [30]. Pairing of a sensory cue with an aversive stimulus will enhance the response of that stimulus, as indicated by increased field potentials in the amygdala. While the cellular correlates of this memory paradigm remain speculative, regulation of cFOS, an early marker of gene activity, is directly related to learned associations. CFOS transcription is upregulated in response to meaningful activation. This expression may serve to mediate the structural or functional reorganization necessary for learning.

The amygdala is subdivided into discrete nuclei, including but not limited to the lateral amygdala, the basolateral amygdala, and the central nucleus of the amygdala. The lateral amygdala receives direct information about sensory input, including both the conditioned and unconditioned stimulus, while the basolateral amygdala receives integrated input from the hippocampus. The role of the central nucleus, in contrast, is to project learned behavior to downstream effector targets, including the hypothalamus and brainstem. Sensory information about the unconditioned stimulus, such as the foot-shock, appears to reach the amygdala via two parallel pathways. Single lesions of either posterior thalamus

or the insular cortex alone will not prevent the learning of conditioned fear [31]. However, the exact route of progression is not completely clear. The route of the conditioned stimulus is better understood [28]. Injections into the LA reveal direct projections from the medial subdivisions of the medical geniculate body (MGm), as well as accessory projections from the suprageniculate and PIN [29,32-34]. Besides these thalamic projections, the LA also receives projections from the primary auditory cortex and the auditory association cortex (Fig. 3-1). The different roles of the cortico-amygdala and thalamo-amygdala pathways are not completely understood. A general hypothesis is that while the cortical pathway is required for the learning of complex auditory cues, the direct thalamic pathway is able to convey sufficient information about rudimentary stimulus [28]. Enough, at least, to elicit a fear response. This direct pathway may confer an advantage in behavioral situations where a quick response is necessary. The best evidence supporting the importance of the thalamo-amygdala pathway are lesion studies demonstrating that the auditory cortex is not necessary for conditioning of an auditory cue [33]. With that in mind, singular lesions of the thalamic pathway also do not completely disrupt learning, indicating that the cortical pathway is indeed sufficient for learning [35].

The visual route to the thalamus shares a parallel structure. While there are no direct projections from the LGd to the amygdala, the pulvinar nucleus (LP) does send projections to the LA [36]. Additional visual information reaches the LA via the perirhinal cortex (Fig. 3-1). Like the auditory cortical lesions, lesions of the primary visual cortex also fail to disrupt learning. Interestingly, this is also evident in humans. Patients with striate cortex lesions still show physical responses to visual stimuli, even though

recognition and discrimination is impaired. This 'blindsight' is thought to occur through a superior colliulus-pulvinar subcortical pathway [37]. Nevertheless, lesions of the perirhinal cortex do disrupt learning of a visual cue – demonstrating that visual access to the amygdala likely progresses through some cortical nuclei.

Despite similar organizational schemes between visual and auditory cues, it is evident that the behaving animal treats these two sensory stimuli differently. As young as p21 rats can and will learn to associate an auditory cue with a paired US, while failing to learn an associated visual cue [38]. In adulthood, while rats can learn to associate a visual cue, many more pairings are required to elicit a response [39]. What remains unknown is whether these differential learning curves represent inherent differences in stimuli, or as suggested previously may reflect differences in the route that the sensory information takes to reach the amygdala.

We asked whether visual information routed through the auditory pathway would show a learning profile similar to auditory or visual cues. If visual information uses the auditory pathway to access the amygdala it should become as robust a sensory cue as the auditory stimulus (Fig. 3-1). We show that rewired mice do, in fact, learn to associate a visual cue more rapidly than sham-lesioned mice. This learning profile is similar to the association of an auditory cue in normal mice. Furthermore, this rapid acquisition is paralleled by differential induction of cFOS in the MGN and lateral amygdala of normal and rewired mice. Rewired mice show visual activation of the MGN and lateral amygdala after only one day of training, while sham lesioned mice do not. Thus, the processing of this visual

stimulus is influenced by the structure it innervates, providing further evidence that properties intrinsic to a target will impact the course of cross-modal input.

Methods

Animals. Surgeries were performed on wild-type 129/SvEv mice (Taconic, Germantown, NY) that were bred and maintained in our in-house colony (Division of Comparative Medicine, MIT). Live animal procedures were approved by the Committee on Animal Care at MIT and conformed to National Institutes of Health guidelines.

Rewiring Surgery. SvEv/129 mice were anesthetized one day after birth by deep hypothermia. We made bilateral inferior colliculus lesions using high temperature microcautery (n=10). For the sham control group, animals were treated similarly except but no lesion was made (n=10). As an additional control, we made bilateral superior colliculus lesions in a subset of animals. Pups were revived under a heat lamp and were reared to adulthood.

Training. Conditioned fear experiments present an emotionally neutral stimulus (conditioned stimulus, CS) paired with an aversive stimulus (unconditioned stimulus, US) after which subsequent exposure to the CS alone elicits a defensive response, like freezing, that reflects an internal state of fear. This response is expressed to both the CS (cued fear) and the context in which the CS-US pairings occurred (contextual fear). As adults, the mice underwent three consecutive sessions of fear conditioning and behavioral testing during the light portion of the light-dark cycle. The sessions occurred in two chambers, a 30 x 26 x 30 cm rectangular Plexiglas conditioning chamber housed inside a sound attenuated chamber and a 35 x 35 x 35 x 40 cm triangular Plexiglas cued testing chamber scented with vanilla extract. The day before the first fear conditioning session,

the mouse freely explored the cued testing chamber for six minutes. The following day the mouse freely explored the inside of the conditioning chamber for ten minutes before experiencing three cue-shock pairings (30 sec interstimulus interval). The cue served as the CS and was either auditory (75 dB noise) or visual (4 diodes flickering at 1 Hz). The visual cue was presented on two panels located on either side of the chamber so that it could not be missed. The cue was presented for five seconds, co-terminating with a mild foot shock (2 sec, 0.3 mA) which served as the US. After each fear conditioning session the mouse experienced two behavioral testing sessions. During contextual testing (24 hours after conditioning) the mouse was placed in the conditioning chamber and allowed to freely explore for five minutes without incident. A ceiling mounted camera recorded the amount of time the mouse spent freezing, and was taken as an indication of contextual fear. During the cued testing session (48 hours after conditioning) the mouse was placed in the cued testing chamber, and was allowed three minutes of free exploration (habituation) followed by a three minute presentation of the CS. A ceiling mounted camera recorded the amount of time the mouse spent freezing. Freezing during the cue presentation period was compared to that during the habituation period, and was taken as an indication of cued fear.

Control of the stimuli, data acquisition and analysis were performed automatically using Image FZ software, which is a modified version of the NIH Image program. Images were captured (1 frame/second) and for each pair of successive frames, the area (in pixels) the mouse moved was measured. If this amount was equal to or above threshold (i.e., 10 pixels), then the mouse was considered "moving", otherwise the mouse was

considered "freezing". The optimal threshold (in pixels) was set to an amount previously determined to yield results that were in good agreement with freezing judgements measured by human observation[42]. Freezing that lasted less than the time threshold of two seconds was not included in our analysis. Statistical analysis was conducted using SPSS and StatView. The data were analyzed by two-tailed paired t-tests for habituation versus cue presentation period comparisons within a group, two-tailed t-tests for between-group or -session comparisons, or a three-way repeated measures ANOVA.

CFos labeling and quantification. Several mice in each group were euthanized (Nembutal, 80mg/kg), and perfused transcardially with phosphate buffered saline followed by fixatives, 30 minutes after cued testing following one session of fear conditioning. Their brains were cryoprotected, coronally sectioned (40-50μm) and immunohistochemically stained for c-fos. Quantification of c-fos labeled cells in the lateral amygdala (LA) was performed using a 3D counting method[43] , which uses stereology to determine the number of cells contained within a tissue volume, on four sections through the LA for each mouse, with the area analyzed held constant across animals. The level of staining was normalized by quantifying c-fos in four additional sections through the primary somatosensory cortex (S1) equal in area to those analyzed for LA. The number of labeled LA cells was then scaled for each section by the mouse's S1 staining level relative to the mean S1 staining level for all sections (n=40). To examine activation of brain pathways by visual stimuli, additional sections through the MGN, LGN and V1 were examined and quantification of c-fos labeled cells was performed. Two sections through these regions were quantified for each mouse after one

session of fear conditioning (n=20). The level of staining was normalized by the c-fos labeling in S1 for each mouse. In Figure 4f the relative staining observed in these regions for the different groups is represented as follows: - = the least amount of c-fos labeling, comparable to background, + = moderate c-fos labeling, ++ = high c-fos labeling, +++ = the most c-fos labeling observed relative to all sections through that region.

Results

Rewired projections

Original rewiring studies all involved lesions of the visual cortex but since that time it has become evident that these cortical lesions are unnecessary. Previous experiments, however, have always necessitated the elimination of at least one visual target – usually the superior colliculus. Unfortunately, these superior colliculus lesions also result in extreme enhanced projections to the lateral posterior nucleus, as well as the SG and PIN. Since these visual pathways are implicated in fear-conditioning, they would likely confound our results. Therefore, we first demonstrate that lesions of the ascending input into the MGN alone are sufficient for inducing aberrant visual projection into this nuclei. Bilateral lesions of the IC lead to visual innervation of the MGN as demonstrated by retinal injections of cholera toxin B (Fig 3-2A,B). Sham lesioned animals show no visual input to the MGN. In contrast, bilateral lesions of the superior colliculus resulted in enhanced retino-LP projections, but showed no retino-MGN projections (Fig 3-2 C).

Fear conditioning

To assess the differential response of rodents to visual and auditory cues, we exposed both sham-lesioned and rewired mice to 3 cue-shock pairings. Learned fear association was assessed by cue-induced freezing two days after training. The cues were either discrete tones or light stimuli, and each mouse was trained on only one of the sensory cues. As expected, after a *single* session of fear conditioning sham-lesioned and rewired mice responded to a paired tone presentation with significantly increased levels of

freezing ($p<0.001$ and $p<0.001$ respectively, paired t-tests; Fig 3-3A). In contrast, training with a light paired cue did not lead to cue-induced freezing ($p<0.01$, paired t-test; Fig 3-3A). Freezing levels during habituation and during cue presentation were not significantly different for light conditioned cues in unlesioned mice. However, rewired mice showed significantly more freezing during light presentation than during habituation after only one session of training. Both the sham lesion and rewired groups of light conditioned mice exhibited an initial decrease in freezing during the thirty seconds following the onset of the light cue (Fig. 3-3B,D), reflecting an initial orienting behavior towards the stimulus. The light stimulus was very different from the lighting experienced in the home cage environment, and the novelty of this stimulus may have provoked the orienting behavior; however the behavior did not persist beyond the initial thirty seconds following light onset.

After three sessions of fear conditioning, light conditioned sham lesion mice froze significantly more during the cue presentation than during the habituation period ($p<0.05$, paired t-test; Fig. 3-3c), as did light conditioned rewired mice, and tone conditioned sham lesion and rewired mice ($p<0.05$, $p<0.01$ and <0.01 respectively, paired t-tests). More generally, a three-way repeated measures ANOVA showed a significant effect of lesion type ($F=4.5$, $p<0.05$), time (habituation vs. cue; $F=81.0$, $p<0.001$) and session ($F=6.5$, $p<0.01$). There were also significant interactions between lesion type x time ($F=25.2$, $p<0.01$), lesion type x cue type x session ($F=10.2$, $p<0.01$) and lesion type x cue type x time ($F=3.9$, $p=0.05$). Separate two-way repeated measures ANOVAs were run on the data collected after either one or three fear conditioning sessions. The ANOVA on the

data collected after one fear conditioning session showed a significant effect of group ($F=2.7$, $p=0.05$) and time (habituation vs. cue; $F=87.1$, $p<0.001$) as well as a significant interaction between group x time ($F=26.9$, $p<0.001$). The ANOVA run on the data collected after three fear conditioning sessions showed a significant effect of time (habituation vs. cue; $F=53.39$, $p<0.001$), but no effect of group ($F=1.29$, $p=0.29$) and no interaction between group and time ($F=0.57$, $p=0.64$).

The direct projections from the LP and SG to the amygdala offer an alternative path for rewired projections. We therefore performed an additional set of experiments on the SC-lesioned mice. These mice, despite increased visual projections to the LP and SG, did not freeze significantly more to light after a single learning session ($p>0.1$, t-test, comparing sham lesion mice, $n=15$, and SC lesion mice, $n=5$, after one session of fear conditioning). This suggests that enhanced visual drive to the amygdala is not sufficient to produce this change in behavior. Instead direct retino-MGN inputs underlie this rapid learning.

CFOS expression in fear-conditioned mice

CFOS is an immediate early gene whose expression is often upregulated in to response to relevant activity. Its expression pattern often coincides with sites of neural plasticity. cFOS expression is known to increase in the amygdala in response to fear acquisition, in addition to other sites of plasticity within the fear network. We asked whether cFOS expression in the amygdala and other structures in the fear pathway would support our behavioral results. As expected, in tone-conditioned mice cFOS is expressed in the MGN

in response to an auditory cue after only one session of fear conditioning (Fig 3-4 A,B). In light conditioned normal and rewired mice, the LGN andV1 show similar levels of cFOS expression in response to a visual cue. In rewired mice, but not in sham-lesioned controls, cFOS is also induced in the MGN in response to a visual cue (Fig 3-4 A,B). This expression indicates that visual information potently drives cells in the MGN.

Importantly, cFOS expression in the lateral amygdala is markedly different in rewired and sham-lesioned mice (Fig 3-5). In tone conditioned mice, there is increased cFOS expression in the lateral amygdala in response to cue presentation after only one session of fear conditioning (Fig. 3-5B). This is consistent with previous results indicating an important role for cFOS in the induction and expression of learned fear. There is no activation of cFOS in normal light-conditioned mice in response to cue paralleling the behavioral response (Fig. 3-5A). In contrast, light-conditioned rewired mice induce expression of cFOS in the amygdala in response to the cue ($p<0.01$, t-test; Fig. 3-5A,D). The combined cFOS pattern in the MGN and LA in both tone-conditioned and rewired light-conditioned mice indicates that this pathway is activated similarly during these two conditions and may underlie learned fear. The absence of activation in the LA of the normal light-conditioned mice – despite receiving sufficient drive to the visual network – demonstrates the superiority of the MGN pathway to activate the amygdala.

Discussion

Visual and auditory cues show different abilities to induce cued fear in rodents. Auditory cues can induce learned fear early in life, with the ability to associate visual cues developing later. Additionally, while mice will learn to associate an auditory cue with a foot-shock after only 3 tone-shock pairings, it takes many more pairings to elicit a fear response to a light stimulus. While it is potentially acknowledged that an underlying pathway difference between these two modalities may explain the difference, this has remained unresolved. We show here that in fact activity of the MGN gives light new meaning. Visual cues can be learned as rapidly as tone cues if they are routed through the MGN. Visual input activates the MGN, as indicated by increased cFOS expression in the MGN of rewired vs. normal mice. Furthermore, this same visual cue will also induce cFOS expression in the amygdala, the proposed sight of fear plasticity after only three cued pair associations. CFOS expression is not induced in normal light-conditioned mice. Finally, enhanced visual activation of the amygdala cannot explain these differences as superior colliculus lesions, which enhance visual projections to LP, do not show this steeper learning curve.

Instruction during development vs. adulthood

These results seemingly contradict previous rewiring behavioral data, which suggested that the auditory pathway would shape itself during development such that activation resulted in the perception of 'vision' rather than audition. This perception is difficult to measure but was assumed based on the behavioral responses of the animals. These

animals treated visual stimuli as visual despite its use of auditory substrates. In these animals, visual information reaches the auditory cortex as it making its connections. Thus, visual input is available to guide the interpretation of a visual cue. Our results demonstrate that this choice of connections is not always as plastic. It is possible that the differences lie in the developmental age at which a structure receives instruction from it's input. In rewired mice, although an MGN neuron is receiving visual input, it still makes functional connections to the auditory – not the visual cortex – and to the amygdala. This is in apparent contrast to the results in rewired ferrets. It is possible that without necessary pressure to guide appropriate connections, visual input to the MGN-amygdala pathway does not instruct sensory-specific development. Only when plasticity is induced in pathway, does the relative dependence on input become apparent. If a pathway receives novel input after it has already made its connections, activation results in a perception natural to its own pathway – AKA the labeled line. In contrast, if a pathway develops under the guidance of particular sensory information, downstream networks – including those that guide behavior - may be shaped by information linked to the input. However, this instruction is likely influenced by pressure exerted during development.

Where information goes gives it new meaning

Importantly, our work demonstrates that by routing information through a novel pathway we can give that information new meaning, or a new behavioral advantage. This is evidence that segregation and independent processing of sensory inputs gives unique information to the input it processes.

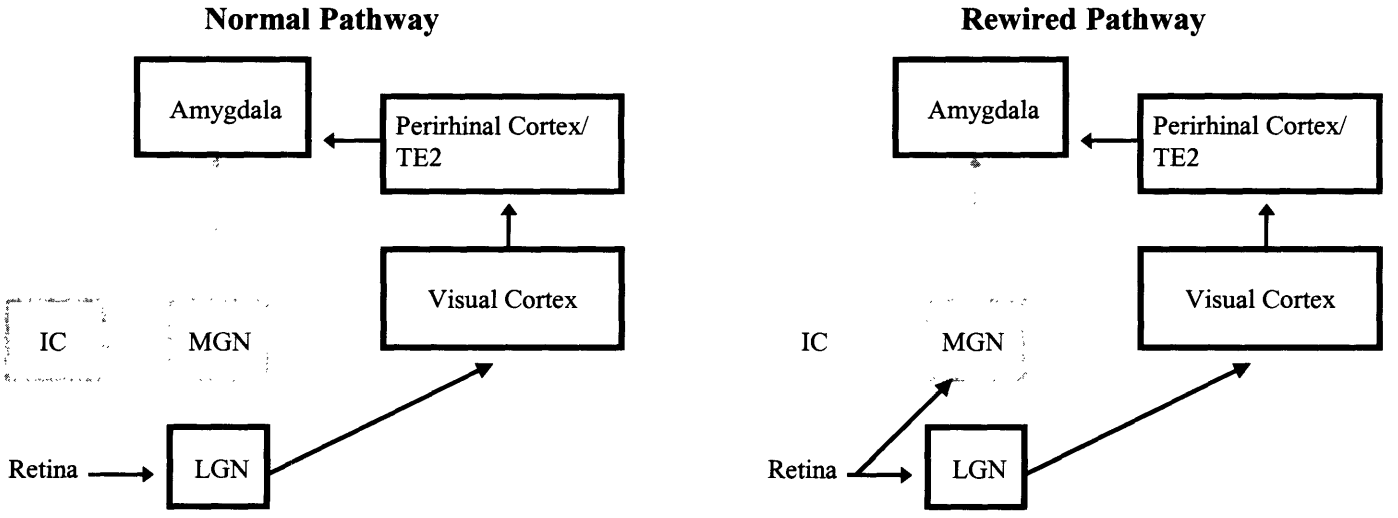

Figure 3-1. Simplified fear conditioning pathways in normal and rewired mice.

(Left) Schematic of the principal visual (black) and auditory (gray) cued conditioned fear pathways in normal mice. (Right) Schematic of the rewired visual (black) cued conditioned pathway. The IC (shown as a dotted box) was lesioned bilaterally in neonatal mice to induce retinal projections to the MGN. IC = inferior colliculus, LGN = lateral geniculate nucleus, MGN= medial geniculate nucleus.

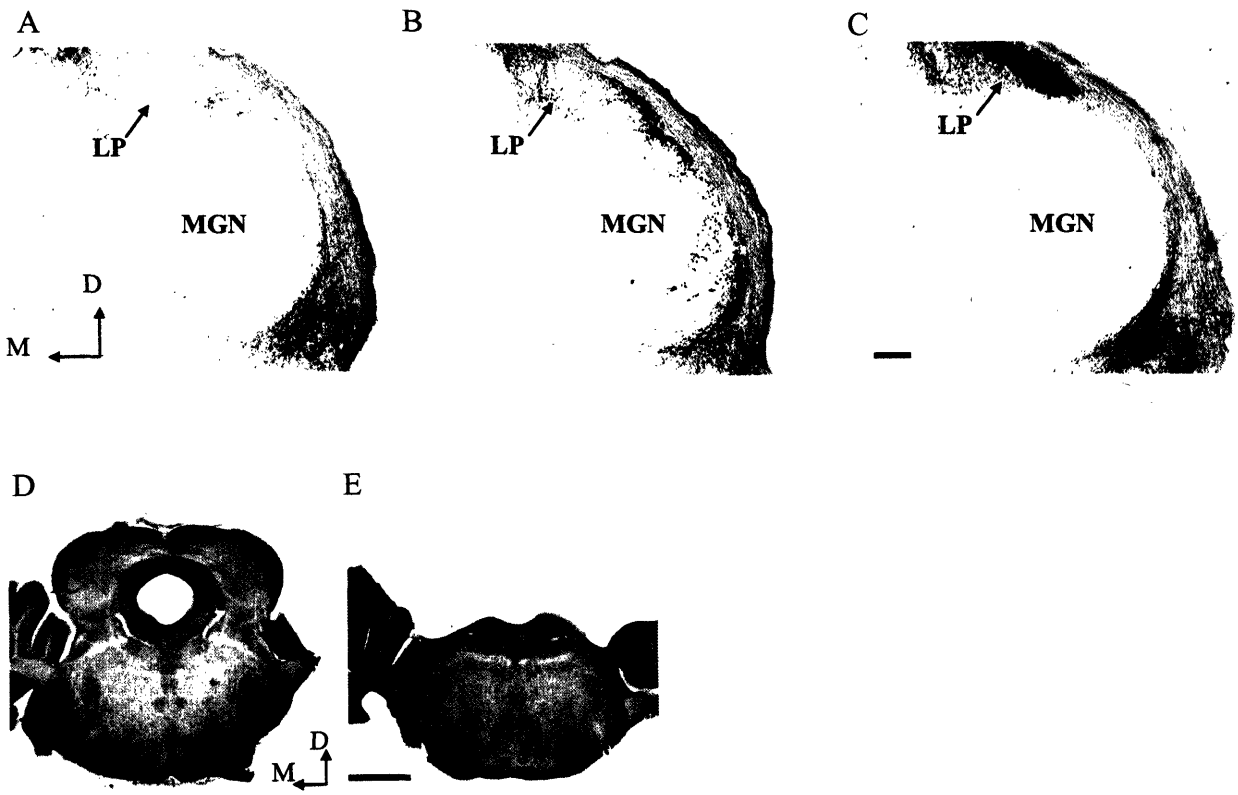

Figure 3-2. Rewired visual projections to MGN and LP

A. Sham-lesioned adult mice. Retinal axons innervate the lateral geniculate nucleus (LGN), as indicated by bilateral intraocular injections of CTB. B. Adult Mice with bilateral inferior colliculus lesions. Intraocular injections of CTB show retinal innervation into both the LGN and the MGN. C. Adult mice with bilateral lesions of the superior colliculus. Retinal CTB injections show enhanced retinal innervation to the lateral posterior nucleus (LP) but not the MGN. D,E. Section through normal (D) and lesioned (E) inferior colliculus in adult mice.

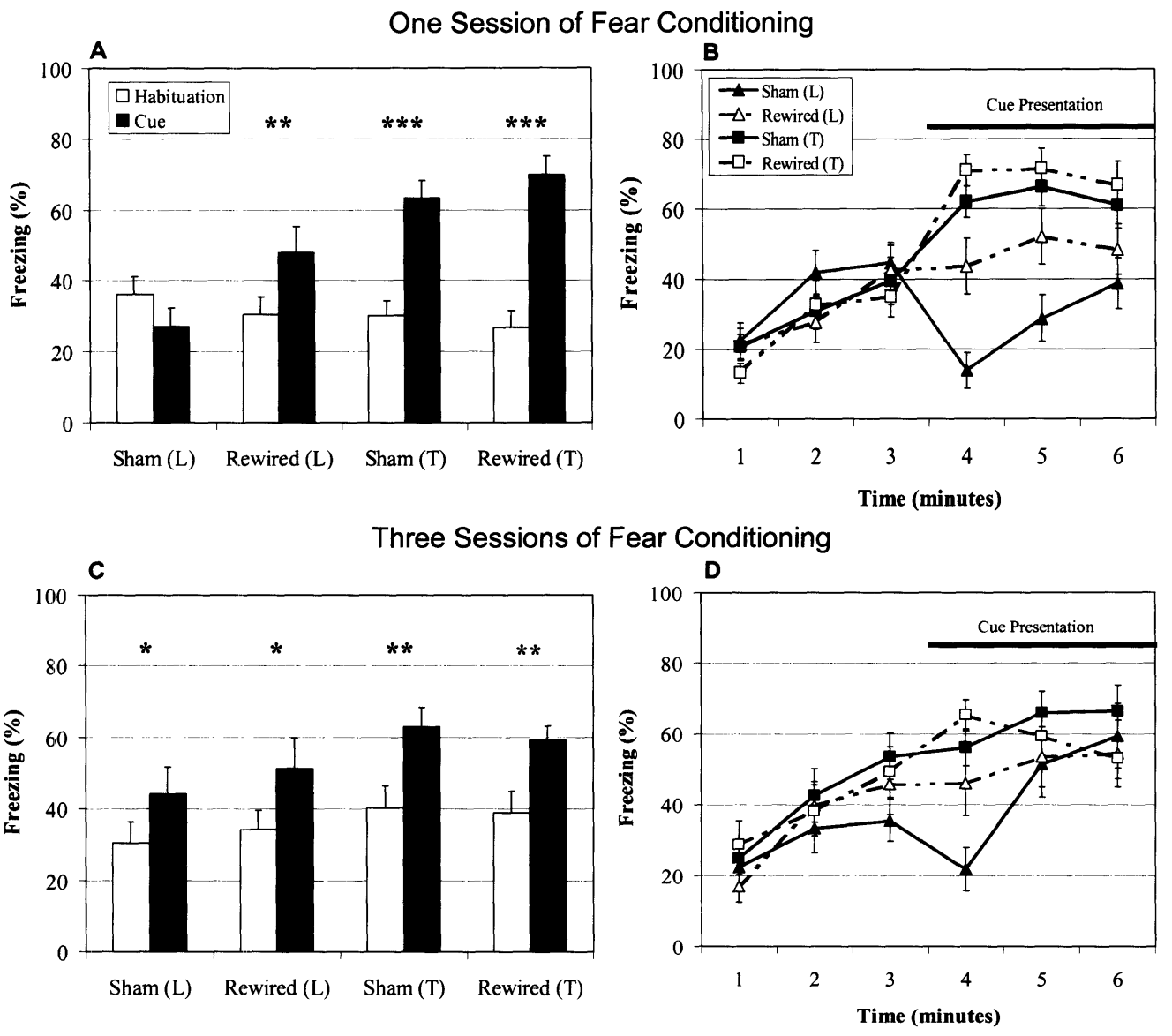

Figure 3-3. Fear conditioning in sham-lesioned and rewired mice

Cued testing behavior in normal and rewired mice. **(A and C)** The mean freezing per group during the habituation (white bar) and cue presentation (black bar) periods of the cued testing session after one or three sessions of fear conditioning, respectively (significant paired t-tests, * $p<0.05$, ** $p<0.01$, *** $p<0.001$). Error bars denote standard error of the mean. L = light conditioned, T = tone conditioned. **(B and D)** The mean freezing per minute after one or three sessions of fear conditioning, respectively. Light conditioned sham (□), rewired (□), tone conditioned sham (□) and rewired (□) groups are shown. The black line represents the duration of the cue presentation. Error bars denote standard error of the mean..

A

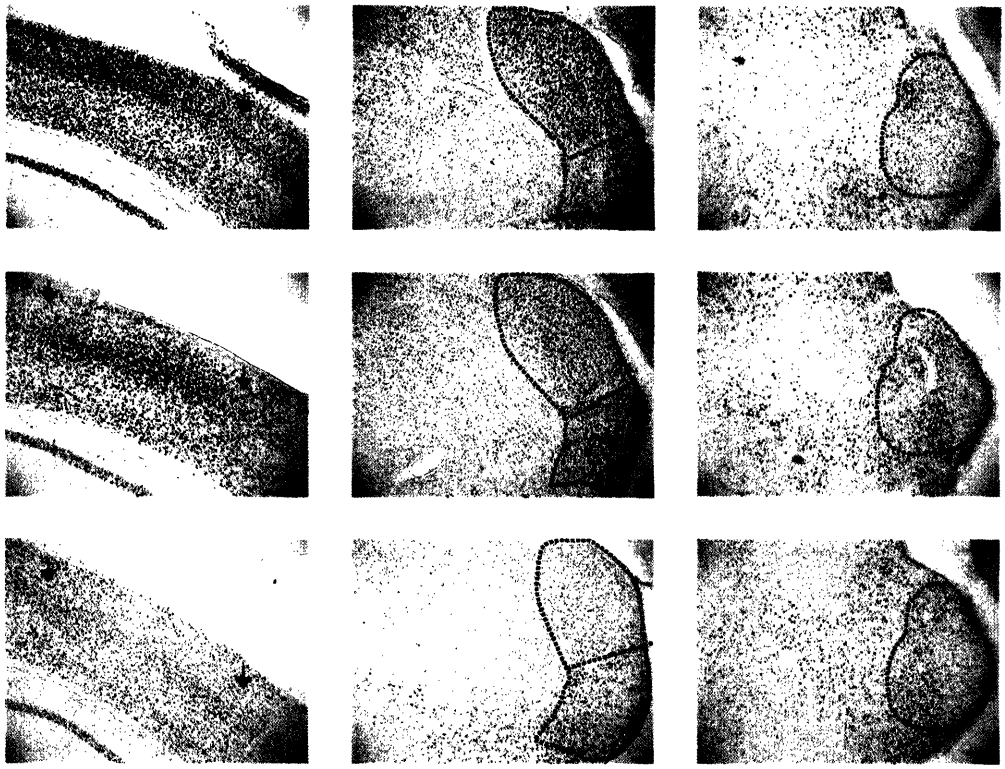

B

	V1	LGN	MGN
Sham (L)	+++	++	-
Rewired (L)	+++	++	++
Sham/Rewired (T)	+	-	++

Figure 3-4. cFOS activation of auditory structures in rewired mice

50μm coronal sections through: (left column), primary visual cortex (V1); (middle column), the lateral geniculate nucleus (LGN); and (right column), the medial geniculate nucleus (MGN). Sections are taken from: (top row) a light conditioned sham lesion mouse; (middle row) a light conditioned rewired mouse; and (bottom row) a tone conditioned sham lesion mouse. The arrowheads in the left column delineate the extent of V1; the dotted lines in the middle column contain the LGN, including the dorsal LGN at the top of the picture and the ventral LGN below; and the dotted line in the right column outlines the MGN , including the dorsal, ventral and medial divisions. Scale bar at bottom right, 0.1mm. (f) A table depicting the levels of c-fos expression in the V1, LGN and MGN of the three groups of mice. -, +, ++, +++ = increasing levels of c-fos expression compared to the other groups.

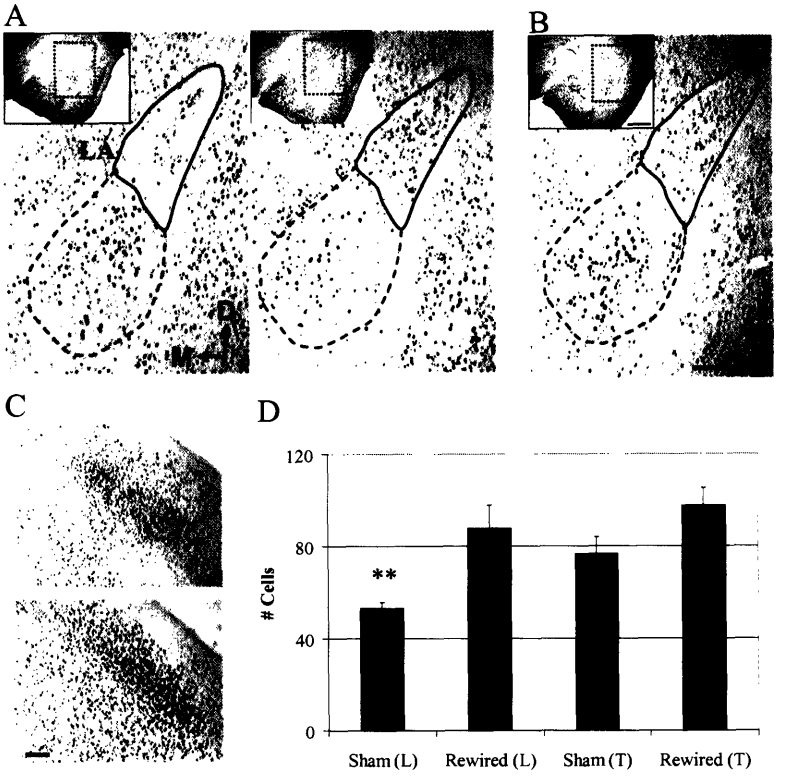

Figure 3-5. cFOS activation of the amygdala after one session of fear conditioning

(A) 50μm coronal sections at 10x magnification at the same level of the amygdala for a light conditioned sham lesion (left) and a light conditioned rewired mouse (right). The lateral nucleus of the amygdala (LA) is contained within the solid lined region. The basolateral nucleus is indicated by the dotted line. D = dorsal, M = medial. (Insets) the same sections at 4x magnification. (B) 50μm coronal section through the amygdala of a tone conditioned sham lesion mouse at 10x magnification. Scale bar, 0.5mm, and applies to (a) as well. (Inset) the same section at 4x magnification. (C) 50μm coronal sections through S1 in the same light conditioned sham lesion (top) and rewired mouse (bottom) shown in (a). Scale bar, 0.1mm. (D) The scaled mean number of c-fos labeled cells per group; error bars denote standard errors of the mean (** $p<0.01$, t-test). L = light conditioned, T = tone conditioned

Chapter 4: Differential gene expression in the developing thalamus

Introduction

The thalamus is the gateway to the cortex. Sensory information, with the exception of olfaction, gains access to the cortex by first synapsing on thalamic relay neurons. The traditional view that the thalamus functions simply as a relay station has been replaced with an appreciation for a more complex regulatory role [40]. The multiple functions of the thalamus are reflected in its elaborate architecture and organization. The thalamus derives from the early diencephelon, which will eventually develop into dorsal and ventral thalamus, as well as the epithalamus and hypothalamus. Only the dorsal thalamus sends direct projections to the cortex, and within the dorsal thalamus are housed the principle sensory nuclei. The basic structure of each primary sensory nucleus, which includes the ventrobasal nucleus (VB), the dorsal subdivision of the lateral geniculate nucleus (LGd) and the ventral subdivision of the medial geniculate nucleus (MGv), is highly similar. These sensory nuclei consist primarily of thalamic relay neurons but may also include local inhibitory neurons. Each nucleus maintains the order, ie – retinotopy, and temporal precision of its sensory input. However, each nucleus also develops unique properties. This is reflected in the local organization of each nucleus. For example, in higher mammals the LGd is organized into stereotyped eye-specific lamina, as well as retinal cell-class specific sublamina. The MGv instead has frequency-specific lamellae. The VB subdivides facial sensory information from the trigeminal nucleus and body representation from the dorsal column nucleus. Differences are also reflected in the

neuronal make-up of the nucleus. In rodents, for example, only the LGd contains local inhibitory neurons [41]. Even despite the unique properties of each primary sensory nucleus, the differences between them are minute compared to other nuclei within the thalamus.

The major differences between the sensory nuclei are their input-output connections. The process of development, and the forming of connections, unfolds concurrently in the thalamus, the cortex, and the midbrain. In rats, neurogenesis in the LGd occurs from at E14 and E15 [42]. The LGd is innervated directly by the retina, through the optic tract, in a process that begins at E17 and is largely complete by birth. Neurons in the MGv are born slightly earlier from E13-E15 [43]. The MGv receives direct auditory input from cells in the central nucleus of ipsilateral inferior colliculus (IC) and minor input from the contralateral IC. The VB receives somatosensory information from both the contralateral trigeminal nucleus and dorsal column nucleus in the brainstem. Thalamic nuclei have reciprocal connections with their matching sensory target in the cortex. Neurons in the LGN, MGN and VB send thalamocortical projections to the visual, auditory, and somatosensory cortices respectively. Thalamic axons project from their nucleus and ascend to the cortex through the internal capsule and eventually synapse onto layer IV cells of the cortex [44]. Thalamic axons rarely fail to reach their appropriate cortical area despite a complex trajectory and amid a milieu of guidance molecules.

Gene expression profiles reflect the differences between thalamic nuclei. Nakagawa and O'Leary examined the developmental expression pattern of multiple transcription factors

known to play a role in cortical development [45]. They defined a set of differentially expressed genes in the thalamus that included the LIM homeodomain genes Isl1, and Lhx 1,2,5 and 9, as well as Gbx2, Ngn2 and Pax6. Their distinct expression patterns are evident at the onset of neurogenesis, and the authors suggested that they may act in a combinatorial manner to control the specification of thalamic nuclei. For example, Gbx2 is expressed only in MGN, and is conspicuously absent from the LGd and VB nucleus [45]. Other research has identified genes that are differentially expressed in the thalamus, and may serve to match thalamic nuclei with their cortical targets. For example, limbic system-associated membrane protein (LAMP) is a membrane bound glycoprotein exclusively expressed in the limbic associated anterior and medial thalamic nuclei, and in medial prefrontal, insular and perirhinal cortical areas. The expression of LAMP promotes thalamocortical axon extension from limbic thalamus but not non-limbic thalamus, in vitro and in vivo [46,47]. A subset of Eph receptors is expressed in both the lateral posterior nucleus in the thalamus, and in extrastriate visual cortex where these axons will project. Expression of EphR is distinctly absent in the nearby striate cortex, where LP axons do not synapse, and in the dorsal division of the lateral geniculate nucleus [48-50]. Similarly, cadherin-6 is discretely expressed in the medial geniculate nucleus of the thalamus, while cadherin 8 and cadherin 11 are not. The auditory cortex also expresses cadherin-6 [51].

As mentioned above, the thalamus and cortex develop simultaneously and their relationship is of obvious importance. Significantly more effort has been made to elucidate the development of sensory-specific domains in the cortex. Insight into the

uncovered mechanisms will undoubtedly also shed light on the development of the thalamus. In the cortex, distinction between sensory cortical regions includes differences in gene expression, laminar histology and network organization, including afferent and efferent connections. There is overwhelming evidence that intrinsic factors instruct the regional development of the brain. In E12 mice, before thalamocortical axons even reach the cortex, distinct molecular markers are evident in the cortex. While some of these markers are expressed in gradients in the cortex, others show discrete profiles that closely match functional borders. Transcription factors show the clearest regional profile. Among the most well-defined are Pax6, Emx2, Otx1 and 2, Coup-TF1 and Tbr-1 [52-54]. While these genes may or may not provide instruction about development, they certainly impose positional identity to the neurons and this may dictate further choices. Among these choices is the differential expression of cell-surface molecules. As described above, the ephrins and the Eph receptors, as well as the cadherins, are all differentially expressed in the developing cortex and, to a large extent, match functional boundaries [48-51]. It is clear that thalamocortical innervation is not essential for the maintenance of regional information. The molecular profile of the cortex is remarkably unchanged in mice lacking thalamocortical input, including both Gbx2 mutant and Mash-1 knockout mice [55,56]. Furthermore, gene expression profiles are highly interdependent. Misexpression of key genes has a profound effect on the genetic and functional organization of the developing cortex. Knocking out the rostral expression of Pax6 shifts the gene expression pattern in the caudal direction. More importantly, this shifting also results in the misdirection of visual thalamocortical axons to inappropriately rostral positions. The opposite effect is

seen in the Emx2 mutant, where both genetic expression patterns and thalamocortical organization is shifted rostrally [57].

It is not clear what information in the early developing brain may set up differences in regional identity. In the very early developing nervous system, signaling centers aligned along the neural axis provide positional information [53,54]. The best characterized of these is sonic hedgehog. Cells underneath the developing neural plate secrete sonic hedgehog (SHH). SHH induces the nearby neural cells to take on a ventral fate, and does so in a concentration dependent manner [58,59]. SHH is also expressed in the developing ventral prosencephalon, and provides dorsoventral information to the developing cortical tissue [60]. At least three additional signaling centers are proposed to pattern the cortex [53,54]. The anterior neural ridge expresses FGF, providing anterior/posterior information to the cortex. In fact, ectopically expressed FGF in the brain will induce cells to take on an anterior-like profile [61]. A signal center at the isthmus of the midbrain and prosencephalon, which includes the future cortex and thalamus, provides additional anterior/posterior information. The Wnt family of molecules are expressed at this junction [62,63]. Finally, bone morphogenic proteins (BMPs) are expressed in the dorsal midline of the developing telecephelon, and may be available to provide additional dorsoventral information[64]. These multiple signaling centers create a series of gradients in the brain and may be sufficient to induce a multitude of molecularly distinct areas. This theory has proved true in the developing spinal cord where the overlapping BMP and SHH expression gradient induces a complex expression pattern of LIM homeodomain transcription factors [65].

Over the last decade, cDNA microarrays have been used to construct an emerging map of gene expression across neuronal types, brain regions, and developmental stages. Most reports, however, have provided little more than an extensive list of genes. Few have attempted to uncover the relationship between differentially expressed genes [66]. Here we use a cDNA microarray to identify genes that differentiate the visual and auditory thalamus in the P0 mouse. Moreover, we employ an algorithm designed to search for common regulatory sequences enriched in a set of co-regulated genes [67]. Numerous transcription factors are differentially expressed in the LGN and MGN, consistent with known literature. We searched for putative binding sites for our LGN-specific transcription factors in the promoter sequences of co-regulated LGN specific genes. We show that one potential pathway of induction, through Pax 6, may involve the Zic family of proteins, heretofore uncharacterized in the developing thalamus. We confirm the LGN-specific expression of the Zic genes, and potential downstream targets. In addition, we demonstrate the restricted expression of a subset of MGN-specific genes and suggest a role for retinoic acid in the development of this nucleus.

Methods

Animals. Dissections were performed on wild-type 129/SvEv mice (Taconic, Germantown, NY) that were bred and maintained in our in-house colony (Division of Comparative Medicine, MIT). Live animal procedures were approved by the Committee on Animal Care at MIT and conformed to National Institutes of Health guidelines.

Normal LGN/MGN Tissue. P0 mice were sacrificed using deep hypothermia. Tissue was extracted from a P0 mouse thalamic whole mount immersed in RNA later (Qiagen), (Fig. 4-1). Boundaries of the LGN were identified in representative animals by a 5% unilateral intraocular injection of WGA-HRP, stained with a tetra-methyl benzadine reaction. Left and right LGN and MGN were extracted from the same animal, amounting to approximately .5mg of nucleic-specific tissue per animal. Ten animals were used for each of two biological replicates (n=20 mice total). New tissue was extracted for RT - PCR.

RNA extraction and labeled cRNA synthesis. Total RNA was isolated from the samples (LGN, MGN) using a standard phenol-chloroform extraction. A cDNA copy of the mRNA transcripts was made with Superscript-T7 kit protocol using a T7 oligo-dT primer (Invitrogen; Genset). Labeled cRNA was made with an In Vitro Transcription reaction using biotinylated nucleotides (Enzo Biolabeling Kit).

Hybridization. 15-20ug of labeled cRNA for all conditions was run separately on the Affymetrix murine U74-v2 series by the Biopolymers lab at MIT.

Data analysis. Robust Multi-chip Analysis. Data was first normalized using robust multichip analysis (RMA). RMA is an additive linear model, which normalizes data on the basis of probe intensity levels. In this way, RMA is highly resistant to extreme values. RMA returns background adjusted, normalized, log transformed expression levels based on perfect match probe values. A version of this software is available at **www.bioconductor**.org [68]. Previous results have demonstrated that measurements obtained with RMA are more precise and reliable than with other methods. We employed a method of least partial error (Bonferoni adjustment p=.05) to evaluate average expression values across replicates and to determine significance.

Identification of Cis-Regulatory Elements. Briefly, the algorithm we used was designed to search for the combination of transcription factor binding sites that are enriched in a set of potentially co-regulated genes with respect to the whole genome [67]. Given a set of genes, the program searches for the possible cis-regulatory elements of the transcription factors included in LGN-set. The preferred binding sequences of the differentially expressed transcription factors were identified using TRANSFAC® 6.0 – Public Database (http://www.gene-regulation.com/) or by literature searches using Pubmed. For some transcription factors, a matrix of possible binding sites was used to identify common regulatory sequences in our data set. For some transcription factors only single potential binding sites were available from the literature. The search allowed for one mis-matched nucleotide per sequence for individual binding sequences. A list of transcription factor binding sites is included in Appendix A. The promoter sequence for

each gene was identified from NCBI. 5,000 base pairs up and downstream of the transcription start site were searched for each gene.

Expression pattern of genes

RT-PCR. RNA was extracted from new samples as described above. Single strand cDNA was produced using Superscript First-strand cDNA synthesis (Invitrogen). 26 repetitive rounds of amplification maximized differential expression.

In situ hybridization. PCR was used to create templates for our in situ hybridization probes, using primers including the T7 promoter sequence (Proligo). We used the PCR product as a template for our IVT reaction using Dig-labeled nucleotides (Roche). Probes were quantified using RiboGreen. The in situ was carried out either on free floating 50um fixed sections or 15um sections mounted on slides. 50ng of probe were used for the free floating tissue. 100ng of probe were used for the mounted tissue. Probes were detected using either an AP coupled anti-DIG antibody or a biotinylated anti-DIG antibody (Roche). For the biotinylated antibodies, we used a TSA amplification kit for detection using the protocol provided (Perkin Elmer).

Immunohistochemistry. We used 50um fixed sections from p0 mice for the detection of a subset of differentially expressed genes. Antibodies to the Zic1 protein were obtained from Abcam and used at a 1:100 dilution. Biotinylated secondary antibodies were detected using an ABC kit, and a DAB reaction.

Results

Differential gene expression in the LGN and MGN

We made intraocular injections of WGA-HRP in a P0 mouse to identify the approximate posterior boundaries of the LGN (Fig. 4-1A). Using this histological marker as a guide, we dissected fresh tissue from P0 thalamic whole mounts (n=7-10) (Fig. 4-1B,C). Samples from MGN and LGN were taken from the same animals. Post dissection sections of the tissues demonstrated that we dissected the appropriate tissue, although the samples did not encompass the entire nucleus. RNA was extracted from these tissues and analyzed using Affymetrix mU74-v2 series of cDNA microarrays. The entire process was repeated, resulting in two biological replicates. Robust Multichip Analysis software (RMA) normalized the data from each sample and replicate and was used to calculate the average expression level for each probe set across replicates. This average number was used for all future analysis. From these numbers, we calculated the fold change between LGN and MGN. For the purposes of our analyses, we focused on genes whose expression level differed at least by a factor of 2. ~34,600 transcripts are represented on the mU74-v2 microarray chips. Of those genes, only sixty-four probe sets were differentially expressed according to the criteria described above; 31 sets showed greater expression in the LGN, 33 showed greater expression in the MGN. Because Affymetrix chips are designed such that genes may be represented on more than one transcript, these sets represented 22 and 19 genes respectively. A full list of differentially expressed genes is included in Figure 4-2.

Our screen was consistent with previous work demonstrating LGN and MGN specific genetic profiles, including those characterized by Nakagawa and O'Leary such as Pax6, Dlk 1,2,5, Lhx5 (LGN-specific) and Gbx2 (MGN-specific) [45]. We chose a strict 2-fold criteria limit to decrease the amount of noise within our data. However, additional genes that did not reach our 2-fold criteria but were significantly different between the nuclei ($p<0.05$), are also known to be differentially expressed in the thalamus. For example, in our screen Cadherin 6 showed a 1.7 fold higher expressed in the MGN versus the LGN. This is consistent with previous work on the Cadherin family [51]. Peg3/PW1, a known imprinted gene, was also identified with a 1.5 fold higher expression in the MGN. Previous work in mice demonstrated that expression of this gene was restricted to the MGN and the auditory brainstem nucleus, the inferior colliculus, implicating a role in auditory pathway development [69].

Analysis of cis-regulatory elements in LGN-specific genes

Upon initial inspection of our genes, it was apparent that many transcription factors were differentially expressed in the two nuclei. To confirm our initial assessment, we ran our gene set using GoTree Machine and Mapp Finder software. As expected, the only gene ontology biological group over-represented in this analysis was transcription factors ($p<.005$). Many transcription factors are involved in regionalizing the developing brain, as discussed above. However, the complexity of their regulation has yet to be appreciated. Transcription factors can be positively or negatively regulate downstream genes. Furthermore, a single mammalian gene is likely to be regulated by 10-15 transcription factors [65,70]. Understanding the pattern of a single transcription factor is thus

likely to be under informative. We therefore sought to determine whether any of our sensory specific transcription factors may be working in concert to regulate gene expression in their nuclei. To address this question, we used an algorithm designed to search for common cis-regulatory elements in a set of co-regulated genes [67]. The validity of this method for identifying relevant regulatory elements was previously tested using a set of drosophila genes known to be co-regulated in dorsalization of the embryo. In this study, no knowledge of the transcription factors involved in dorsalization was assumed but instead a list of 13 co-regulated gene promoters was searched for common regulatory sets. The algorithm independently identified a module of transcription factors that are necessary for dorsalization, as determined by previous reports in the literature.

We asked whether the transcription factors preferentially expressed in the LGN could potentially regulate the set of co-expressed LGN genes. Because the binding kinetics of transcription factors are highly dose dependent, we did not initially impose a two-fold criteria. We included all transcription factors that were differentially expressed ($p<.05$). These additional TFs are listed in the bottom table of Figure 4-2. We could identify binding sequences for 11 of our 17 LGN-specific transcription factors. Those transcription factors that were included in the analysis are highlighted with an asterisk in Table 4-1. In some cases, a binding sequence matrix has been characterized and was available either through literature (for example Pbx3) or through the TRANSFAC database (for example Pax6). In some cases where no matrix was available we identified one or more binding sequences from the literature (for example, Isl1). Dlx 1, 2 and 5 bind a common cis-regulatory element. We could not discriminate between these three binding

sites. The sequence of the cis-regulatory sequence for each transcription factor is available in Appendix A.

For our analysis, we included 5,000 base pairs upstream and the first exon and intron downstream of the transcription start site for each of our differentially expressed genes. Using these boundaries, and including all TFs described above, 23 of the 27 analyzed genes contained one or more binding sequence for the LGN-specific transcription factors (Fig.4-3). While the analysis is designed to limit the number of false positive binding sites within the promoter sequences, there is the likelihood that the co-regulation of developmentally related genes may enhance this probability. To better confirm the reliability of our data, we performed an identical analysis using LGN-specific transcription factors on a random set of twenty or thirty genes. The proportion of genes containing binding sites for our transcription factors was significantly higher for our LGN-specific genes compared to a random set of genes ($p<.05$).

Many of the gene interactions identified in our promoter analysis are confirmed in the literature. For example, Isl1 is known to bind to and regulate the Somatostatin promoter. Similarly, Pitx2 binds to a bicoid-like response element in the Dlx2 promoter and can upregulate Dlx2 expression up to 45 fold in certain cell lines [18]. Other relationships have not been directly established but are consistent with known co-expression patterns in the diencephelon. As an example, Pax6, Dlx, Isl1, and Lim1 are co-expressed in a set of differentiating progenitor neurons the differentiating ventral thalamus.

Our analysis also suggested novel co-regulation patterns. The pattern of binding sites suggested that the transcription of downstream targets may be regulated in two parallel streams. Coup_tf2, a DNA transcription factor, has a putative binding site on both the Pax 6 and Lhx1/Lim1 promoter sequences. Our data suggests that Pax 6 and Lhx1 proceed through activating the Isl1 or Zic 3,4 promoters respectively. These two transcription cascades in turn activate a set of unique, but overlapping, downstream effectors (Fig. 4-4). The Isl1 cis regulatory sequence is found on multiples genes including somatostatin, neuropeptide y, and proenkephelon. All of these genes are expressed in the reticular thalamic nucleus, located in close proximity to the LGN, and ventral LGN. In contrast, several proteins involved in neurotransmitter processing, including GluR1 and Gad1, instead contain putative binding sites for the Zic family of transcription factors. While these transcription binding sites are still putative, the interactions provide a framework by which to consider the relationship between upstream signaling molecules, such as Pax6, and downstream effectors. A brief description of those genes considered in our analysis is available in Appendix B.

LGN specific genes

The Zic family

The above binding site analysis suggested a role for the Zic family in mediating the transcription of several genes involved in neurotransmitter pathways. This role is consistent with previously identified roles for the Zic proteins, which serve as a bridge between signaling molecules, such as SHH and BMP, and downstream effectors. Of the

five known Zic homologues, Zic 1-5, four showed at least a 2-fold higher expression in the LGN, compared to the MGN, in our cDNA microarray experiment (Fig. 4-2). The only Zic family member not expressed in the LGN, Zic 2, *is* highly expressed in retinal ganglion cells during development. To confirm the differential Zic expression in the LGN, we performed RT-PCR on a new sample of tissue from the LGN and MGN. RT-PCR confirmed the differential expression of Zic 1,3 and 4, with all three genes being more highly expressed in the LGN (Fig 4-5A). We further characterized the expression pattern of two of these genes, Zic 1 and Zic 4 using in situ hybridization (Zic 4 in Fig 4-5B; Zic1 in 4-6A). In situ hybridization confirmed that these genes are expressed highly in both dorsal and ventral LGN. Furthermore, there is little or no expression in the MGN (Zic4 in Fig. 4-5B; Zic1 in Fig. 4-6C). In fact, their expression pattern closely matches the posterior and medial boundaries of the LGN. In anterior sections, there is additional mRNA expression in dorsal thalamus.

While transcription influences the level of a given gene product in a cell, post transcription modulation can also contribute to the level of protein expressed. Thus, to determine whether the shown differential mRNA expression translated into differential protein expression, we performed immunohistochemistry with a Zic1 antibody. For Zic1, the in situ hybridization pattern closely matched the protein expression pattern (Fig 4-6). Zic1 protein was present in the LGN, and other regions of the dorsal thalamus, but was absent from the MGN.

Zic and other LGN-specific genes

Restricted expression in the LGN suggested that the Zic family may be important in the development of this sensory nucleus. To further assess its relevance, we also considered three additional genes that are closely associated with the Zic family; GluR1, Reelin, and Ten-M3. Both GluR1 and Reelin contain a putative Zic 3 binding sequence, and show at least a 2.0 fold higher expression in the LGN compared to the MGN. In an independent experiment in our laboratory, GluR1 antibody staining in the P27 ferret thalamus showed marked staining of the LGN, with lower staining in surrounding nuclei. Its expression pattern closely marks the borders of the LGN (Fig 4-7A). Reelin expression was previously characterized in the P0 mouse brain. Using in situ hybridization, Alcatara et al showed that ventral LGN showed high Reelin expression (Fig. 4-7B). The overlap of expression of the Zic genes with GluR1 and Reelin is evidence for a functional role for Zic in regulating transcription of these genes.

In drosophila, the Zic homologue, opa is expressed in a striped pattern along the anterior posterior axis, and, thus, are members of the pair-rule class of segmentation genes. Its expression pattern coincides with other pair-rule genes, including Ten-m. Mutational analysis by Baumgartner et al., indicated that Ten-m initiates a signal transduction cascade via or in concert with *opa* receptor (Baumgartner et al., 1994). Our microarray analysis also identified Tenm3 as a gene with significantly higher expression in the LGN, although with only a 1.5 fold expression difference ($p < .01$). Interestingly, a parallel experiment in our laboratory identified Tenm3 as a gene with restricted expression in visual cortex in the P0 mouse brain. *In situ* hybridization confirmed Tenm3 expression in

V1, and also demonstrated restricted expression in the LGN, consistent with our microarray data (Fig 4-7C). This independent confirmation of the microarray data highlights the reliability of these methods for identifying region specific genes. Together our results suggest that this molecule may be an important player in visual pathway development. Of interest, Tenm1, another Ten-M family member showed significantly higher expression in the MGN ($p<.01$).

MGN specific genes

As in the LGN, the MGN also expresses a unique set of transcription factors. Ten out of the nineteen MGN-enriched genes identified in our screen were transcription factors (Fig. 4-2). This set of transcription factors included only two genes with well-defined cis-regulatory element matrices. Lessening our criteria to include transcription factors that did not meet our two-fold restriction added on an additional six genes. These genes are listed in the bottom table of Figure 4-2. Of these additional genes, none had well-defined binding information. A literature search identified single binding sites for an additional seven genes. With these binding sites, we performed an identical analysis on MGN-specific transcription factors as described above for the LGN (Fig. 4-8). Unfortunately, the lack of information on the binding elements prevented us from forming a clear picture of MGN development. Fewer MGN-specific genes had putative TF binding sites. For those genes that did, the binding sites were more sparsely located throughout the promoter sequence. Of interest, however, Calbindin 1 and 2 both contain putative binding sites for a number of our MGN-specific transcription factors. In fact, the regulation of the two genes appears to be very similar – including binding sites for Gbx2, Bcl11a/Ctip1,

and Ldb2. Again, the sequence of the cis-regulatory sequence for each transcription factor is available in Appendix A.

Despite the lack of information obtained from promoter analysis, our results are a necessary first step for understanding how the relationships between transcription factors might lead to the functional identity of the MGN. We confirmed the restricted expression of transcription factors including Mtsh and FoxP2 using RT-PCR (Fig 4-9A). Mtsh is a mouse homologue of the drosophila t-shirt gene and is implicated in trunk development [71]. FoxP2 is a homeobox protein, most recognized for its putative role in speech development [72]. Both of these transcription factors showed a higher expression in the MGN compared to LGN at P0. In situ hybridization for FoxP2 confirmed that this transcription factor showed higher expression in the MGN versus the LGN. In fact, its expression was further restricted to a sub-division of the medial geniculate nucleus, with borders closely approximating the MGv (Fig 4-9B). The expression pattern of Fox P2 was similar to the restricted MGN expression shown for Gbx2 (Fig 4-9C) [55]. Though FoxP2 did show higher expression in the MGN, its pattern was not exclusive to that nucleus. In fact, there was FoxP2 expression in dorsal thalamus with some expression in dorsal LGN.

As described above for the LGN, differential expression of transcription factors results in the sensory –specific expression of downstream effector targets. Of those genes that were more highly expressed in the MGN, neurotensin and neurogranin may provide

unique information to sensory input passing through this nucleus. Again, neurotensin was independently identified in a screen for genes showing restricted cortical expression. In this case, neurotensin was shown to have low expression in visual cortex. *In situ* hybridization confirmed restricted expression of neurotensin in the MGN consistent with our microarray data (Fig. 4-9D).

While were not able to create a putative framework for MGN development, we noticed that a significant number of our MGN-specific genes were involved in the processing and transport of retinoic acid. Crabp2, a cellular retinoic acid binding protein, showed the most marked expression difference between MGN and LGN. Crabp2 expression was eleven times higher in the MGN. We confirmed this differential expression using RT-PCR (Fig 4-9A). The level of cellular retinal binding protein (RBP1) expression was also significantly higher in the MGN vs. the LGN ($p<.05$). Prostaglandin d-synthase (Ptgds), a lesser known retinoic acid binding partner of the lipocalin family, also showed preferential expression in the MGN. We also performed a literature search on our MGN-specific genes, to ascertain whether any additional MGN-specific genes are regulated by retinoic acid. In fact, Gbx2, whose differential expression was pulled out in our screen and confirmed in Nakagawa and O'Leary, is positively regulated. The neurogranin, Calbindin 1 and 2 are also under the direct regulation of retinoic acid, while Casein kinase 1alpha (Ck2a) interacts with the retinoid X receptor. A similar search using the LGN specific gene failed to identify any genes that were known direct targets of retinoic acid signaling. In fact, both Dlx1 and Neuropeptide Y appear to be negatively regulated by retinoic acid.

Discussion

Using microarray analysis we identified a set of genes that were differentially expressed in the LGN and MGN. The majority of these genes are known transcription factors, previously characterized in other early developmental systems. By analyzing the promoter sequences of the LGN-specific genes, we were able to identify putative binding sites for many of these transcription factors. This analysis offers a first look at how transcription factors in the developing brain may cooperate to confer identity to a developing sensory nucleus. Furthermore, they provide a link between gene expression and functional differences, such as neurotransmitter expression. We confirmed the differential expression of a subset of these transcription factors, and their potential downstream targets using RT-PCR and in situ hybridization. We suggest that the development of the LGN importantly involves Pax 6 and Zic protein expression. In contrast, MGN development, may instead involve retinoic acid.

Relationship between transcription factors and signaling centers

A novel method for identifying relationships between co-regulated genes

Transcription factors exert their affects by binding to and activating the transcription of multiple gene targets. In mammalian systems, transcription factors can positively or negatively regulate gene transcription up to 10,000 base pairs away from the transcription start site. Furthermore, binding specificity is not unique. Cis-regulatory elements, the specific DNA sequence to which a TF binds, can vary by multiple sites and this will influence the extent of interaction. Finally, binding may rely on multiple TFs acting in

concert [73,74]. Thus, the identification of binding sites within the promoters of genes is a difficult task [75]. However, determining the relationship between transcription factors and downstream targets is absolutely necessary for understanding how these genes may cooperate to confer regional information to the developing brain. The program used in our analysis was designed with the complex binding of transcription factors in mind. Instead of using single binding sites, it relies largely on matrices designed to encompass multiple possible binding sites, akin to real biological interactions. By allowing only 1 mismatched pair, it can predict a putative TF binding site with a false positive every 1 in 100 genes [67].

Putative transcription pathway may influence vLGN development

We used this program to identify putative binding sites for our LGN-specific transcription factors within the promoters of all our LGN-specific genes. Many of the putative interactions have been confirmed in vivo or in vitro in the literature. For example, the transcriptional control of somatostain by Isl1 was previously reported [76]. However, a large number of the putative interactions have not been previously reported. They are, however, consistent with known overlapping expression patterns. To better understand out data we developed a model of interaction between the LGN-specific genes. This model suggests that there are two parallel pathways of transcription occurring in the LGN, or potentially in nearby nuclei. In the first putative pathway, Lim1 binds to the Isl1 promoter, which in turn activates many downstream effectors, including cadherin 8, somatostatin, and neuropeptide Y. This above model has never been characterized in the literature, but is consistent with the development of the ventral LGN. Isl1 shows

restricted expression in the ventral thalamus [45]. The neuropeptides Sst and Npy are also expressed in vLGN, as well as the reticular thalamic nuclei, where they are important for synaptic modulation .

Zic proteins as mediators of transcription in the developing LGN

The second putative pathway progresses through Pax 6, which in turn binds to the Zic family of proteins (either Zic3 or Zic4). The Zic proteins may act mediators between Pax6 and downstream effector targets such as GluR1 and Gad1, both of which are preferentially expressed in the LGN. Pax 6 shows restricted expression in the thalamus, and mutations in pax6 result in a ventralization of the thalamus, including misepxression of ventral marker Isl1 [45,77]. However, this is the first characterization of restricted Zic expression in the developing thalamus. The Zic family of genes plays multiple roles during development [78,79]. The family includes 5 different genes, perhaps evolutionary replicates, conserved in mice, xenopus, c elegans, and drosophila. Previous reports have proposed that the Zic genes act as bridges between secreted neural tissue induction signals and downstream targets [78]. For example, at early stages of development, Zic3 expression is regulated by BMP signaling and is necessary for the development of the neural crest cells [80,81]. In a second phase of contribution, Zics are downregulated by sonic hedgehog, and are necessary for the dorsalization of the neural tube [80,82]. Our results suggest an additional role for the Zic proteins in the patterning of the developing thalamus. The Zics are known for their multiple effects on development, including neurogenesis, regionalization, and cerebellar patterning [78]. We propose that by acting as mediators between signaling molecules and downstream targets they can affect multiple

levels of patterning in the LGN, including neurotransmitter synthesis and potentially afferent and efferent projections. In fact, we demonstrate that putative downstream targets of Zic, GluR1 and Reelin, are also highly expressed in the LGN. As a side note, the only Zic family member not identified in our screen was Zic2. Interestingly, Zic2 is expressed in the developing retina and its expression is restricted to ipsilaterally projecting retinal ganglion cells [83].

Retinoic Acid signaling and MGN development

While many of the LGN-specific gene transcripts could be linked to high rostral expression of Lim1 and/or Pax 6, many of the genes preferentially expressed in the MGN are involved in retinoic acid signaling. Retinoic acid is involved in multiple aspects of development [84-86]. In all systems, retinoic acid regulates gene expression via activating nuclear retinoic acid receptors. The level of retinoic acid that reaches these receptors is determined by RA transport both intra and extracellularly. This graded expression level of RA is integrally involved in the patterning of the hindbrain[84,85]. Specifically, high levels of retinoic acid confer posterior identity to neurons in the hindbrain, in its absence neurons take on a default identity. Several key players can determine how much retinoic acid reaches the RA receptors, including the retinol binding proteins (Rbp), the cellular retinol binding proteins (Crbps) and the cellular retinoic acid binding proteins (Crabp2) [87,88]. Together these constitute the lipocalin-like family of transporters. Both Crabp2 and CRbp1 were preferentially expressed in the MGN compared to the LGN. In fact, Crabp2 showed the highest fold change between the nuclei. In addition, Prostaglandin d synthase was recently identified as a retinoic acid binding partner with affinities similar to the

known retinoic acid transporters [89]. Ptgds also showed preferential MGN specific expression. While it is known that these genes are positively regulated by retinoic acid, thus creating a complex regulatory loop, it is not evident from our data whether high expression of the signaling proteins suggests a posteriorizing role for retinoic acid. For example, high levels of Crabp2 may sequester retinoic acid and prevent it from reaching the nuclear receptors. In this way it may serve to distinguish the MGN from the nearby, but more posterior, midbrain.

Micoarray analysis – too much data, too little time

Over the last ten years, the use of the cDNA microarrays has created a mass of information about gene expression in the brain and elsewhere [90] [66]. In previous work, the efforts resulted in list of genes with differential expression. This list either confirmed previously known data or identified novel genes influenced by a given variable, ie - time or space. However, there is a growing frustration with how best to interpret this plethora of data [66]. Our approach resulted not just in a list of genes, but allowed us to propose a conceptual framework for how these genes may interact [67]. The use of tools such as those used here, in addition to databases such as GeneMapp and BioCarta, are means to understanding the co-regulation of genes. Together these techniques allowed us see new relationships between genes, and to consider a role for known genes, such as the Zic family, in novel roles.

The goal of this microarray analysis was to establish a framework for understanding how early genetic patterning might lead to functional differences between nuclei in the

thalamus. By determining the relationship between signaling centers, prepatterning genes, and functional differences in gene expression we can begin to understand how sensory specific nuclei are established. As an example, neurons in the auditory pathway exhibit a number of specializations for transmitting signals at high rates, including expression of unique glutamate receptors with rapid kinetics. These characteristics allow auditory neurons to extract relevant information from auditory stimuli [92]. Such functional differences may develop as a combined result of differential gene expression and sensory-specific patterns of activity. Our data offer a putative explanation for the differential expression of glutamate receptor subunits in the thalamus.

As mentioned previously, differential expression of genes in the cortex and thalamus has been thoroughly described in the literature. Our work paves the way for a series of experiments aimed at understanding the consequence of such expression patterns. Biochemical techniques can demonstrate transcription factor binding at regulatory sites to verify our computational approach. Interruption of transcription factor binding, or the misexpression of such genes in vivo or in vitro, could confirm whether these genes regulate downstream proteins of interest. Misexpression of functional genes, such as Reelin or GluR1, might hint at the mechanisms that provide unique function to sensory-specific nuclei, including but not limited to afferent and efferent connectivity and the processing of sensory-specific activity patterns. Most certainly, gene expression patterns are only one of many pieces of information that the thalamus receives during development. By understanding the contribution of this differential gene expression and

being able to manipulate these profiles, we can begin to ask real questions about how activity patterns and genetic patterns interact to form the developed brain.

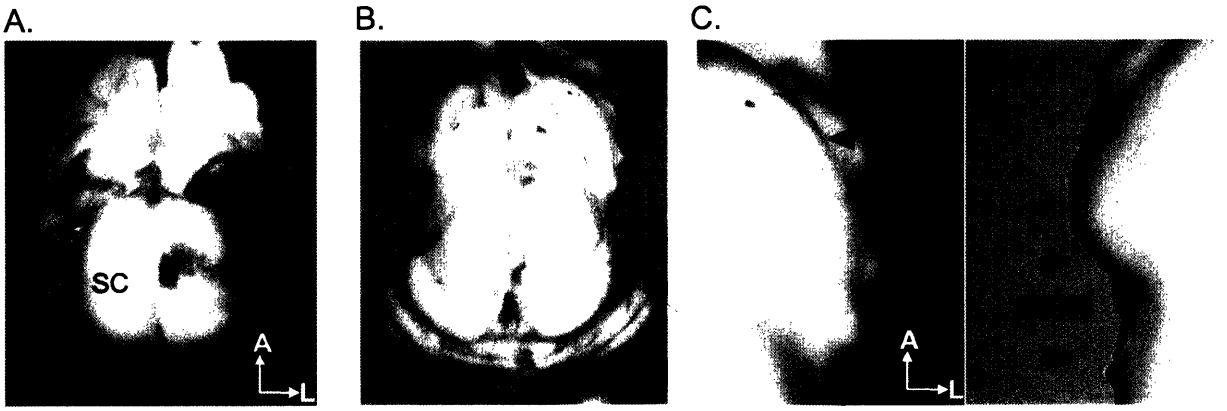

Figure 4-1. Thalamic whole mount. Sections of dissected LGN and MGN

A. Thalamic whole mount of P0 mouse with unilateral intraocular injections of WGA-HRP. Red arrows mark the boundaries used to guide LGN and MGN dissections. L, LGN. M, MGN. SC, superior colliculus. B. Thalamic whole mount of a P0 mouse after removal of LGN (right) and MGN (left) tissue used for RNA extraction and microarray analysis. C. A higher magnification of the dissections depicted in B.

A.

Affymetrix ID	Gene	Fold Change
98394_at	Dlx1 *	7.00
166042_f_at	Arx	5.72
103061_at	Gad1	3.47
95436_at	Sst	3.45
96591_at	Reelin	2.99
108899_at	Zic4	2.94
138483_at	Cad8	2.92
92515_at	Isl1 *	2.91
92271_at	Pax6 *	2.71
133116_at	Edil3	2.62
116989_at	Evi3	2.53
104169_at	Zic1 *	2.50
101420_at	Viatt	2.41
98330_at	Zic3 *	2.36
116403_at	Zic5	2.30
117269_at	Nef3	2.29
117291_at	GluR1	2.22
164128_at	Cnr1	2.11
92332_at	Dlx2 *	2.10
92930_at	Dlx5 *	2.04
94516_f_at	Penk1	2.03
103235_at	Npy	2.02

134006_at	Coup_TF2 *	1.79
92697_at	Foxa1/Hnf3*	1.64
102788_s_at	Pitx2 *	1.59
93615_at	Pbx3	1.56
92961_at	Lhx1	1.53
97988_at	Meis2 *	1.52
101192_at	Lhx5	1.47

B.

Affymetrix ID	Gene	Fold Change
100127_at	Crabp2	11.07
94200_at	Gbx2 *	9.97
99042_s_at	Shox2 *	5.47
106265_at	Mtsh1 *	5.32
92545_f_at	Ptgds	4.14
137034_f_at	Tpbg	3.61
134688_at	Foxp2	3.55
162651_at	Ldb2 *	3.49
113610_at	Tmod2	3.38
166833_at	Neurogranin	2.79
114774_at	Tcf712 *	2.57
98133_at	Calb1	2.56
106292_at	Bcl11a *	2.40
95036_at	Calb2	2.40
109653_at	Neurotensin	2.13
93669_f_at	Sox11 *	2.11
112175_at	Tox	2.08
94689_at	Rnpc2	2.08
135338_s_at	Ck2_alpha	2.03

101451_at	Peg3/Pw1	1.89
129880_s_at	bHLHb5	1.87
163242_at	Rbm9	1.82
110860_at	Copeb *	1.66
105625_at	Ssbp	1.65
93643_at	Lhx9 *	1.45

☐ transcription factors

Figure 4-2. List of genes differentially expressed in the LGN and MGN.

A. LGN-specific expression. Top table: Genes showing at least a 2-fold expression difference between LGN and MGN. Bottom table: Additional transcription factors that did not meet our 2-fold restriction but were included in analysis of cis-regulatory elements. Asterisks indicate transcription factors used for promoter analysis. B. MGN-specific expression. Same as in A.

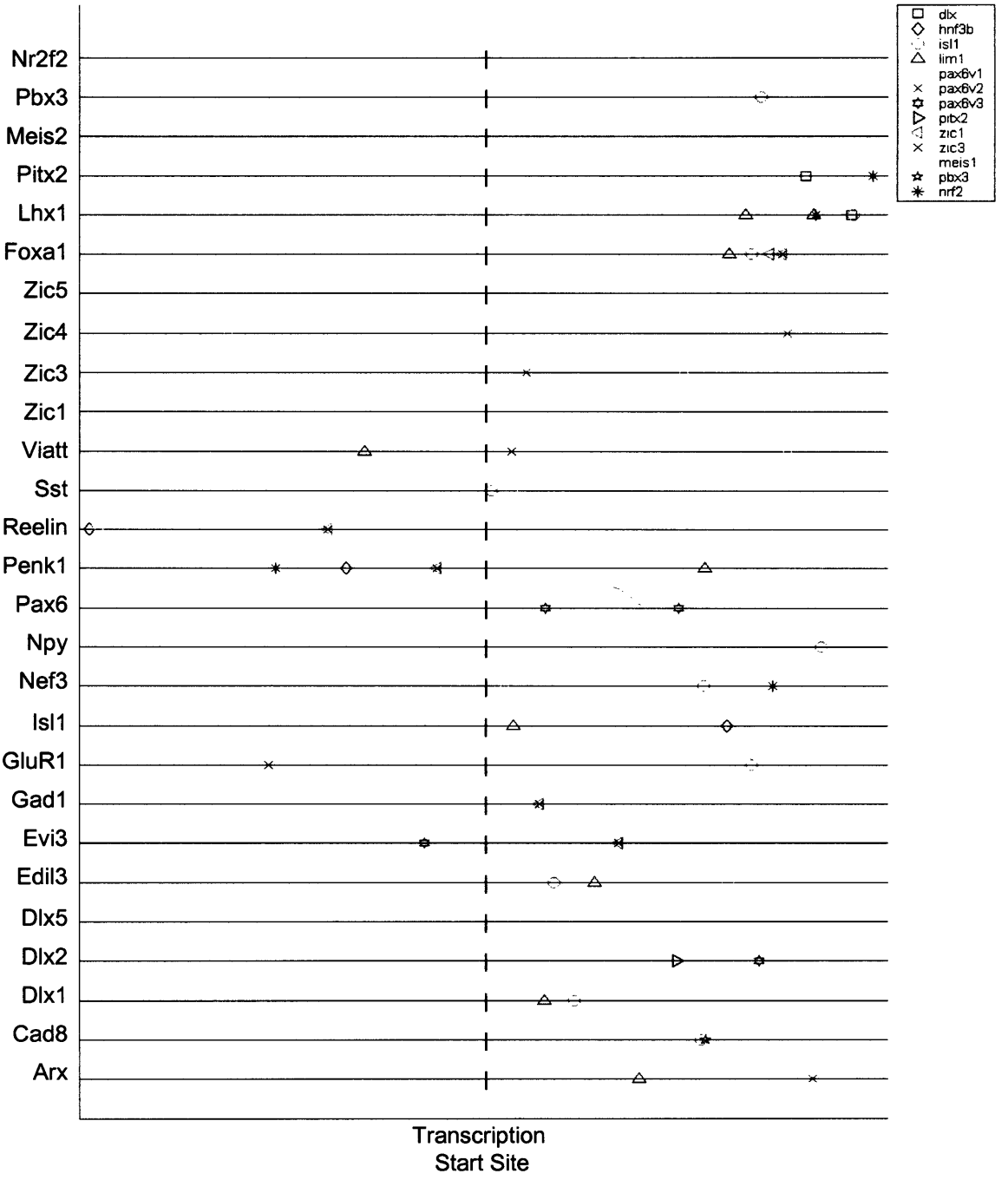

Figure 4-3. Potential binding sites for LGN-specific transcription factors

The complete list of genes showing 2-fold higher expression in the LGN compared to MGN (Y-axis). Schematic of the regulatory sequence 5,000 base pairs upstream and downstream of the putative transcription start site (X-axis). Colored shapes show the relative position of putative cis-regulatory elements for LGN-specific transcription factors. Inset – the list of transcription factors used in our algorithm.

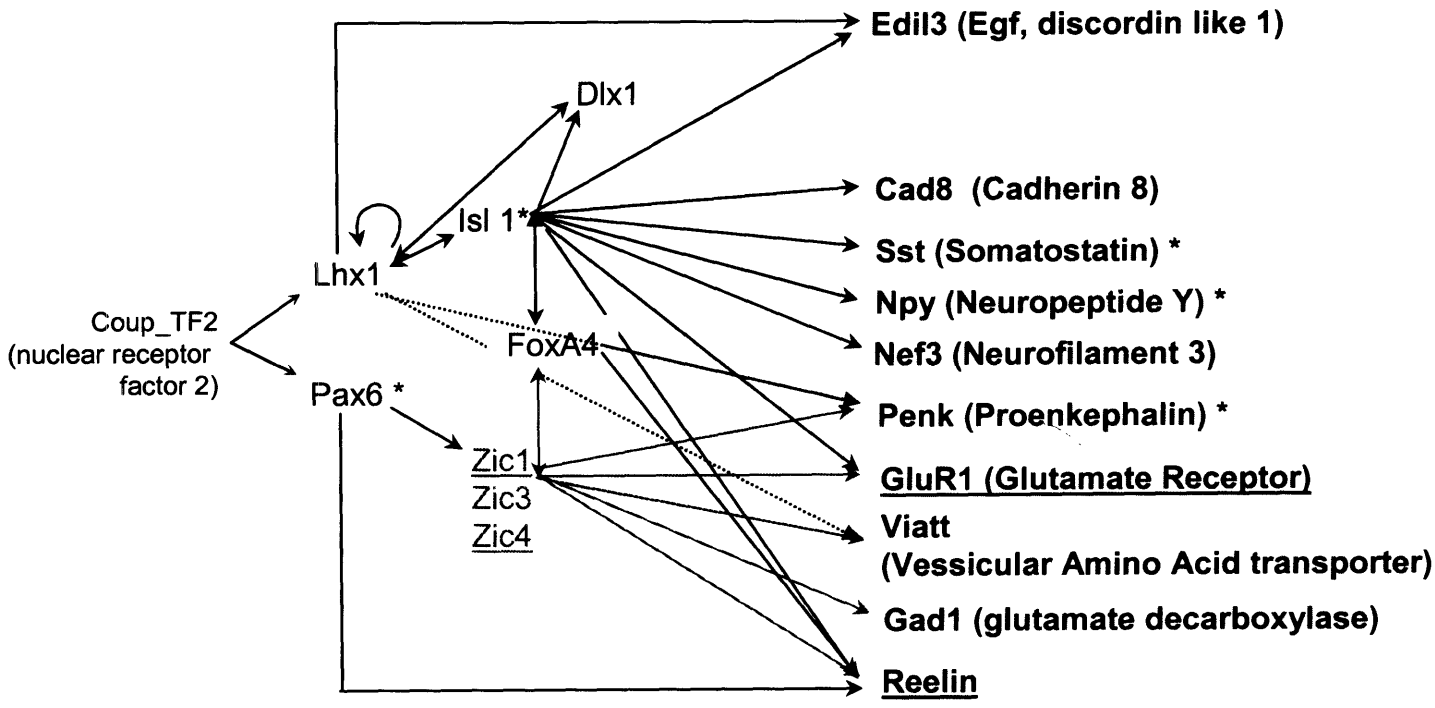

Figure 4-4. Potential network of transcriptional regulation.

The regulatory relationship between co-expressed genes in the LGN, as identified from Figure 4-2. Transcription Factors are labeled in Purple, Red, or Orange; Non-transcription factors are labeled in Green. Arrows mark potential regulation as indicated by the presence of a putative binding site in a gene's promoter sequence. Double arrows mark genes with putative reciprocal regulation. Regulatory interactions involving Arx, Evi3, Pitx2, and Dlx2 were excluded for simplicity.

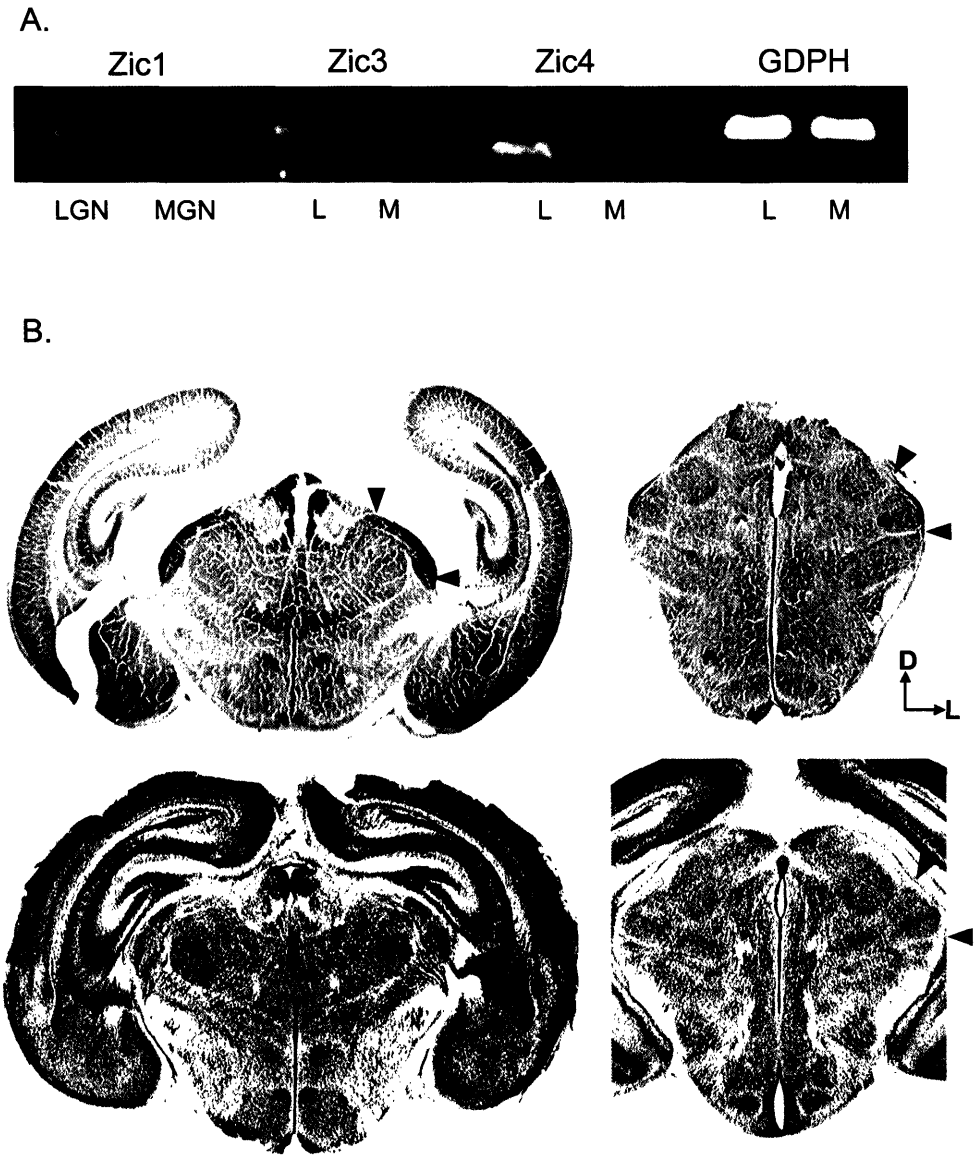

Figure 4-5. Confirmation of Zic mRNA expression in the LGN

A. RT-PCR using Zic1, Zic3, and Zic4 specific primers on RNA isolated from P0 LGN (L, left lane in all cases) or MGN (M, right lane in all cases). Gdph primers were used as a control to ensure equal RNA quantities. B. In situ hybridization of Zic4 mRNA antisense in 50um coronal sections through the P0 LGN (L) and MGN (M) detected with Alkaline-phosphatase coupled antibody to the Zic4 probe. Red arrows mark the approximate boundaries of the LGN and MGN. C Matched sections stained with cresyl violet.

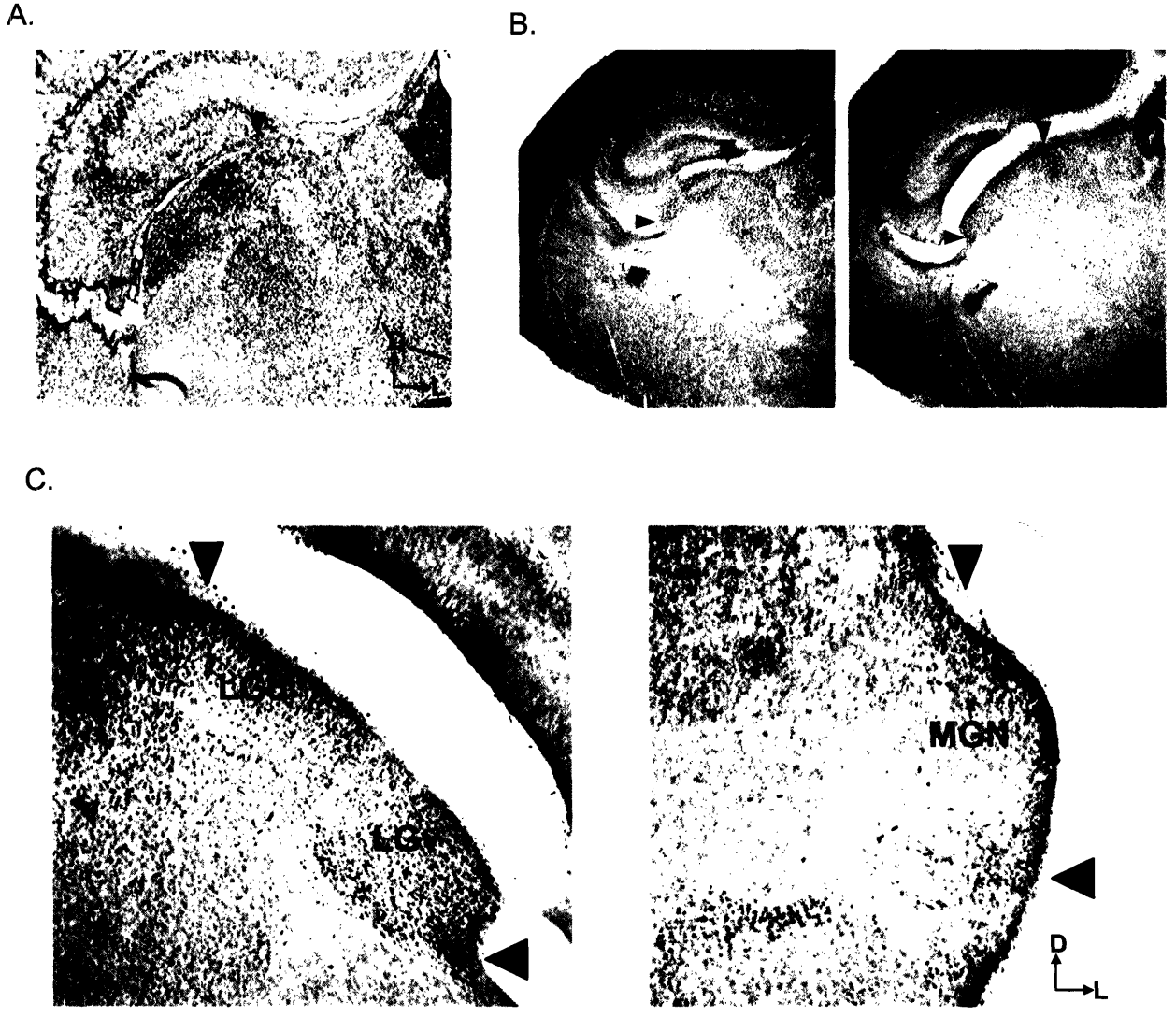

Figure 4-6. Confirmation of Zic mRNA andprotein expression in the LGN

A. In situ hybridization of Zic1 mRNA anti-sense. 50um coronal sections through the P0 LGN (L) detected with Alkaline-phosphatase coupled antibody to the Zic1 probe. B. Protein expression of Zic1 in two 50um sections through the LGN. Left, anterior; Right, posterior. Black arrows mark the approximate boundaries of the LGN. C. High magnification of LGN shown in B (right) and MGN.

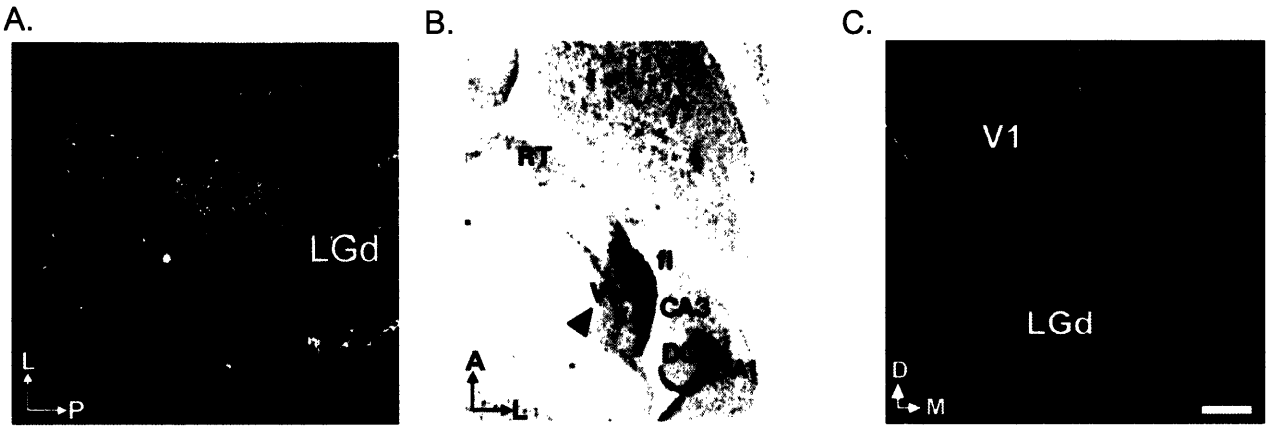

Figure 4-7. Expression of downstream Zic targets and related genes: GluR1, Reelin, and TenM3

A. GluR1 protein expression detected with an antibody to the GluR1 protein subunit. 40um horizontal section through p28 ferret thalamus. Blue line marks the approximate boundary of the LGN. B. In situ hybridization of Reelin mRNA [91]. C. *In situ* hybridization of Ten-M3 mRNA antisense. 50um coronal section through P0 LGN detected with TSA-amplification of a phosphatase-coupled antibody to the TenM3 probe.

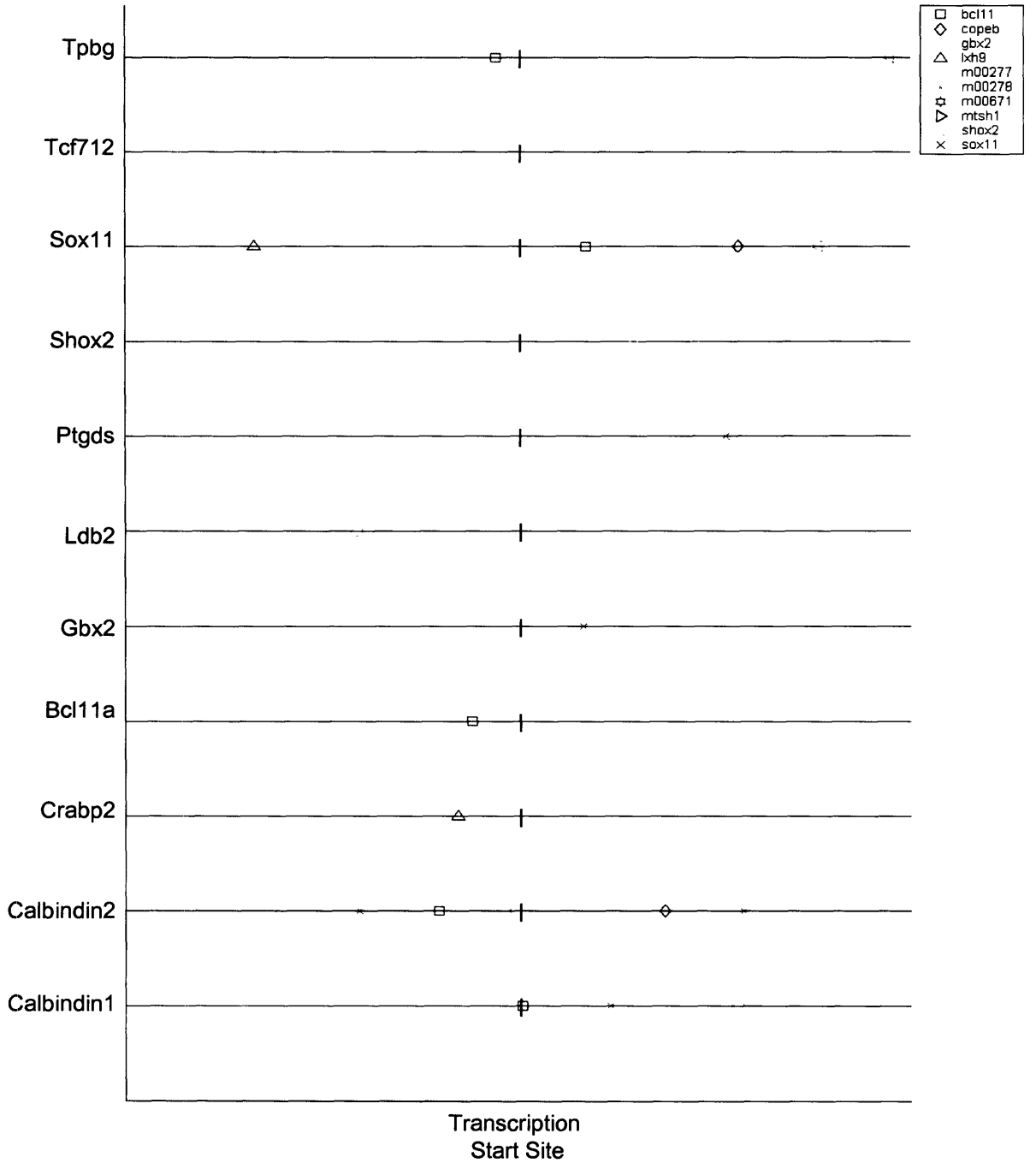

Figure 4-8. Potential binding sites for MGN-specific transcription factors

The complete list of genes showing 2-fold higher expression in the MGN compared to LGN (Y-axis). Schematic of the regulatory sequence 5,000 base pairs upstream and downstream of the putative transcription start site (X-axis). Colored shapes show the relative position of putative cis-regulatory elements for LGN-specific transcription factors. Inset – the list of transcription factors used in our algorithm. M00277, M00278 correspond to the matrices of putative binding sites for Lbd2. M00671 corresponds to the matrix of binding sites for Tcf712.

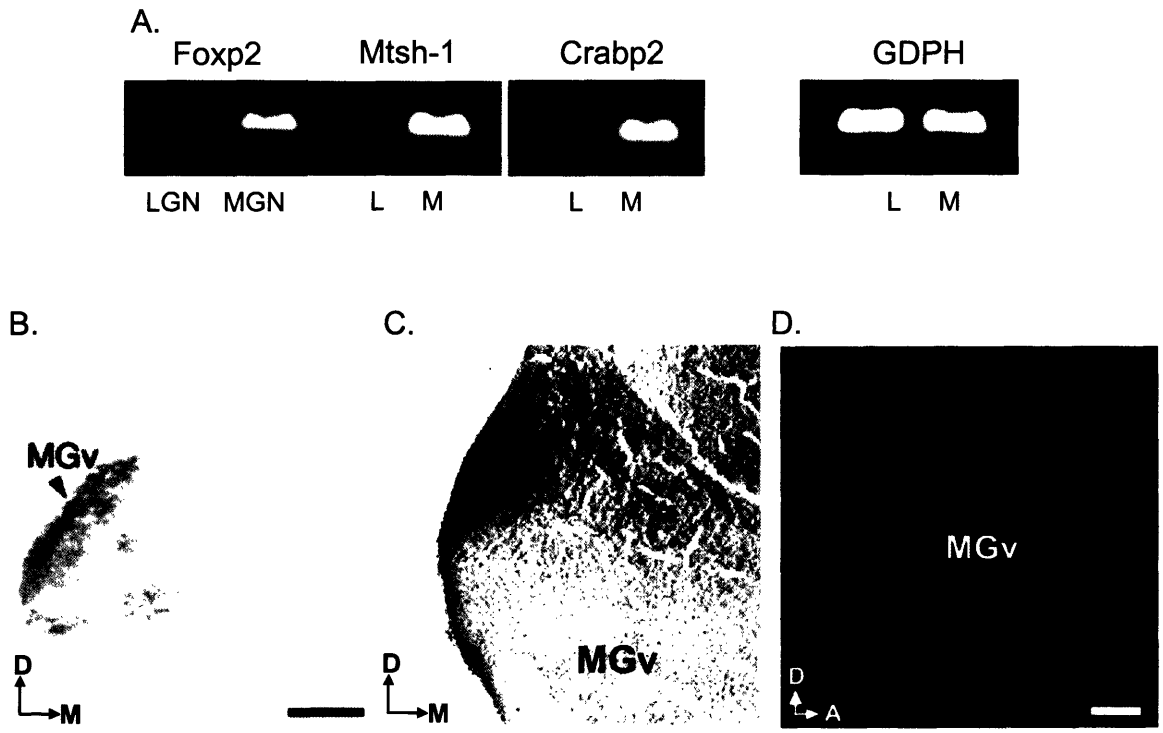

Figure 4-9. Confirmation of MGN-specific genes.

A. RT-PCR using FoxP2, Crabp2, Mtsh, or Tpbg specific primers on RNA isolated from P0 LGN (L, left lane in all cases) or MGN (M, right lane in all cases). Gdph primers were used as a control to ensure equal RNA quantities. B. In situ hybridization of FoxP2 mRNA antisense 50um coronal sections through the P0 MGN (M) detected with Alkaline-phosphatase coupled antibody to the FoxP2 probe. C. In situ hybridization of neurotensin mRNA antisense. 50um coronal sections through the P0 MGN (M) detected with TSA-amplification of a phosphatase-coupled antibody to the neurotensin probe.

Chapter 5: Molecular profile of the rewired MGN

Introduction

Schneider first described cross modal reorganization in the thalamus in hamsters [2]. In these experiments, he showed that deafferentation of ascending auditory input via ablation of the inferior colliculus along with ablation of the visual cortex, resulted in aberrant visual innervation of the MGN [2]. This cross modal reorganization was achieved as long as surgery was performed near birth. Since that time, similar surgeries in ferrets and mice were shown to induce the same novel retino-MGN projections [1,3]. While many papers have characterized the novel projections that result from deafferentation, as well as their influence on anatomical organization and behavior, few studies have asked what affect deafferentation has on the molecular profile of the MGN. Such changes will likely provide insight into how denervation induces the in-growth of novel retinal projections. Furthermore, they are a first step at determining whether sensory-specific profiles are coupled to the input they receive.

The lack of information about sensory-specific gene expression in the LGN and MGN during normal development hinders our understanding of such developmental plasticity. The data in chapter four provides us with the foundation by which to examine the effects of this cross modal reorganization. The analyses in chapter four highlighted the differences in the expression profiles of the LGN and MGN during development. They demonstrated the importance of transcription factors in establishing sensory-specific features of a nucleus, such as GluR1 expression. These features likely impact the way

that sensory information is organized and processed in a nucleus, including the afferent and efferent projections of that nucleus.

We compared the genetic expression profiles of the rewired P5 MGN to normal P0 LGN and MGN, using an Affymetrix cDNA microarray. Deafferentation of the MGN results in numerous changes in gene expression compared to normal MGN. We see an increase in the expression level of known genes implicated in neurite outgrowth, in addition to a down-regulation of extracellular matrix proteins. These changes may create an environment that promotes axon collateralization and in-growth into the deafferented MGN. Importantly, when we compared these results with those of chapter four, we find very little overlap in expression sets. More specifically, of those genes that differentiate normal MGN from LGN, few change in response to deafferentation. Thus, the molecular profile of a target is largely independent of the input it receives.

Methods

Animals. Surgeries were performed on wild-type 129/SvEv mice (Taconic, Germantown, NY) that were bred and maintained in our in-house colony (Division of Comparative Medicine, MIT). Live animal procedures were approved by the Committee on Animal Care at MIT and conformed to National Institutes of Health guidelines.

Rewiring MGN Tissue SvEv/129 mice were anesthetized one day after birth by deep hypothermia. We made bilateral superior and inferior colliculus lesions using high temperature microcautery. Pups were revived under a heat lamp and returned to their home cage. At P5, mice were sacraficed by deep hypothermia. Tissue was extracted from these animals and processed as described above. Seven to ten animals were used for each of two biological replicates. New tissue was extracted for RT-PCR. We also extracted the LGN of these 'rewired' mice for use in PCR.

RNA extraction and labeled cRNA synthesis and data analysis were the same as described in chapter 4.

Results

Bilateral ablations of the superior and inferior colliculus in P0 mice result in massive retinal input in the MGN (personal observation). We used this paradigm to induce the maximum amount of aberrant innervation. We extracted left and right MGN tissue 5 days after the rewiring surgeries. We confirmed that retinal input has reached the MGN by day 5 (data not shown). RNA was extracted from the tissue, processed, and analyzed on mU74-v2 chips. This process was repeated to create two biological replicates. The expression levels from normal P0 MGN and LGN, as described in chapter four, and rewired MGN were normalized using RMA analysis. Significant differences in expression were determined using Least Partial Error analysis.

Normal vs. Rewired MGN

Initially, we compared the gene expression profiles of rewired MGN and normal P0 MGN. As suspected, there are numerous genes whose expression profiles are changed as a result of deafferentation. Using the criteria outlined in Chapter 4, 80 genes were downregulated in response to deafferentation (Fig 5-1A), while 60 genes were upregulated in response to deafferentation (Fig 5-1B). A full list of genes that are significantly influenced by rewiring, and their expression levels, is included in Appendices C and D.

Surprisingly few genes were upregulated in response to deafferentation. An analysis of the results using GoTree Machine revealed an overrepresentation of genes involved in

cell/ ion homeostasis ($p<.05$), including sodium and calcium ion transport. An additional inspection of the data revealed a large number of genes known to promote neurite extension. Neurotrimin (HNT), for example, which promotes axon outgrowth and synaptogenesis, is upregulated in response to deafferentation [93]. Neurexin 3, which is implicated in the stabilization of synapses, is also upregulated. Additional genes were downregulated in response to deafferentation. An analysis of the downregulated probe sets showed an overrepresentation of genes located in the extracellular matrix. Interestingly, four genes implicated in the production of collagen (Col1a1and a2,Col5a2,and Col3a1) are downregulated in response to deafferentation. Nidogen-2, which is co-expressed with Type 5 collagen on basement membranes [94,95], is also significantly downregulated, as is reticulon 1, a homolog of Nogo. Previous research suggests that both of these genes create a nonpermissive environment for axonal growth [95, 96]. Additional extracellular matrix proteins are marked with asterisks in Appendix C.

Comparison of rewired MGN to normal LGN

The dramatic changes we see in the deafferented MGN are not surprising given the massive changes in input and reorganization resulting from the rewiring surgery. However, we wanted to know whether rewiring would specifically change the developmental genetic profile of the MGN, described above, to an LGN-like profile. We therefore compared the deafferented MGN to normal LGN. Specifically, we did a three-way comparison of genes: Normal P0 MGN, Normal P0 LGN, and Rewired P5 MGN. We identified genes that met three criteria; 1) they were significantly different between rewired MGN and normal MGN; 2) they were significantly different between normal

LGN and MGN; and 3) they were *not* significantly different between rewired MGN and normal LGN. In other words, we searched for genes whose expression level changed to resemble the LGN. This is a first step in asking whether sensory-specific genetic profiles are dependent on input.

Only one gene initially met the direct criteria outlined above. Two probe copies of the prostaglandin d-synthase were downregulated in response to deafferentation such that its expression was now similar to LGN levels (Fig. 5-2B, red). It is possible that the expression level of an LGN-specific gene may not require identical levels to create similar instructive effects. Therefore, we also looked for genes which met criteria (1) and (2) above, but whose expression was still significantly different than LGN. By using these criteria, we could also include both Crabp2 and Tpbg whose expression in rewired MGN falls between normal MGN and LGN (Fig. 5-2B, blue). It is worth noting that neurotrimin (Hnt), although it did not reach our two-fold criterion, has higher expression in LGN versus normal MGN. A 2-fold change in response to deafferentation makes its expression nearly indistinguishable from LGN (Fig. 5-2A, blue). Expression levels of these genes in normal LGN, MGN and rewired MGN can be found in Appendices C and D.

Discussion

The re-routing of retinal input into the deafferented MGN has been used as a paradigm to study the mechanisms and consequences of cross-modal reorganization in the thalamus. The efforts have focused on how input influences the organization and processing of a sensory pathway. We used a cDNA microarray comparison of rewired MGN to normal MGN and LGN to ask how the genetic expression profile of the MGN changes in response to deafferentation. Several gene expression levels change in response to rewiring. Importantly, rewiring upregulates the expression of genes previously implicated in axonal sprouting and neurite outgrowth. In addition, there is a downregulation of extracellular matrix proteins. However, our results demonstrate that important MGN-specific molecules do not change as a result of deafferentation. By comparing the genetic profiles of normal MGN and LGN with rewired MGN, it is clear that denervation does not make the MGN more "LGN-like". Together, these results support two conclusions. Importantly, they demonstrate that the gene expression pattern of the auditory thalamus is largely independent of the type of input it receives. This is important for examples of cross-modal plasticity, where sensory input is constrained by the molecular profile of the target. Additionally, they suggest that deafferentation does not specifically instruct visual axons to innervate the auditory thalamus. Instead, it creates an environment that is permissive for axon in-growth in general, and visual axons in particular.

Anomalous retinal input to the MGN

This comparison of normal to rewired MGN is an important first step in understanding the molecular changes that induce cross-modal reorganization. The earliest descriptions of sensory reorganization in the thalamus included a reduction of normal retinal targets, via an ablation of the superior colliculus and/or lateral geniculate nucleus. However, Angelucci et al demonstrated that deafferentation of the MGN alone was sufficient to induce this novel targeting. The amount of deafferentation correlated well with the extent of retino-MGN projections, suggesting that availability of target space was the critical factor. In fact, intact retinal pathways were *necessary* to generate a retino-MGN projection. The authors hypothesized that deafferentation of the MGN might trigger the release of a molecule or factor that would stimulate axonal collateralization from a primary axon. Such target-derived factors are integral for the development and arborization of normal axon projections systems. A wide variety of membrane-associated and soluble proteins direct growing axons toward their targets via growth-promoting and -inhibiting effects. Some of these interactions are likely cell type specific, promoting distinct homophilic (or heterophilic) interactions, as in the cadherins or the ephrins [97]. Others promote non-specific neurite growth. Visual axons are one of many sets attracted to the deafferented MGN, including ascending input from the trigeminal nucleus, as well as the spinal cord. Such non-specific innervation implies that any induced chemoattractant factor, if it were to exist, is likely to act in a non cell-type specific manner.

Our screen identifies candidates for such a target-derived factor. Neurotrimin expression, for example, increased greater than two-fold in response to deafferentation. This molecule belongs to a family of immunoglobulin cell adhesion molecules (IgCam),

which also includes opioid-binding cell adhesion molecule and limbic associated membrane protein (LAMP) [98]. These glycosylphosphatidylinositol (GPI)-anchored proteins are expressed in distinct neuronal systems during development. Previous work demonstrated that neurotrimin promotes neurite outgrowth. Of note, it has opposing effects on the outgrowth of sensory neurons and sympathetic neurons, promoting and inhibiting their outgrowth, respectively [93,99]. Angelucci et al noted the preferential targeting of sensory axons into the denervated MGN. Non-lemniscal axons from local nuclei, such as the substantia nigra, failed to innervate the MGN. Thus, neurotrimin is one candidate involved in the induction of retinal growth into the deafferented MGN.

Regeneration and extracellular matrix proteins

After CNS trauma, changes in the deposition of extracellular matrix proteins, as well as glial formation, prevent recovery and axonal regeneration. Extracellular matrix proteins, including collagen V, laminin, and nidogen form a barrier, the basement membrane, which inhibits axon growth [96,100]. Glial production of proteoglycans and Nogo are also specifically implicated in the failure of CNS axons to regenerate. Interestingly, many of the genes involved in axon regeneration were downregulated in response to rewiring. Deafferentation of the medial geniculate nucleus results in a dramatic decrease in ascending input which is likely to have a large effect on gene expression. The proximity of the surgery (superior and inferior colliculus) to the deafferented nucleus is also likely to impact gene expression. It is difficult to distinguish between those genes that promote axon in-growth into the MGN versus those that result from the physical trauma of lesion. However, it is known that changes in extracellular matrix proteins regulate levels of

plasticity in the developing and adult CNS. Dissolving the extracellular matrix proteins in the visual cortex, for example, upregulates spine motility and may allow for enhanced reorganization of input [101]. Thus, deafferentation may down-regulate those genes that interfere with axonal regeneration and thus create an environment permissive for axon in growth.

Plasticity as a function of time

In the last decade, cDNA microarrays have been used extensively to identify molecules involved in plasticity and reorganization after trauma, including expression changes as a result of epilepsy, spinal cord transection, and ischemia. Many of the genes identified in our screen are consistent with previous plasticity-inducing paradigms. For example, molecules implicated in homeostasis, particularly those that regulate ion transport, are consistently upregulated in these experiments. However, a subset of the genes we've identified shows an opposite profile. Neurotrimin, implicated in neurite outgrowth both in vivo and in vitro, and neurexin, implicated in synaptic plasticity, are significantly downregulated twelve hours after ischemia induction [96]. Our data show an upregulation of both neurotrimin and neurexin. In contrast, ischemia induction upregulates cellular retinol binding protein within twelve hours, and sciatic nerve injury increases mRNA levels of crpb1 and crabp2 [102]. In our paradigm, crbp1 and crabp2 were significantly downregulated. One interpretation of these findings is that the molecular determinants of plasticity vary greatly with time. In the experiments described above, RNA was extracted and analyzed within twelve hours of perturbation. It is possible that the immediate

molecular response may be to respond to changes in activity and/or to ensure cell survival, while genes that promote new in-growth of axons are upregulated later in time.

At this point in our analysis, however, it is also important to remember that levels of mRNA are affected both by the level of transcription and the level of translation. Confounding any genome-scale analysis of gene expression after trauma is a change in protein synthesis. The increased translation of essential genes will result in an artificially decreased level of mRNA and vice versa. By examining mRNAs bound to the ribosome after ischemia induction, MacManus et al demonstrated that total mRNA levels in a tissue is not necessarily a perfect indicator of essential genes [103]. Such translational modulation is still being explored, and its temporal profile is unknown. However, it is possible that five days post-perturbation is sufficient to reestablish the homeostatic balance between transcription and translation.

Hypothesis driven microarray analysis

Chapters 4 and 5 demonstrated two ways of using microarray results to provide information. In this second approach, we used microarray data to test our hypothesis that gene expression in the rewired MGN would come to resemble gene expression in the LGN. Such an approach takes advantage of high-throughput, large-scale data and asks not only about the action of an individual gene but how multiple genes are co-affected as a result of manipulation.

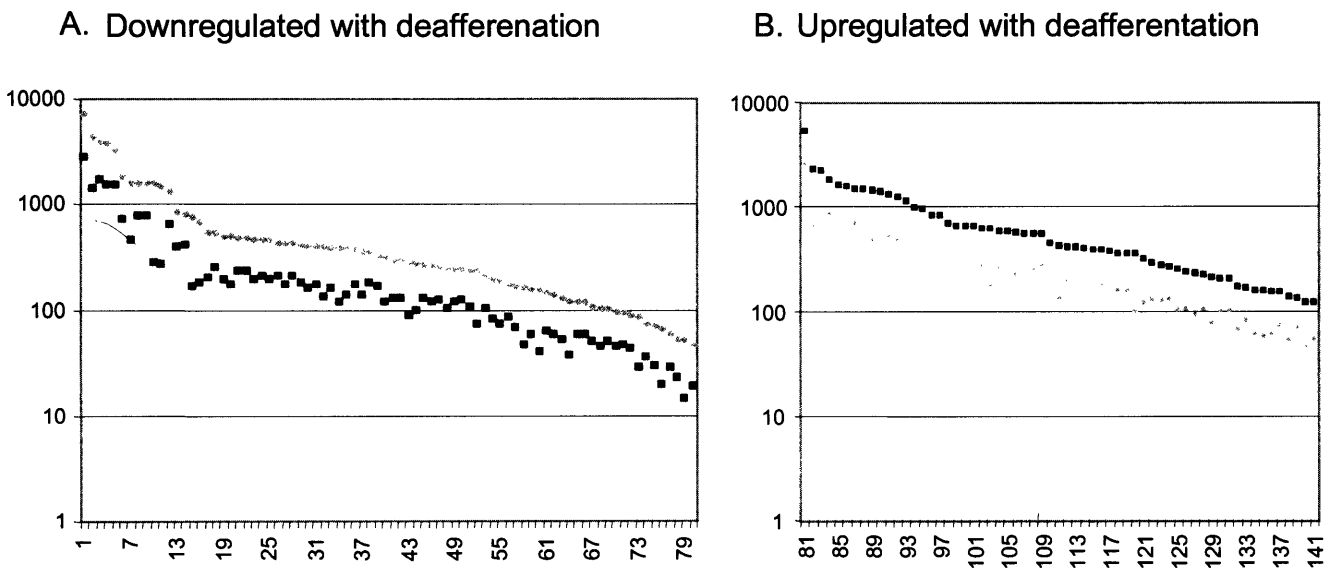

Figure 5-1. Genes expressed in the rewired MGN

A. Genes showing a significant 2-fold downregulation in response to rewiring. Red squares – expression level in normal MGN. Green diamonds – expression level in rewired MGN. Y axis – Logarithmic expression level. X-axis – List of genes, ordered from highest to lowest expression level in normal MGN. The corresponding names of these genes and their expression levels are listed in Appendix C. B. Genes showing a significant 2-fold upregulation in response to rewiring. Same as in A. Gene names and expressions levels are listed in Appendix D.

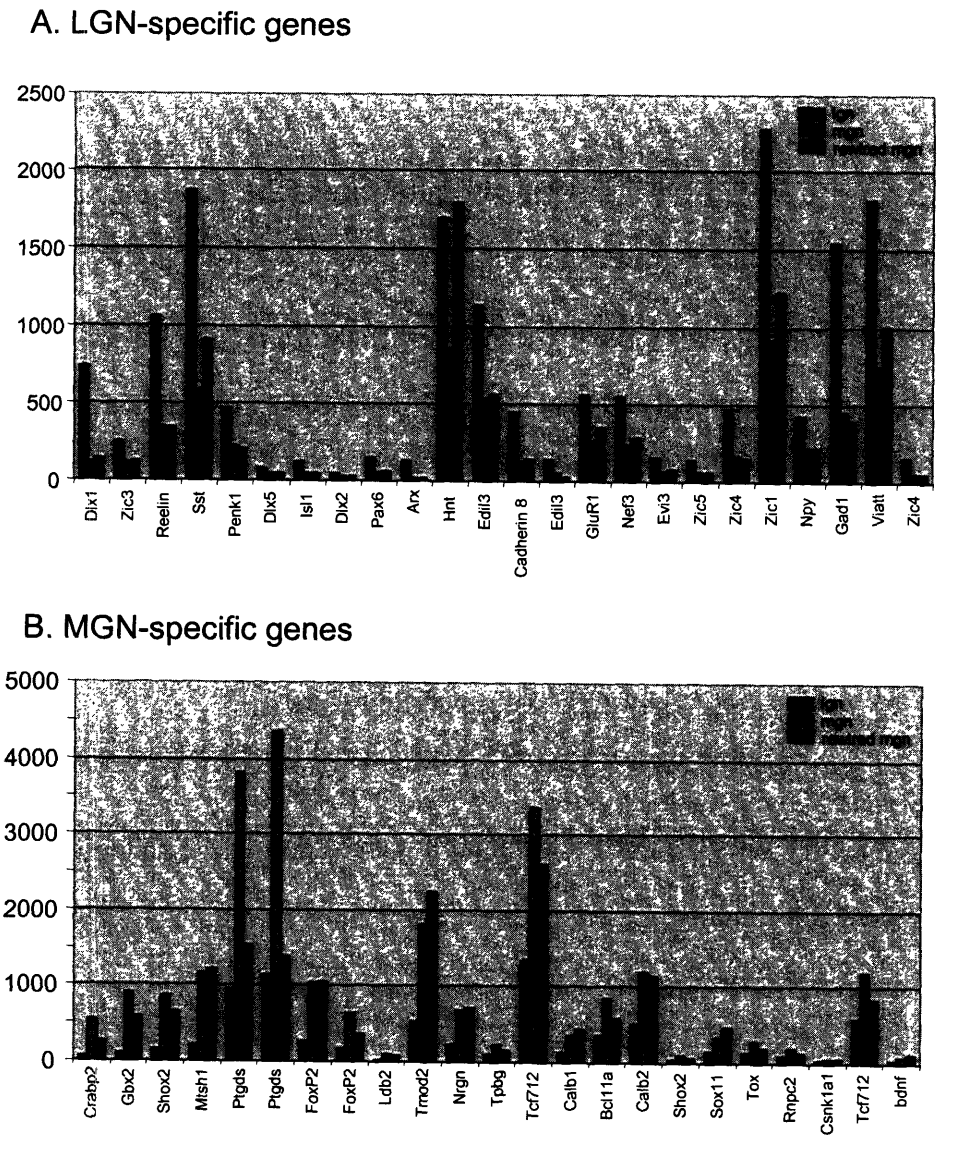

Figure 5-2. Changes in the MGN-specific gene profile in response to rewiring.

Average probe expression levels for the set of LGN or MGN -specific genes identified in Fig. 4-2, in normal LGN (blue), normal MGN (light green), and in rewired MGN (dark green). X-axis; genes identified in figure 4-2. Y-axis averaged probe intensity values as normalized by RMA. Red diamond indicates those genes whose expression profile are significantly different between MGN and rewired MGN, but similar between LGN and rewired MGN. Blue diamond indicate a similar expression change, but with less stringent criteria.

Chapter 6: Conclusions

In the introduction, I emphasized the remarkable plasticity of the developing brain. There are many examples in which extrinsic cues will determine the organization and functioning of a brain area. In our rewired animals, visual information is routed through the auditory pathway. This novel pathway is not only functional, but also remarkably similar to the normal visual pathway. We demonstrate, however, that cues intrinsic to a target, in this case the medial geniculate nucleus, will impact the way in which input is organized and interpreted. In addition, we begin to explore these sensory-specific cues and demonstrate that they do not change in response to rewiring.

Chapter 2 explored the role of the ephrin/Eph family of proteins in the patterning of novel retinal projections to the auditory pathway. In wild-type mice, ephrin is expressed in similar gradients in the LGN and MGN, while the retina expresses a graded Eph distribution. Retinal axons use ephrin/Eph interactions to guide normal retinotopic organization at multiple points along the visual pathway. Furthermore, this retinotopy is reflected in the patterning of eye-specific projections to visual nuclei. More specifically, ipsilateral axons with high receptor expression map to areas of the LGN with low ephrin expression. We show that this repulsive-mediated interaction also maps novel retinal projections in the MGN. Ipsilateral axons also avoid high ephrin expression in the MGN. Thus, we demonstrate that the molecular cues present in a target shape incoming axons, independent of modality. This may constrain the organization of cross-modal input. We

also show that the same cues can be used for multiple levels of patterning, including retinotopy and eye-specific patterning. The use of conserved guidance mechanisms in the visual, auditory, and somatosensory pathways highlights the evolutionary conservation of development and the commonality of sensory organization.

Chapter 3 explored the behavioral consequences of routing visual information through the auditory pathway. Fear-conditioned auditory and visual cues show distinct learning profiles in normal mice. Animals are able to associate an auditory cue paired with a noxious stimulus earlier in development than they are able to learn a visual cue association. Even in adult mice, it takes many more cue-shock pairings to associate a visual cue than an auditory. This may be due to differences between auditory and visual thalamic projections to the amygdala, with the MGN having a more direct route. We demonstrate that when visual information is routed through the MGN, its learning profile is similar to auditory stimuli. Rewired mice learn to associate a visual cue in fewer pairings than wild-type mice. This rapid association of the visual cue in rewired mice is accompanied by increased cFOS expression in the MGN and the amygdala after only a single day of training. In normal mice, visual stimuli do not induce cFOS expression in either the MGN or the amygdala, although cFOS is induced in the visual thalamus and cortex. These findings suggest that when input is routed to a novel target, the target may influence its processing. In our paradigm specifically, the influence may be due to differences in the efferent projection patterns of the visual and auditory thalamus.

The above experiments demonstrate the differences between the visual and auditory pathways and suggest that intrinsic molecular cues may have a role in the organization and processing of input. Chapter 4 begins to explore the differences in the molecular structure of the visual and auditory thalamus. Using a cDNA microarray, we identify multiple genes that are differentially expressed between the LGN and MGN in a P0 mouse. We find that the majority of these differentially expressed genes are transcription factors. By analyzing the promoter sequences of genes preferentially expressed in the LGN, we explore how these differential gene profiles develop. Specifically, we identified putative binding sites for LGN-specific transcription factors in co-regulated genes. We propose that there are two parallel streams of induction, one through Isl1 and a second through the Zic family of proteins. We demonstrate that four of the five Zic proteins are preferentially expressed in LGN, compared to the MGN and confirm this expression using in situ hybridization and immunohistochemistry. Furthermore, we show that putative downstream targets of the Zic family, including GluR1 and Reelin, are also preferentially expressed in the LGN. We also demonstrate enhanced expression for a subset of MGN-specific genes, many of which are responsive to retinoic acid. Thus, we identify novel genes that are preferentially expressed in either the visual or auditory pathway, and propose how transcription factors may cooperate to confer identity to a sensory nucleus. These cues intrinsic to thalamic nuclei, as demonstrated above, are likely to influence the organization and patterning of cross modal input.

Chapter 5 addressed how deafferentation of the MGN, which results in aberrant retinal innervation, influences the molecular structure of the MGN. Using a cDNA microarray,

we identified a set of genes that showed differential expression in the normal and deafferented MGN. Many of these genes are also altered in response to other plasticity inducing paradigms, including seizure induction and transection of the spinal cord. Multiple genes implicated in neurite outgrowth were upregulated in response to rewiring, including Neurotrimin. In addition, one eighth of the down-regulated genes were extracellular matrix proteins. This list included many collagen genes, as well as reticulon-1, a NOGO homolog. We propose that deafferentation creates an environment that is permissive for the in-growth of nearby axons in general, and visual axons in particular. Furthermore, we compared the expression profiles of the normal LGN to the normal and rewired MGN. Of those genes that differentiate LGN from MGN in normal development, few changed in response to rewiring to make the MGN appear more 'LGN-like'. Thus, molecular cues unique to the MGN are likely to guide the organization and processing of rewired visual input.

This thesis emphasizes the importance of intrinsic factors on the organization and function of visual input in the rewired MGN. However, rewiring clearly demonstrates the remarkable capabilities of the brain to reorganize in response to perturbations in activity. Retinal input is able to drive neurons in the MGN and their downstream targets, including the amygdala and A1. For the associations required for a cued-fear response, the amygdala is equally influenced by auditory drive (as in normal animals) and by visual drive (as in rewired animals). Thus, the capability of areas in the brain to use and functionally map novel input demonstrates the important interplay between intrinsic and extrinsic factors in the development of sensory projections and function.

The targets of sensory input do not act alone in shaping networks, for normal or novel projections. In rewired ferrets, the influence of visual activity on connections and behavior is apparent when structures downstream of the MGN develop under visual instruction. Visually driven activity patterns relayed to primary auditory cortex (A1) induce changes in network connections such that orientation selective cells and an orientation map arise in A1. Horizontal connections in A1 also come to resemble those in primary visual cortex. It is unlikely that molecular cues in A1 guide the development of these connections. Similarly, the behavioral role of A1 appears to be altered in these rewired ferrets: visual stimuli that activate the auditory pathway, including A1, are perceived as visual rather than as auditory. Common to the behavioral findings in rewired ferrets and in rewired mice is the observation that pathways and networks downstream of the MGN derive (visual) function from their inputs.

Pathways laid down during development are invariably specific and must rely on specific molecular matches between projection axons and their targets. In contrast, plasticity, particularly functional cross-modal plasticity, appears to start with molecules that are not uniquely specific to one target or source alone. Thus, while the LGN and MGN express unique molecules during normal development deafferenting the MGN regulates nonspecific molecules that attract retinal axons. These novel axons must in turn find specific cues that allow them to make orderly connections. For example, retinal axons need EphA receptors in order to recognize an ephrin gradient in the MGN. In these ways, plasticity requires that factors intrinsic to the MGN must work together with extrinsic

factors, including molecules on retinal axons as well as the activity these neurons provide, to enable cross modal rewiring and functional plasticity.

Appendix A: Transcription factor binding sites

1. LGN transcription factors

Gene ID	Binding sequence
Arx	Unavailable
Dlx1	Unavailable
Dlx2	CAC**TAATT**GAG
Dlx5	CAC**TAATT**GAG
Evi3	Unavailable
Foxa1; HNF3B	TRANSFAC
Isl1	G**CTAATG**G; **CTAATG**GTG
Lhx1	Unavailable
Lhx5	Unavailable
Pax6	TRANSFAC
Pitx2	TRANSFAC
Zic1	TRANSFAC
Zic3	TRANSFAC
Zic4	Unavailable
Zic5	Unavailable
Mrg1; Meis2	Matrix
Pbx3	Matrix
Nr2f2	TRANSFAC

2. MGN transcription factors

Gene ID	Binding Sequence
Bcl11a/Evi9/CTIP1	GGCCGGAGG
FoxP2	Matrix
Ldb2	Transfac
Lhx9	CGCT**A**AC**A**AGCCGC
Mtsh1	CATTGGAAAAATA; GTTCCGCCATTTAC
Shox2	TAATGGCATTA
Sox11	AAA**CAA**AGA
Tcf7 12/Tcf4E	Transfac
Tox	UNAVAILABLE
Gbx2	G**ATTAA**GACAATG; TCACTC**ATTAA**CC; TACAA**ATTAA**CTGG
Peg3/Pw1	UNAVAILABLE
bHLHb5	UNAVAILABLE
Copeb	CTC**CACCCA**; CC**CCACCCA**
Rbm9	UNAVAILABLE
Rnpc2	UNAVAILABLE
Ssbp2	UNAVAILABLE

Appendix B: Description of LGN-specific genes

Abbreviations	Gene Name	Function
Arx	Aristaless Related homeobox gene	Transcription Factor. Vertabrate homolog of aristaless - a pair rule gene. Expressed in NPY containing Gaba-ergic interneurons. Deficiency in Arx seems to inhibit migration of GABAergic interneurons, distinct from the actions of Dlx. Linked to mental retardation and epilepsy.
Cad8	Cadherin 8	Cell adhesion. Hypothesized to play roles in axon growth and synaptic targeting during development. Expression domain of Cad8 is restricted to rostral neocortex and anteroventral thalamic nucleus
Coup_tf2	Coup_TF2 (chicken ovalbumin upstream promoter transcription factor)	Nr2f2. Transcription factor. Orphan Nuclear receptor. Binds to and negatively regulates the activation function of thyroid hormone and retinoic acid thru the retinoid X receptor. Involved in neurogensis and axon growth.
Dlx1	Distal-less homeobox 1	Transcription Factor. Necessary for the migration of Gaba-ergic interneurons from the ganglionic eminence to the neocortex. Co-expressed with Pax6, MAsh1, Isl1, Lhx1, and Lhx5.
Dlx2	Distal-less homeobox 2	Transcription factor. See above
Dlx5	Distal-less homeobox 5	Transcription factor. See above
Edil3	EGF-like repeats & discordin I-like domains 3	Uncharacterized. Cell adhesion and development inferred from sequence. Discordin
Foxa1	Forkhead box A1	(HNF3alpha) Transcription Factor. Forkhead box. Potentially involved in the induction of floor plate by SHH. Also regulates multiple metabolic proteins
Gad1	Glutamate Decarboxylase	Neurotransmitter biosynthesis. Converts glutamic acid to the inhibitory neurotransmitter, GABA
GluR1	Glutamate Receptor subunit	Neurotransmitter receptor
Isl1	Islet 1	Transcription Factor. LIM homeodomain. Expressed in ventral neural tube, and ventral diencephalic and telecephalic neurons. Potentially induced by SHH.
Lhx1/Lim1	LIM homeobox protein 1	Transcription Factor. LIM-homeodomain. Co-expressed with Isl1 and Pax6 in the differentiating neurons.
Lhx5/Lim5	LIM homeobox protein 5	Transcription Factor. See above
Meis2	Myeloid ecotropic viral integration site-related gene 1	Transcription Factor. Co-factor that binds to and enhances specificity of hox genes regulation. May stabilize Pbx proteins to regulate hindbrain patterning.
Nef3	Neurofilament 3	Intermediate filament protein. Neurofilament proteins define regional patterns of cortical organization in primate visual system. Distribution matches extent of axonal projections in visual pathways
Npy	Neuropeptide Y	Neuropeptide. Mediator of neuronal excitability and synaptic transmission. Expressed in Gaba-ergic interneurons, largely non-overlapping with Sst
Pax6	Paired box gene 6	Transcription factor. Paired-box. High rostrolateral to low caudomedial gradient in the forebrain.Mutation results in a caudalization of neocortical areas.
Pbx3	Pre B-cell leukemia transcription factor 3	Transcription factor. Co-factor that binds to and enhances specificity of hox genes regulation. Functions with Meis2 proteins to regulate hindbrain patterning.
Penk1	Proenkephalin	Neuromodulator. Expressed in GABAergic interneurons in the neostriatum and LGv. Expression regulated through NMDA and GABA receptors.
Pitx2	Paired-like homeodomain transcription factor 2	Transcription factor. Bicoid-related homeodomain. Activated and stabalized by the Wnt/Dvl/beta-catenin pathway. Involved in cell-type-specific proliferation and left/right axis patterning.
Reelin	Reelin	Cell adhesion. Secreted by nerouns into extracellular space to provide an architectonic signal. *reeler* mutations fail to recognize location and orientation during migration.
Sst	Somatostatin	Neuropeptide. Mediator of neuronal excitability and synaptic transmission. Expressed in Gaba-ergic interneurons, largely non-overlapping with Npy
Viatt	Vesicular Inhibiotory Amino Acid Transporter	Vesicular neurotransmitter transporter. Takes up and packages inhibitory amino acids including glycine and GABA into synaptic vesicles at nerve endings. ATP-dependent
Zfp521	Zinc finger protein 521	Transcription factor. Zinc finger protein. Uncharacterized.
Zic1	Zinc Finger of the Cerebellum 1	Transcription Factor. Vertebrate homolog of odd-paired, a pair-rule gene. Involved in neurogenesis, neural crest development, cerebellar patterning, and left-right axis. May bridge indicution signals and bhelix loop helix transcriptional regulators.
Zic3	Zinc Finger of the Cerebellum 3	Transcription Factor. See above. Human mutation of Zic3 results in holoprosencephaly.
Zic4	Zinc Finger of the Cerebellum 4	Transcription Factor. See above
Zic5	Zinc Finger of the Cerebellum 5	Transcription Factor. See above

Appendix C: Genes down regulated with deafferentation

	Affymetrix	GENE	MGN	RW MGN	Fold Change	LGN
1	98623_g_at	Igf2	7167.78	2778.21	2.58	
2	**92546_r_at**	**Ptgds**	**4355.78**	**1389.67**	**3.13**	**1134.95**
3	167869_f_a	Rtn1	3904.11	1737.82	2.25	
4	**92545_f_at**	**Ptgds**	**3796.65**	**1524.08**	**2.49**	**954.26**
5	130532_at	Riken	3178.82	1506.35	2.11	
6	167615_s_a	Riken	1830.39	715.23	2.5 n	
7	100600_at	Cd24a	1610.25	465.23	3.46	
8	168186_f_a	Riken	1608.06	781.69	2.06	
9	129203_at	Idb4	1582.61	776.30	2.04	
10	**93028_at**	**H19**	**1562.86**	**284.62**	**5.49**	**891.43**
11	135314_at	Unknown	1479.58	267.67	5.53	
12	165624_i_a	Nol4	1314.03	650.42	2.02	
13	98627_at	Igfbp2	821.53	397.68	2.07	
14	165601_f_a	Slc13a4	814.71	402.32	2.03	
15	166160_f_a	Cpne8	750.85	167.71	4.48	
*** 16	101130_at	Col1a2	662.40	177.91	3.72	
*** 17	94305_at	Col1a1	541.47	200.21	2.70	
18	**100127_at**	**Crabp2**	**536.45**	**252.96**	**2.12**	**47.72**
19	134797_at	Riken	492.32	194.66	2.53	
20	166084_f_a	Plagl1	485.62	175.56	2.77	
21	99010_at	Islr	470.50	234.62	2.01	
*** 22	100928_at	Fbln2	469.53	234.15	2.01	
23	101069_g_a	Mkrn1	460.20	196.13	2.35	
24	111759_at	Riken	460.17	206.14	2.23	
25	129147_r_a	Igsf9	451.95	190.80	2.37	
26	**101975_at**	**Dlk1**	**433.13**	**211.41**	**2.05**	**273.94**
27	95471_at	Cdkn1c	422.13	170.90 --	2.47	
28	97960_at	Usp22	420.81	204.77	2.06	
*** 29	8549_at	Vtn	405.33	177.37	2.29	
30	111455_at	Xtrp3s1	396.36	159.40	2.49	
31	102259_at	Ywhag	395.59	171.42	2.31	
32	**137034_f_a**	**Tpbg**	**387.11**	**130.49**	**2.97**	**101.92**
33	93534_at	Dcn	385.11	159.65	2.41	
*** 34	105100_at	Adam22	383.92	118.20	3.25	
35	104249_g_a	Ssr3	373.44	139.82	2.67	
36	100927_at	Pltp	366.95	171.55	2.14	
37	138986_at	Centuar	358.41	139.26	2.57	
38	113932_g_a	EST	356.20	179.08	1.99	
39	112722_at	D6Ertd2	327.86	164.44	1.99	
40	**104716_at**	**Rbp1**	**315.19**	**120.55**	**2.61**	**201.74**
41	166683_r_a	Est	294.81	128.73	2.29	
42	138988_at	Centuar	287.77	126.92	2.27	
43	168282_r_a	Son	276.57	87.48	3.16	
44	162689_at	Rbm9	271.71	99.86	2.72	
45	137065_at	Innp5f	263.55	125.75	2.10	
46	93918_at	Taf9	256.89	118.33	2.17	
47	165464_r_a	Riken	253.36	121.81	2.08	
48	166513_at	Riken	245.32	102.07	2.40	
49	104486_at	A2m	244.77	116.65	2.10	
50	113047_at	Pdzrn3	244.66	120.74	2.03	
51	96011_at	Matr3	234.91	107.63	2.18	
52	138993_r_a	Gtl2	231.45	72.33	3.20	
*** 53	92567_at	Col5a2	208.90	103.32	2.02	
54	165706_r_a	Tdrd3	195.67	80.77	2.42	
55	167342_r_a	Riken	187.83	71.51	2.63	
56	95466_at	Cotl1	171.88	82.87	2.07	
57	133130_at	Scn3b	168.09	66.73	2.52	
58	113431_at	Rnf14	160.74	45.86	3.51	
59	166370_at	Scamp1	153.82	57.36	2.68	
60	135720_at	Riken	153.73	40.39	3.81	
61	109529_at	Riken	143.20	62.61	2.29	
62	133906_at	Est	138.70	58.46	2.37	
63	**97560_at**	**Psap**	**129.24**	**50.92**	**2.54**	**85.70**
64	168379_i_a	Colec12	119.80	37.39	3.20	
65	93212_at	AW74231	118.97	58.36	2.04	
66	166262_f_a	Gpc2	117.43	58.68	2.00	
67	139980_g_a	Ndufs1	106.17	50.28	2.11	
*** 68	92593_at	Postn	102.87	45.25	2.27	
69	168147_s_a	Dcamkl1	101.01	49.21	2.05	
70	167886_f_a	Rnf138	93.84	43.84	2.14	
71	93164_at	Rnf2	92.80	45.51	2.04	
72	166897_at	Riken	88.12	43.46	2.03	
73	131756_at	Xtrp3s1	83.02	28.05	2.96	
74	165785_f_a	Porcn	73.36	35.52	2.07	
75	168297_f_a	Riken	68.70	29.48	2.33	
76	140565_f_a	Unknown	65.57	19.83	3.31	
*** 77	102990_at	Col3a1	58.54	28.68	2.04	
*** 78	93563_s_at	Nid2	51.37	22.84	2.25	
79	133559_at	Rnpc2	50.94	14.68	2.47	
80	129302_at	Calm	46.16	18.76	2.46	

Appendix D: Genes upregulated with deafferentation

	Affymetrix	GENE	MGN	RW MGN	Fold Change LGN	
♦81	95356_at	Apoe	2557.81	5336.61	2.09	
82	99057_at	Thy1	650.48	2280.47	3.51	
83	140546_at	Gfap	777.13	2209.49	2.84	
♦84	**163670_f_at**	**Hnt**	**851.48**	**1798.79**	**2.11**	**1699.40**
85	101578_f_at	Actb	599.76	1623.16	2.71	
86	162658_at	Riken	650.22	1548.26	2.38	
87	93573_at	Mt1	700.32	1458.33	2.08	
88	101887_at	Agt	493.70	1449.77	2.94	
89	95705_s_at	Actb	475.57	1417.25	2.98	
♦90	105808_at	Nrxn3	634.83	1367.51	2.15	
91	105895_at	Camk2d	520.23	1307.19	2.51	
92	166999_at	Riken	473.21	1231.39	2.60	
93	166472_i_at	Kif21	447.25	1143.64	2.56	
94	102704_at	Aqp4	371.61	984.80	2.65	
95	106477_at	Riken	420.64	961.77	2.29	
96	**105725_at**	**C230027C17**	**323.10**	**822.64**	**2.55**	**753.88**
97	95092_at	Ppp3ca	406.18	818.87	2.02	
98	169012_s_at	Camk2d	276.53	686.84	2.48	
99	100959_at	S100a13	303.57	652.79	2.15	
100	117118_at	Sfxn5	209.60	650.53	3.10	
101	113537_at	Riken	242.62	646.69	2.67	
102	101216_at	Unknown	275.29	613.18	2.23	
103	113013_s_at	Slc4a4	177.02	607.98	3.43	
104	102703_s_at	Aqp4	258.87	575.61	2.22	
105	161121_f_at	S100a13	260.55	571.85	2.19	
106	92378_at	Ptprz1	224.78	556.58	2.48	
107	**96055_at**	**Cck**	**210.65**	**547.35**	**2.60**	**386.46**
108	163510_at	Basp1	241.86	545.85	2.26	
109	112898_at	Klf7	268.59	544.68	2.03	
110	94464_at	Clcn3	209.12	449.80	2.15	
111	168478_s_at	Riken	132.85	420.46	3.16	
112	98782_at	Cplx2	190.21	415.18	2.18	
113	161436_s_at	Adarb1	166.80	403.88	2.42	
114	116919_f_at	Riken	188.61	400.57	2.12	
115	102305_at	Gpr37l1	186.05	389.98	2.10	
116	139207_s_at	Riken	176.94	383.81	2.17	
117	117080_at	Ubxd4	191.33	379.55	1.98	
♦118	116425_at	Ntrk2	157.72	357.69	2.27	
119	111716_at	Arhgef12	155.04	352.40	2.27	
120	164262_at	Ror-A	98.82	350.73	3.55	
121	112493_at	D1Ertd471e	118.57	318.75	2.69	
122	93964_s_at	Ddx6	127.40	288.35	2.26	
123	117013_at	Unknown	123.32	272.21	2.21	
124	95944_at	Dhx36	126.19	261.16	2.07	
125	110372_at	D11Bwg0414	102.21	252.91	2.47	
126	116905_at	Riken	105.27	238.04	2.26	
127	115779_at	AI853548	89.14	226.72	2.54	
128	113319_at	Rbm5	105.58	219.29	2.08	
129	95453_f_at	S100a1	76.63	212.25	2.77	
130	161610_at	Unknown	99.71	206.26	2.07	
131	116883_at	Kcnj10	101.74	205.82	2.02	
132	101923_at	Pla2g7	68.08	171.75	2.52	
133	110994_at	AI316882	81.31	168.02	2.07	
134	163286_at	Bcas1	60.13	157.76	2.62	
135	114563_at	Riken	57.39	156.73	2.73	
136	135364_at	Riken	60.20	153.96	2.56	
137	102712_at	Saa3	71.42	153.63	2.15	
138	110850_f_at	Slc14a1	51.58	137.25	2.66	
139	113792_at	Klf12	66.65	133.49	2.00	
140	105257_at	AI842293	45.09	122.40	2.71	
141	103550_at	Ednrb	54.19	119.52	2.21	
142	107385_at	Lix1	58.23	115.43	1.98	
143	96311_at	Mbp	41.51	108.40	2.61	
144	102726_at	Tac1	43.80	96.81	2.21	
145	163548_at	Pik3r1	40.83	84.95	2.08	
146	163364_at	Riken	30.57	71.91	2.35	
147	163931_at	Pkn2	29.07	71.75	2.47	
148	161270_i_at	Prkwnk1	26.77	65.49	2.45	

References

1. Lyckman, A. W. et al. Enhanced plasticity of retinothalamic projections in an ephrin-A2/A5 double mutant. *J Neurosci* **21**, 7684-90 (2001).
2. Schneider, G. E. Early lesions of superior colliculus: factors affecting the formation of abnormal retinal projections. *Brain Behav Evol* **8**, 73-109 (1973).
3. Sur, M., Garraghty, P. E. & Roe, A. W. Experimentally induced visual projections into auditory thalamus and cortex. *Science* **242**, 1437-41 (1988).
4. Pallas, S. L., Roe, A. W. & Sur, M. Visual projections induced into the auditory pathway of ferrets. I. Novel inputs to primary auditory cortex (AI) from the LP/pulvinar complex and the topography of the MGN-AI projection. *J Comp Neurol* **298**, 50-68 (1990).
5. Angelucci, A., Clasca, F., Bricolo, E., Cramer, K. S. & Sur, M. Experimentally induced retinal projections to the ferret auditory thalamus: development of clustered eye-specific patterns in a novel target. *J Neurosci* **17**, 2040-55 (1997).
6. Angelucci, A., Clasca, F. & Sur, M. Brainstem inputs to the ferret medial geniculate nucleus and the effect of early deafferentation on novel retinal projections to the auditory thalamus. *J Comp Neurol* **400**, 417-39 (1998).
7. Roe, A. W., Pallas, S. L., Hahm, J. O. & Sur, M. A map of visual space induced in primary auditory cortex. *Science* **250**, 818-20 (1990).
8. Sharma, J., Angelucci, A. & Sur, M. Induction of visual orientation modules in auditory cortex. *Nature* **404**, 841-7 (2000).
9. Feldheim, D. A. et al. Topographic guidance labels in a sensory projection to the forebrain. *Neuron* **21**, 1303-13 (1998).
10. Cheng, H. J., Nakamoto, M., Bergemann, A. D. & Flanagan, J. G. Complementary gradients in expression and binding of ELF-1 and Mek4 in development of the topographic retinotectal projection map. *Cell* **82**, 371-81 (1995).
11. Cheng, H. J. & Flanagan, J. G. Identification and cloning of ELF-1, a developmentally expressed ligand for the Mek4 and Sek receptor tyrosine kinases. *Cell* **79**, 157-68 (1994).
12. Drescher, U. et al. In vitro guidance of retinal ganglion cell axons by RAGS, a 25 kDa tectal protein related to ligands for Eph receptor tyrosine kinases. *Cell* **82**, 359-70 (1995).
13. Monschau, B. et al. Shared and distinct functions of RAGS and ELF-1 in guiding retinal axons. *Embo J* **16**, 1258-67 (1997).
14. Yates, P. A., Roskies, A. L., McLaughlin, T. & O'Leary, D. D. Topographic-specific axon branching controlled by ephrin-As is the critical event in retinotectal map development. *J Neurosci* **21**, 8548-63 (2001).
15. Feldheim, D. A. et al. Genetic analysis of ephrin-A2 and ephrin-A5 shows their requirement in multiple aspects of retinocollicular mapping. *Neuron* **25**, 563-74 (2000).
16. Frisen, J. et al. Ephrin-A5 (AL-1/RAGS) is essential for proper retinal axon guidance and topographic mapping in the mammalian visual system. *Neuron* **20**, 235-43 (1998).
17. Vanderhaeghen, P. et al. A mapping label required for normal scale of body representation in the cortex. *Nat Neurosci* **3**, 358-65 (2000).
18. Green, P. D. et al. Antagonistic regulation of Dlx2 expression by PITX2 and Msx2: implications for tooth development. *Gene Expr* **9**, 265-81 (2001).
19. Frost, D. O. Orderly anomalous retinal projections to the medial geniculate, ventrobasal, and lateral posterior nuclei of the hamster. *J Comp Neurol* **203**, 227-56 (1981).

20. Prakash, N. et al. Malformation of the functional organization of somatosensory cortex in adult ephrin-A5 knock-out mice revealed by in vivo functional imaging. *J Neurosci* **20**, 5841-7 (2000).
21. Frost, D. O. Anomalous visual connections to somatosensory and auditory systems following brain lesions in early life. *Brain Res* **255**, 627-35 (1982).
22. Pickles, J. O., Claxton, C. & Van Heumen, W. R. Complementary and layered expression of Ephs and ephrins in developing mouse inner ear. *J Comp Neurol* **449**, 207-16 (2002).
23. Pickles, J. O. Expression of Ephs and ephrins in developing mouse inner ear. *Hear Res* **178**, 44-51 (2003).
24. Yun, M. E., Johnson, R. R., Antic, A. & Donoghue, M. J. EphA family gene expression in the developing mouse neocortex: regional patterns reveal intrinsic programs and extrinsic influence. *J Comp Neurol* **456**, 203-16 (2003).
25. Huberman, A. D., Stellwagen, D. & Chapman, B. Decoupling eye-specific segregation from lamination in the lateral geniculate nucleus. *J Neurosci* **22**, 9419-29 (2002).
26. Muir-Robinson, G., Hwang, B. J. & Feller, M. B. Retinogeniculate axons undergo eye-specific segregation in the absence of eye-specific layers. *J Neurosci* **22**, 5259-64 (2002).
27. von Melchner, L., Pallas, S. L. & Sur, M. Visual behaviour mediated by retinal projections directed to the auditory pathway. *Nature* **404**, 871-6 (2000).
28. LeDoux, J. E. Emotion circuits in the brain. *Annu Rev Neurosci* **23**, 155-84 (2000).
29. LeDoux, J. E., Cicchetti, P., Xagoraris, A. & Romanski, L. M. The lateral amygdaloid nucleus: sensory interface of the amygdala in fear conditioning. *J Neurosci* **10**, 1062-9 (1990).
30. Clugnet, M. C. & LeDoux, J. E. Synaptic plasticity in fear conditioning circuits: induction of LTP in the lateral nucleus of the amygdala by stimulation of the medial geniculate body. *J Neurosci* **10**, 2818-24 (1990).
31. Shi, C. & Davis, M. Pain pathways involved in fear conditioning measured with fear-potentiated startle: lesion studies. *J Neurosci* **19**, 420-30 (1999).
32. LeDoux, J. E., Ruggiero, D. A. & Reis, D. J. Projections to the subcortical forebrain from anatomically defined regions of the medial geniculate body in the rat. *J Comp Neurol* **242**, 182-213 (1985).
33. LeDoux, J. E., Sakaguchi, A. & Reis, D. J. Subcortical efferent projections of the medial geniculate nucleus mediate emotional responses conditioned to acoustic stimuli. *J Neurosci* **4**, 683-98 (1984).
34. Doron, N. N. & Ledoux, J. E. Organization of projections to the lateral amygdala from auditory and visual areas of the thalamus in the rat. *J Comp Neurol* **412**, 383-409 (1999).
35. Romanski, L. M. & LeDoux, J. E. Equipotentiality of thalamo-amygdala and thalamo-cortico-amygdala circuits in auditory fear conditioning. *J Neurosci* **12**, 4501-9 (1992).
36. Shi, C. & Davis, M. Visual pathways involved in fear conditioning measured with fear-potentiated startle: behavioral and anatomic studies. *J Neurosci* **21**, 9844-55 (2001).
37. Morris, J. S., Ohman, A. & Dolan, R. J. A subcortical pathway to the right amygdala mediating "unseen" fear. *Proc Natl Acad Sci U S A* **96**, 1680-5 (1999).
38. Campbell, B. A. & Ampuero, M. X. Dissociation of autonomic and behavioral components of conditioned fear during development in the rat. *Behav Neurosci* **99**, 1089-102 (1985).

39. Heldt, S., Sundin, V., Willott, J. F. & Falls, W. A. Posttraining lesions of the amygdala interfere with fear-potentiated startle to both visual and auditory conditioned stimuli in C57BL/6J mice. *Behav Neurosci* **114**, 749-59 (2000).
40. Jones, E. G. Thalamic organization and function after Cajal. *Prog Brain Res* **136**, 333-57 (2002).
41. Steriade, M. Synchronized activities of coupled oscillators in the cerebral cortex and thalamus at different levels of vigilance. *Cereb Cortex* **7**, 583-604 (1997).
42. Altman, J. & Bayer, S. A. Development of the rat thalamus: VI. The posterior lobule of the thalamic neuroepithelium and the time and site of origin and settling pattern of neurons of the lateral geniculate and lateral posterior nuclei. *J Comp Neurol* **284**, 581-601 (1989).
43. Altman, J. & Bayer, S. A. Development of the rat thalamus: V. The posterior lobule of the thalamic neuroepithelium and the time and site of origin and settling pattern of neurons of the medial geniculate body. *J Comp Neurol* **284**, 567-80 (1989).
44. Molnar, Z., Higashi, S. & Lopez-Bendito, G. Choreography of early thalamocortical development. *Cereb Cortex* **13**, 661-9 (2003).
45. Nakagawa, Y. & O'Leary, D. D. Combinatorial expression patterns of LIM-homeodomain and other regulatory genes parcellate developing thalamus. *J Neurosci* **21**, 2711-25 (2001).
46. Barbe, M. F. & Levitt, P. Attraction of specific thalamic input by cerebral grafts depends on the molecular identity of the implant. *Proc Natl Acad Sci U S A* **89**, 3706-10 (1992).
47. Mann, F., Zhukareva, V., Pimenta, A., Levitt, P. & Bolz, J. Membrane-associated molecules guide limbic and nonlimbic thalamocortical projections. *J Neurosci* **18**, 9409-19 (1998).
48. Donoghue, M. J. & Rakic, P. Molecular evidence for the early specification of presumptive functional domains in the embryonic primate cerebral cortex. *J Neurosci* **19**, 5967-79 (1999).
49. Donoghue, M. J. & Rakic, P. Molecular gradients and compartments in the embryonic primate cerebral cortex. *Cereb Cortex* **9**, 586-600 (1999).
50. Sestan, N., Rakic, P. & Donoghue, M. J. Independent parcellation of the embryonic visual cortex and thalamus revealed by combinatorial Eph/ephrin gene expression. *Curr Biol* **11**, 39-43 (2001).
51. Suzuki, S. C., Inoue, T., Kimura, Y., Tanaka, T. & Takeichi, M. Neuronal Circuits Are Subdivided by Differential Expression of Type-II Classic Cadherins in Postnatal Mouse Brains. *Mol Cell Neurosci* **9**, 433-47 (1997).
52. Zhou, C., Tsai, S. Y. & Tsai, M. J. COUP-TFI: an intrinsic factor for early regionalization of the neocortex. *Genes Dev* **15**, 2054-9 (2001).
53. Rubenstein, J. L. Intrinsic and extrinsic control of cortical development. *Novartis Found Symp* **228**, 67-75; discussion 75-82, 109-13 (2000).
54. Rubenstein, J. L. et al. Genetic control of cortical regionalization and connectivity. *Cereb Cortex* **9**, 524-32 (1999).
55. Nakagawa, Y., Johnson, J. E. & O'Leary, D. D. Graded and areal expression patterns of regulatory genes and cadherins in embryonic neocortex independent of thalamocortical input. *J Neurosci* **19**, 10877-85 (1999).

56. Miyashita-Lin, E. M., Hevner, R., Wassarman, K. M., Martinez, S. & Rubenstein, J. L. Early neocortical regionalization in the absence of thalamic innervation. *Science* **285**, 906-9 (1999).
57. Bishop, K. M., Goudreau, G. & O'Leary, D. D. Regulation of area identity in the mammalian neocortex by Emx2 and Pax6. *Science* **288**, 344-9 (2000).
58. Ericson, J., Muhr, J., Jessell, T. M. & Edlund, T. Sonic hedgehog: a common signal for ventral patterning along the rostrocaudal axis of the neural tube. *Int J Dev Biol* **39**, 809-16 (1995).
59. Briscoe, J. et al. Homeobox gene Nkx2.2 and specification of neuronal identity by graded Sonic hedgehog signalling. *Nature* **398**, 622-7 (1999).
60. Gunhaga, L., Jessell, T. M. & Edlund, T. Sonic hedgehog signaling at gastrula stages specifies ventral telencephalic cells in the chick embryo. *Development* **127**, 3283-93 (2000).
61. Fukuchi-Shimogori, T. & Grove, E. A. Emx2 patterns the neocortex by regulating FGF positional signaling. *Nat Neurosci* **6**, 825-31 (2003).
62. Gunhaga, L. et al. Specification of dorsal telencephalic character by sequential Wnt and FGF signaling. *Nat Neurosci* **6**, 701-7 (2003).
63. Nordstrom, U., Jessell, T. M. & Edlund, T. Progressive induction of caudal neural character by graded Wnt signaling. *Nat Neurosci* **5**, 525-32 (2002).
64. Furuta, Y., Piston, D. W. & Hogan, B. L. Bone morphogenetic proteins (BMPs) as regulators of dorsal forebrain development. *Development* **124**, 2203-12 (1997).
65. Shirasaki, R. & Pfaff, S. L. Transcriptional codes and the control of neuronal identity. *Annu Rev Neurosci* **25**, 251-81 (2002).
66. Henry, G. L., Zito, K. & Dubnau, J. Chipping away at brain function: mining for insights with microarrays. *Curr Opin Neurobiol* **13**, 570-6 (2003).
67. Kreiman, G. Identification of sparsely distributed clusters of cis-regulatory elements in sets of co-expressed genes. *Nucleic Acids Res* **32**, 2889-900 (2004).
68. Irizarry, R. A. et al. Exploration, normalization, and summaries of high density oligonucleotide array probe level data. *Biostatistics* **4**, 249-64 (2003).
69. Relaix, F. et al. Pw1, a novel zinc finger gene implicated in the myogenic and neuronal lineages. *Dev Biol* **177**, 383-96 (1996).
70. Levine, M. & Tjian, R. Transcription regulation and animal diversity. *Nature* **424**, 147-51 (2003).
71. Manfroid, I., Caubit, X., Kerridge, S. & Fasano, L. Three putative murine Teashirt orthologues specify trunk structures in Drosophila in the same way as the Drosophila teashirt gene. *Development* **131**, 1065-73 (2004).
72. Lai, C. S., Gerrelli, D., Monaco, A. P., Fisher, S. E. & Copp, A. J. FOXP2 expression during brain development coincides with adult sites of pathology in a severe speech and language disorder. *Brain* **126**, 2455-62 (2003).
73. Hecht, A. & Stemmler, M. P. Identification of a promoter-specific transcriptional activation domain at the C terminus of the Wnt effector protein T-cell factor 4. *J Biol Chem* **278**, 3776-85 (2003).
74. Mannervik, M., Nibu, Y., Zhang, H. & Levine, M. Transcriptional coregulators in development. *Science* **284**, 606-9 (1999).
75. Wasserman, W. W. & Sandelin, A. Applied bioinformatics for the identification of regulatory elements. *Nat Rev Genet* **5**, 276-87 (2004).

76. Leonard, J., Serup, P., Gonzalez, G., Edlund, T. & Montminy, M. The LIM family transcription factor Isl-1 requires cAMP response element binding protein to promote somatostatin expression in pancreatic islet cells. *Proc Natl Acad Sci U S A* **89**, 6247-51 (1992).
77. Pratt, T. et al. A role for Pax6 in the normal development of dorsal thalamus and its cortical connections. *Development* **127**, 5167-78 (2000).
78. Aruga, J. The role of Zic genes in neural development. *Mol Cell Neurosci* **26**, 205-21 (2004).
79. Aruga, J. et al. The mouse zic gene family. Homologues of the Drosophila pair-rule gene odd-paired. *J Biol Chem* **271**, 1043-7 (1996).
80. Rohr, K. B., Schulte-Merker, S. & Tautz, D. Zebrafish zic1 expression in brain and somites is affected by BMP and hedgehog signalling. *Mech Dev* **85**, 147-59 (1999).
81. Nakata, K., Nagai, T., Aruga, J. & Mikoshiba, K. Xenopus Zic family and its role in neural and neural crest development. *Mech Dev* **75**, 43-51 (1998).
82. Aruga, J., Tohmonda, T., Homma, S. & Mikoshiba, K. Zic1 promotes the expansion of dorsal neural progenitors in spinal cord by inhibiting neuronal differentiation. *Dev Biol* **244**, 329-41 (2002).
83. Herrera, E. et al. Zic2 patterns binocular vision by specifying the uncrossed retinal projection. *Cell* **114**, 545-57 (2003).
84. Begemann, G. & Meyer, A. Hindbrain patterning revisited: timing and effects of retinoic acid signalling. *Bioessays* **23**, 981-6 (2001).
85. Gavalas, A. ArRAnging the hindbrain. *Trends Neurosci* **25**, 61-4 (2002).
86. McCaffery, P. J., Adams, J., Maden, M. & Rosa-Molinar, E. Too much of a good thing: retinoic acid as an endogenous regulator of neural differentiation and exogenous teratogen. *Eur J Neurosci* **18**, 457-72 (2003).
87. Parenti, R. & Cicirata, F. Retinoids and binding proteins in the cerebellum during lifetime. *Cerebellum* **3**, 16-20 (2004).
88. Wolf, G. Cellular retinoic acid-binding protein II: a coactivator of the transactivation by the retinoic acid receptor complex RAR.RXR. *Nutr Rev* **58**, 151-3 (2000).
89. Tanaka, T. et al. Lipocalin-type prostaglandin D synthase (beta-trace) is a newly recognized type of retinoid transporter. *J Biol Chem* **272**, 15789-95 (1997).
90. Bonaventure, P. et al. Nuclei and subnuclei gene expression profiling in mammalian brain. *Brain Res* **943**, 38-47 (2002).
91. Alcantara, S. et al. Regional and cellular patterns of reelin mRNA expression in the forebrain of the developing and adult mouse. *J Neurosci* **18**, 7779-99 (1998).
92. Sugden SG, Zirpel L, Dietrich CJ, Parks TN. Development of the specialized AMPA receptors of auditory neurons. *J Neurobiol* **52,** 189-202 (2002).
93. Gil, O. D., Zanazzi, G., Struyk, A. F. & Salzer, J. L. Neurotrimin mediates bifunctional effects on neurite outgrowth via homophilic and heterophilic interactions. *J Neurosci* **18**, 9312-25 (1998).
94. Erickson, A. C. & Couchman, J. R. Still more complexity in mammalian basement membranes. *J Histochem Cytochem* **48**, 1291-306 (2000).
95. Hermanns, S., Klapka, N. & Muller, H. W. The collagenous lesion scar--an obstacle for axonal regeneration in brain and spinal cord injury. *Restor Neurol Neurosci* **19**, 139-48 (2001).

96. Grandpre, T. & Strittmatter, S. M. Nogo: a molecular determinant of axonal growth and regeneration. *Neuroscientist* **7**, 377-86 (2001).
97. Tessier-Lavigne, M. & Goodman, C. S. The molecular biology of axon guidance. *Science* **274**, 1123-33 (1996).
98. Struyk, A. F. et al. Cloning of neurotrimin defines a new subfamily of differentially expressed neural cell adhesion molecules. *J Neurosci* **15**, 2141-56 (1995).
99. Chen, S. et al. Neurotrimin expression during cerebellar development suggests roles in axon fasciculation and synaptogenesis. *J Neurocytol* **30**, 927-37 (2001).
100. Silver, J. & Miller, J. H. Regeneration beyond the glial scar. *Nat Rev Neurosci* **5**, 146-56 (2004).
101. Mataga, N., Nagai, N. & Hensch, T. K. Permissive proteolytic activity for visual cortical plasticity. *Proc Natl Acad Sci U S A* **99**, 7717-21 (2002).
102. Zhelyaznik, N., Schrage, K., McCaffery, P. & Mey, J. Activation of retinoic acid signalling after sciatic nerve injury: up-regulation of cellular retinoid binding proteins. *Eur J Neurosci* **18**, 1033-40 (2003).
103. MacManus, J. P. et al. Translation-state analysis of gene expression in mouse brain after focal ischemia. *J Cereb Blood Flow Metab* **24**, 657-67 (2004).